

Appendix I

Identification, mapping, and analysis of offshore wave-cut platforms and
strandlines (Paleoshorelines) in the Shoreline fault zone study area,
San Luis Obispo County, California

TABLE OF CONTENTS

	Page
1.0 INTRODUCTION	1
1.1 BACKGROUND.....	1
1.2 PURPOSE AND OBJECTIVES.....	2
1.3 ACKNOWLEDGMENTS	2
2.0 GEOMORPHIC SETTING	3
2.1 ONSHORE GEOMORPHOLOGY	3
2.2 CONTINENTAL SHELF GEOMORPHOLOGY	4
3.0 DATA SETS.....	5
3.1 PROJECT DEM	5
3.2 DIGITAL GEOLOGIC DATA SETS MAPPED ONTO THE COMPOSITE DEM.....	7
3.3 HIGH-RESOLUTION SEISMIC-REFLECTION SURVEY.....	7
4.0 IDENTIFICATION AND MAPPING OF PALEOSHORELINE FEATURES	7
4.1 SHORELINE GEOMORPHOLOGY	8
4.2 METHODS USED TO MAP AND EVALUATE OFFSHORE PLATFORMS AND BEDROCK SURFACES.....	9
4.2.1 Submerged Strandline and Wave-Cut Platform Mapping.....	9
4.2.1.1 Relative Confidence Assessment Levels.....	11
4.2.1.2 Relationship of Submerged Strandlines to Rock Structure.....	13
4.2.2 Holocene Wave-Cut Platform Mapping	14
4.2.3 Top-of-Bedrock Contouring	15
4.3 TYPES OF UNCERTAINTIES	16
5.0 WORLDWIDE SEA-LEVEL CURVES.....	17
5.1 POST-GLACIAL SEA-LEVEL CHANGES.....	19
5.1.1 Onset of Deglaciation	20
5.1.2 Rapid Sea-Level Rise.....	20
5.1.3 Holocene Highstand	22
5.2 MIS 2 (LAST GLACIAL MAXIMUM).....	22
5.3 MIS 3-4.....	23
5.4 MIS 5.....	23
6.0 DATA ANALYSIS AND RESULTS	25
6.1 HOLOCENE PLATFORM DEVELOPMENT.....	25
6.2 SUMMARY OF SUBMERGED WAVE-CUT PLATFORM MORPHOLOGY	27
6.3 CORRELATION OF SUBMERGED STRANGLINES.....	28
6.3.1 Correlation Alternatives 1 and 2	30
6.3.2 Correlation Alternative 3.....	31
7.0 DISCUSSION.....	32
7.1 PATTERNS OF UPLIFT	32
7.1.1 Islay Shelf.....	33
7.1.2 Santa Rosa Reef Shelf.....	33
7.1.3 MIS 5a Wave-Cut Platform	34
7.1.4 Location of Uplift Boundary	35
7.2 AGE ASSESSMENTS	36
7.2.1 Post-LGM Erosion.....	37

TABLE OF CONTENTS

(Continued)

7.2.1.1	Potential Post-LGM Strandlines.....	38
7.2.1.2	Duration of Relative Sea-Level Stability Required to Carve Wave-Cut Platforms	38
7.2.1.3	Estimates of Downcutting	39
7.2.2	Potential Ages of Selected Paleoshorelines on the Islay Shelf	42
7.2.3	Potential Ages of Selected Paleoshorelines on the Santa Rosa Reef Shelf	43
7.2.4	General Age Constraints	43
7.3	CONSTRAINTS ON FAULT DISPLACEMENT	44
7.3.1	N40W Fault	45
7.3.2	Central Segment, Shoreline Fault Zone	45
7.3.3	South Segment, Shoreline Fault Zone	47
8.0	CONCLUSIONS.....	48
9.0	REFERENCES	50

TABLES

Table I-1-1	Definitions
Table I-4-1	Submerged paleoshoreline confidence assessment
Table I-4-2	Uncertainties in assessing elevations of paleoshorelines and ages of past sea level
Table I-5-1	Elevation and age of paleosea-level highstands and lowstands
Table I-6-1	Summary of Holocene platform parameters

FIGURES

Figure I-1-1	Map of Shoreline fault zone study area
Figure I-1-2	Comparison of LTSP paleoshoreline mapping with current mapping
Figure I-1-3	Paleostrandlines and major faults in study area
Figure I-4-1	Schematic diagrams illustrating the coastal geomorphic features formed by marine erosion and their preservation in marine terraces
Figure I-4-2a	Example of strandline and shoreline angle confidence assessment levels A and D
Figure I-4-2b	Example of strandline and shoreline angle confidence assessment level B
Figure I-4-2c	Example of strandline and shoreline angle confidence assessment level C
Figure I-4-2d	Example of submerged strandline and shoreline angle confidence assessment level D
Figure I-4-3	Bathymetric profile location for analysis of submerged strandlines and wave-cut platforms
Figure I-4-4	Distribution of shoreline angles and strandlines
Figure I-4-5	Paleoshoreline angles imaged on USGS high-resolution seismic-reflection profile PBS-021

TABLE OF CONTENTS

(Continued)

- Figure I-4-6a Contours on top of bedrock offshore in the study area
Figure I-4-6b Bathymetric profiles across the inner continental shelf and near Pismo Beach in the study area
Figure I-5-1 Comparison of late Quaternary sea-level curves from oxygen isotope data
Figure I-5-2 Sea level rise since the Last Glacial Maximum
Figure I-5-3 Preferred late Quaternary eustatic sea-level curves and selected data constraints for sea-level stillstands
Figure I-6-1 Mean slopes and maximum widths of submerged wave-cut platforms
Figure I-6-2 Wave-cut platforms wider than 850 m
Figure I-7-1a Map of submerged MIS 5a wave-cut platforms west of San Luis Hill and Olson Hill
Figure I-7-1b Profiles on MIS 5a wave-cut platforms west of San Luis Hill and Olson Hill
Figure I-7-2 Preliminary age assessment of well-developed wave-cut platforms and strandlines in the Islay shelf based on 0.2 mm/yr uplift rate
Figure I-7-3 Preliminary age assessment of well-developed wave-cut platforms and strandlines in the Santa Rosa Reef shelf based on 0.06 mm/yr uplift rate
Figure I-7-4a Wave-cut platform associated with -38m strandline crossing the N40W fault west of Crowbar Canyon
Figure I-7-4b Profiles showing wave-cut platform associated with -38 m strandline crossing the N40W fault west of Crowbar Canyon
Figure I-7-5 The -25m wave-cut platform across the North-Central segment of the Shoreline fault zone at DCP
Figure I-7-6a -21m strandlines and wave-cut platforms crossing the Central segment of the Shoreline fault zone south of DCP
Figure I-7-6b Profiles showing -21 m strandlines and wave-cut platforms crossing the Central segment of the Shoreline fault zone south of DCP
Figure I-7-7a -31m strandlines and wave-cut platform crossing the South segment of the Shoreline fault zone
Figure I-7-7b Profile showing -31 m wave-cut platform across the South segment of the Shoreline fault zone

PLATES

- Plate I-1a Map of submerged wave-cut platforms and strandlines with top of bedrock contours
Plates I-1b-d Maps of submerged wave-cut platforms and strandlines
Plates I-2a-d Maps showing submerged strandlines, wave-cut platforms, and geology
Plate I-3a Longitudinal profile along coastline showing correlation of submerged strandlines
Plate I-3b Longitudinal profile along coastline showing correlation of submerged strandlines (alternative 1)

TABLE OF CONTENTS
(Continued)

Plate I-3c	Longitudinal profile along coastline showing correlation of submerged strandlines (alternative 2)
Plate I-3d	Longitudinal profile along coastline showing correlation of submerged strandlines (alternative 3)

**Identification, Mapping, and Analysis of
Offshore Wave-Cut Platforms and Strandlines (Paleoshorelines)
in the Shoreline Fault Zone Study Area,
San Luis Obispo County, California**

1.0 INTRODUCTION

This appendix presents the results of mapping and analysis of wave-cut platforms and associated paleostrandlines (paleoshorelines) in the offshore part of the Shoreline fault zone study area (herein called study area). The study area is located southwest of the present-day shoreline between Morro Bay and Pismo Beach (Figure I-1-1). These investigations were conducted in 2009 and 2010 as part of the characterization of the Shoreline fault zone. These studies extend the previous analysis of onshore paleoshorelines in the study area that was carried out during the 1985-1991 Diablo Canyon Long Term Seismic Program (LTSP) (Niemi et al., 1987; PG&E, 1988; Response to Question 43i, PG&E, 1989).

The general organization of this appendix is as follows:

- Section 1 provides the overall framework and objectives of the paleoshoreline investigations and acknowledges the individuals who conducted the study.
- Section 2 provides a brief description of the geomorphology of the onshore and offshore regions within the study area.
- Section 3 describes the primary data sets that were used to evaluate and map wave-cut platforms and associated strandlines, both offshore and onshore.
- Section 4 describes the methods and approaches that were used to identify and map geomorphic features related to marine wave-cut platforms and strandlines.
- Section 5 provides a summary of current global sea-level data used to develop a paleosea-level curve that in turn is used to evaluate ages of emergent and submerged paleoshoreline features in the study area.
- Section 6 presents the results of mapping and analysis of paleoshoreline features in the study area
- Section 7 discusses the implications of these results with regard to characterization of the Shoreline fault zone.

Table I-1-1 lists and defines terms used in this appendix.

1.1 BACKGROUND

Onshore and submerged wave-cut platforms and associated strandlines in the study region are important datums that can be used to evaluate locations and rates of Quaternary deformation. As part of the work completed for the LTSP, worldwide data on Quaternary sea levels were

compiled and reviewed in the assessment of the ages and paleosea level (sea level at the time of formation) of onshore marine terrace features in the study area (Hanson et al., 1992, 1994; PG&E, 1988). Submerged shoreline features also were interpreted using the bathymetric chart compilations developed for the LTSP in 1989; however, in the absence of information that could be used to date these submerged paleoshorelines, the correlation and continuity of these offshore features were based entirely on their relative altitudinal spacing (PG&E, 1989).

The greatly improved bathymetry and high-resolution seismic-reflection data recently obtained for the study area and discussed in this Appendix have allowed for more confident identification and more rigorous interpretation of the continuity and relative altitudinal spacing of strandlines in the mid- to upper continental shelf regions in the study area; Figure I-1-2 illustrates the improvement in data resolution. Direct evidence of the ages of sediment associated with or overlying the submerged terrace platforms has not been obtained, so correlation to global eustatic sea-level curves is the only approach available at the time of this study for estimating the age of submerged wave-cut platforms and strandlines.

1.2 PURPOSE AND OBJECTIVES

The primary objectives of the paleoshoreline studies conducted during 2009 and 2010 were to:

- Map submerged wave-cut platforms and strandlines in the study area (Figure I-1-1) using the new bathymetric and high-resolution seismic-reflection data collected in 2008 to 2010.
- Estimate the ages of paleoshoreline features based on available age constraints provided by studies previously completed during the DCPD LTSP (Hanson et al., 1994) and more recent publications regarding paleosea levels from global sea-level studies.
- Evaluate possible displacements of the submerged paleowave-cut platforms where they cross the Shoreline fault zone.

1.3 ACKNOWLEDGMENTS

The AMEC Geomatrix project team consisted of the following individuals: Ms. Kathryn Hanson, Principal Geologist and senior technical lead; Mr. Hans Abramson Ward, Senior Geologist and technical lead for offshore mapping and interpretation; Mr. Brian Gray, Staff Geologist performing offshore mapping and evaluation of the Holocene platform and mapping of submerged wave-cut platforms and strandlines; and Mr. Serkan Bozkurt, Senior GIS Analyst providing GIS database and technical support.

Dr. William Page (Pacific Gas & Electric Company), Drs. William Lettis and Stephen C. Thompson (Fugro-William Lettis & Associates), and Dr. Gary Greene (Professor Emeritus, Center for Habitat Studies, Moss Landing Marine Laboratories) participated in numerous

working meetings to discuss and evaluate interpretations of paleoshoreline features and provided oversight and review throughout the project. Dr. Gary Carver (Carver Geologic), provided technical peer review. Dr. William U. Savage (Consultant) provided additional technical review of the final report.

2.0 GEOMORPHIC SETTING

The general topographic and bathymetric features of the central California coast in the study area are evident in the shaded-relief topography and bathymetric (Figure I-1-3). The area of study focuses on the western margin of the San Luis Range, a prominent west-northwest-trending topographic and structural high that lies within the central part of the Los Osos/Santa Maria structural domain (Lettis et al., 2004). The range is bordered on the northeast by the Los Osos fault zone (Lettis and Hall, 1994) and on the southwest by a diffuse zone of small faults including the Wilmar Avenue, San Luis Bay, Pecho, Los Berros, Oceano, and Nipomo faults, collectively referred to as the Southwestern Boundary zone (Lettis et al., 1994, 2004).

2.1 ONSHORE GEOMORPHOLOGY

Topographically, the San Luis Range is bordered on the north by the Los Osos Valley and associated coastal embayments (Morro Bay and the offshore Estero Bay) and on the south by the onshore Santa Maria Valley, offshore San Luis Obispo Bay, and the Pacific Ocean. The highest, westernmost-part of the range is referred to as the Irish Hills. Point Buchon represents the most westerly point of land associated with this topographic high, which is characterized by rugged headlands, narrow, discontinuous beaches, and flights of emergent marine terraces. At Point San Luis, sea cliffs approach 60 m in height. Between there and Point Buchon (including the DCP site), the cliffs are 12–24 m high and are the lowest step in a flight of marine terraces. Marine sediments overlying the emergent platforms and associated strandlines near the range front commonly are buried by several to tens of meters of Quaternary colluvium, alluvium, and landslide deposits.

Elevations and ages of marine terraces show that the San Luis Range is uplifting as a relatively rigid crustal block with little internal deformation (Lettis et al., 1994). Well-constrained ages for the lower emergent marine terraces, which correlate to marine oxygen isotope stage (MIS) 5e and MIS 5a (about 120 ka and 80 ka, respectively), indicate an uplift rate of 0.2 ± 0.03 mm/yr for the coastal region between Point Buchon and the DCP (Hanson et al., 1994). This uplift rate is inferred by Lettis et al. (1994) for the Irish Hills subblock of the San Luis Range (shown on Figure I-1-3). South of the San Luis Bay fault zone is a separate subblock (herein referred to as the Point San Luis subblock). An uplift rate for this subblock of 0.06 ± 0.2 mm/yr is indicated by the elevation and age of the MIS 5e emergent marine terrace, which is continuous along the

lower flank of San Luis Hill (Hanson et al., 1994). Along the coastline between the Rattlesnake fault and the Olson Hill deformation zone an uplift rate of 0.14 ± 0.03 mm/yr is indicated by well-constrained ages and elevations of marine terraces that correlate to MIS 5e and MIS 5a (Hanson et al., 1994). No separate subblock is defined for this zone of intermediate uplift because the boundary between the Irish Hills subblock and this intermediate zone as well as the southern limit of the zone are not yet well defined.

The Los Osos and Santa Maria valleys are tectonically subsiding basins (Lettis and Hanson, 1992). The morphology of the coastline in these areas is characterized by the broad marine embayments of Estero/Morro Bay and southern San Luis Obispo Bay, low coastline relief, and sand dunes backing a barrier beach or spit (Section 3.0).

2.2 CONTINENTAL SHELF GEOMORPHOLOGY

The continental shelf in the study area is defined as the gently westward-sloping seafloor that lies between the coastline and the break in slope to the steeper (1.0° to 2.0°) continental slope at water depths of 100 m to 225 m that is generally coincident with the Hosgri fault zone (Niemi et al., 1987; Response to Question 431, PG&E, 1989). The seafloor slope along the shelf is generally less than 0.7 degrees. The overall width and character of the continental shelf varies along the coast within the study area. In general, the continental shelf is narrower (5–10 km) and more rugged and irregular adjacent to the uplifted onshore region (Point Buchon to Point San Luis). The shelf is broader (10–25 km) and smoother adjacent to the broad embayments in the coastline (Estero Bay, San Luis Obispo Bay).

The inner part of the continental shelf from southern Estero Bay to northern San Luis Obispo Bay is characterized by broad exposures of deformed, faulted, and differentially eroded bedrock that has generally been eroded to a low angle during multiple sea-level fluctuations. The gently sloping bedrock surface is locally incised with meandering paleostream channels that formed during periods of lower sea level. Well-layered, differentially eroded Tertiary sedimentary rocks underlie the northern part of the study area, whereas pre-Tertiary sedimentary and metamorphic rocks, Tertiary intrusive volcanic rocks, and Tertiary sedimentary rocks underlie the southern part of the study area (Appendix B of this report). In detail, the gently sloping bedrock surface is characterized by irregular relief, numerous sea stacks, and relatively thin, local deposits of Quaternary sediment. Submerged bedrock exposures of the inner shelf give way offshore to modern marine sediments that lap onto bedrock and cover the rocks along the outer continental shelf. Mobile dune-like sand sheets cover the outer continental shelf and locally fill depressions and low areas within the bedrock outcrops in the nearshore.

Numerous submerged marine terraces are preserved on the continental shelf in the study area, both at the seafloor surface and buried by shallow marine sediment. Discussions of the development, distribution, correlation, and timing of formation of these features are provided in Sections 4, 6, and 7.

Based on seafloor morphology and relationship to onshore tectonic subblocks, the continental shelf in the study area is subdivided into three distinct shelf segments. They are the Islay shelf, extending from the southern margin of Estero Bay to Olson Hill south of Diablo Canyon, the Santa Rosa Reef shelf, extending from near Olson Hill to Point San Luis, and the San Luis Bay shelf (Figure I-1-3). The southwestern margin of the Islay and Santa Rosa Reef shelves is defined by the Hosgri fault zone. The southern margin of the San Luis Bay shelf is defined by the southern limit of discontinuous bedrock outcrops.

3.0 DATA SETS

Numerous spatial data sets were compiled within a GIS database. Derivative products from the compiled data were used to map and interpret paleoshorelines features in the study area.

3.1 PROJECT DEM

An integrated digital elevation model (DEM) was compiled for the study region. This DEM, described in Appendix I and elsewhere in this report as the Project DEM, was developed using the following topographic and bathymetric data sets:

- 1 m resolution multibeam bathymetry data (collected for PG&E in 2007, 2009, and 2010)
 - Multibeam echo sounding (MBES) and side-scan sonar data were acquired in the nearshore region from the Estero Bay to San Luis Obispo Bay using a combination of several sonar systems (400 KHz Reson 7125, 240 KHz Reson 8101, SEA SwathPlus) aboard the R/V Ven Tresca. The data were acquired by the Seafloor Mapping Lab at California State University Monterey Bay during 2007, 2009, and 2010. Figure AF-1 in Appendix F shows the areas mapped in 2007 (Point Buchon) and 2009 (Point Buchon to San Luis Obispo Bay) surveys. The 2010 data collection focused on nearshore areas adjacent to the Rattlesnake fault and Olson deformation zone. Elevation data are presented in NAVD88 (North American Vertical Datum 1988). The horizontal datum is NAD1983. Additional information regarding the collection and development of the DEM from these data is provided in Appendix F.
- 1 m resolution near-shore LiDAR topography data (collected for PG&E in 2010)
 - Light Detection and Ranging (LiDAR) data were collected in January 2010 by Tetra Tech along the coastline from Islay Creek in the north to Avila Bay in the south, and extending from the coast to 1.6–2 km inland. The LiDAR data were used to create hillshade images, contours, and slope maps. The data, which were collected at low tide, image the intertidal zone. Stereo photography was collected

along with the LiDAR data at a nominal scale of 1:12,000. Six flight lines were flown, with three flown offshore to afford the best possible view of the seaward-facing cliffs. The photography was flown with airborne GPS collection to minimize the number of ground points necessary to control the photography for mapping. LiDAR collection was done at a density of 8 points per square meter. Multiple static GPS ground surveys, accompanied by a real-time kinematic (RTK) survey of ground points with a roving GPS on selected control points, were conducted simultaneously with the LiDAR collection flight. A total of 129 points were collected to assess the absolute accuracy of the LiDAR data. The root mean square error (RMSE) for the absolute accuracy was calculated at 4–5 cm. The LiDAR data were interpolated into ArcGIS grid files with 1 m grid spacing, and 0.25 m grid spacing on the cliffs and reef outcrops. Elevation data are presented in NAVD88 (North American Vertical Datum 1988).

- 5 m resolution county-wide INSAR topography data (collected for San Luis Obispo County in 2004)
 - InSAR (Interferometric Synthetic Aperture Radar) data collected in July 2004 by Intermap Technologies, Inc. for San Luis Obispo County provides more detailed topographic information than was available during the LTSP. The InSAR DEM was derived from the digital surface model (DSM) using Intermap's proprietary algorithm, and is provided in 7.5-minute by 7.5-minute units, corresponding to the 1:24,000-scale U.S. Geological Survey (USGS) quadrangles. Each DSM is comprised of elevations at 5 m postings, comprising a 5 m grid. The vertical datum used is NAVD88 (Geoid99). Horizontal position accuracy of the data is 2 m or better in areas of unobstructed flat ground. Vertical position accuracy is 1 m or better in areas of unobstructed flat ground.
- 5 m coastal LiDAR topography data (NOAA, 2008)
 - 1996-2000 NOAA/USGS/NASA Airborne LiDAR Assessment of Coastal Erosion (ALACE) Project for the US Coastline, from Department of Commerce (DOC), National Oceanic and Atmospheric Administration (NOAA), National Ocean Service (NOS) Coastal Services Center (CSC).
- 1/3 arc second multibeam bathymetry data (NOAA, 2006)
 - Digital Elevation Model of Port San Luis, California, Integrating Bathymetric and Topographic Datasets, National Geophysical Data Center, NESDIS, NOAA, U.S. Department of Commerce.

These data sets were processed and assembled to create a composite DEM in which the most accurate and detailed data sets supersede less detailed or regional data sets. The composite DEM with merged data sets for both the onshore and offshore regions allows for seamless two-dimensional seafloor profiling across the coastline. Derivative products were developed from the integrated digital terrain model including slope maps, contour maps, and hillshade images of the topography and bathymetry rendered at various sun angles.

Figures and plates presented in this appendix are based on version 6 of the composite DEM data, which was compiled in August 2010 at 1 m raster resolution. The projection system for the data set is Universal Transverse Mercator (UTM), zone 10 North, NAD83 with NAVD88 vertical datum.

3.2 DIGITAL GEOLOGIC DATA SETS MAPPED ONTO THE COMPOSITE DEM

Additional data sets compiled from previous LTSP studies and publications, and from results of ongoing geologic mapping of onshore and offshore portions of the study area were added to the GIS database. These include:

- Detailed Quaternary map information (e.g., marine terrace shoreline angles, locations of marine deposits and pholad-bored wave-cut platforms, borings, and bedrock outcrops) from PG&E (1988), Hanson et al. (1994) Plates 2 and 3, and Response to Question GSG Q16-5 (1990).
- Detailed geologic maps (e.g., PG&E, 1988; Hall, 1973a, 1973b; Hall et al., 1979).
- Onshore-offshore geologic map (Appendix B of this report).

3.3 HIGH-RESOLUTION SEISMIC-REFLECTION SURVEY

Single-channel seismic-reflection data were acquired in 2008 and 2009 by the USGS between Piedras Blancas and Pismo Beach, along shore-perpendicular transects spaced 800–400 m apart extending beyond the 3-mile limit of California State waters. Data were collected by the R/V Parke Snively using a SIG 2Mille mini sparker and an Edgetech SB-0512i chirp system. Water depths in the survey area ranged from 6 m near shore to 210 m at the northwest corner of the survey area. Figures AH-1 and AH-2 in Appendix H show the survey area and individual track lines. Additional information regarding the data collection, processing, and reprocessing of selected lines is provided in Appendix H.

4.0 IDENTIFICATION AND MAPPING OF PALEOSHORELINE FEATURES

Although marine terraces preserved in onshore and offshore environments share common origins and geomorphologic features, they have been subjected to different erosional and depositional environments subsequent to their initial formation. These different environments must be considered in evaluating possible ages and correlations of marine terraces. Section 4.1 provides a description of the formation and basic geomorphic features shared by both emergent and submerged wave-cut platforms and strandlines. Section 4.2 describes the methods and approaches used in this study to identify and map offshore wave-cut platforms and their associated strandlines. Section 4.3 describes potential sources of uncertainty in the mapping and analysis of submerged paleoshoreline features.

4.1 SHORELINE GEOMORPHOLOGY

In general, shoreline features (wave-cut platforms and strandlines) are formed when the local relative sea level remains constant for a sufficient length of time such that coastal erosion is recorded in the landscape. On a high-energy, erosional coastline, such as that along much of California, paleoshorelines are commonly recorded in bedrock as broad, gently sloping wave-cut platforms situated seaward of relatively steep paleosea cliffs. The approximate relative sea level at the time the shoreline was formed is marked by the shoreline angle (generally a point measurement in profile) or strandline, defined as the intersection of the wave-cut platform and the paleosea cliff (Figure I-4-1; Table I-1-1).

Based on their study of several topographic profiles across marine terraces and the active wave-cut platform on the flanks of Ben Lomond Mountain north of Monterey Bay, California, Bradley and Griggs (1976) showed that modern and ancient wave-cut platforms are similar in shape. They have a seaward slope composed of two segments: a steeper, slightly concave inshore segment with gradients of generally 0.02–0.04 (20–40 m/km) and a flatter, planar offshore segment with gradients of 0.007–0.017 (7–17 m/km). The flattest inshore and offshore gradients measured were, respectively, 0.015 (10 m/km) and 0.005 (5 m/km). Bradley and Griggs (1976) interpret these to be close to the minimum gradients for erosional platforms in central California. The inshore segments are generally 300–600 m wide (as measured perpendicular to the sea cliff) and extend to a depth of 8–13 m below the strandline. Bradley and Griggs (1976) note that the platforms are widest in areas where soft sandstone crops out and also where there has been the least uplift (and therefore the coast rises less steeply). It is also likely that the duration of relative sea-level stillstands (that is, the amount of time during which tectonic uplift approximately matches sea-level rise) would tend to increase the width of the platforms.

Many factors contribute to marine erosion, including quarrying (disaggregation of bedrock particles that can range in size from mineral grains to large joint blocks), abrasion, solution of carbonate rocks, and biological activity. Bradley and Griggs (1976) report that quarrying and abrasion are most intense in the zone of breaking waves where fluid drag on the seafloor is the greatest and at the sea cliff where changes in pore fluid pressure, salt wedging, and wetting and drying can cause crumbling. Bradley and Griggs (1976) report that bioerosion of bedrock (i.e., wedging by holdfasts, boring by mollusks and other organisms, and plucking by grazing animals) is best demonstrated in the intertidal zone, and is poorly understood in deeper water. However, the presence of plants that may serve as a baffle to fluid motion, and the relatively lower abundance of marine organisms in deeper water suggest that the rates of bioerosion of bedrock are lower in deeper water than within the intertidal zone. The change in platform gradients from the inshore platform to the offshore platform (at depths of about 8–13 m below

the strandline) likely indicates the water depth of significant marine erosion at the time the wave-cut platform was formed. Below this depth, rates of erosion are likely to be significantly lower.

4.2 METHODS USED TO MAP AND EVALUATE OFFSHORE PLATFORMS AND BEDROCK SURFACES

Offshore geomorphic evaluations included mapping of submerged strandlines and associated wave-cut platforms (Section 4.2.1), Holocene wave-cut platform mapping and analysis (Section 4.2.2), and development of a top-of-bedrock contour map of the offshore region (Section 4.2.3). The approach used to identify and map submerged shoreline features is outlined below.

4.2.1 Submerged Strandline and Wave-Cut Platform Mapping

Figure I-4-2, parts a through d, shows examples of paleostrandline mapping that illustrate the general variability in geomorphic expression of the submerged shorelines. Figures I-4-3 and I-4-4 show the distribution of submerged strandlines and shoreline angles in the study area. The approach used to identify and map submerged shoreline features is outlined below.

1. Examine the project DEM derivative maps, e.g., hillshade images of the seafloor, slope maps, and contour maps. Use derivative maps at various appropriate scales where bedrock is exposed at the seafloor to identify candidate wave-cut platforms and associated paleoshoreline features. Where bedrock is buried by mobile sand sheets, shoreline angles are not evident at the surface, and must be interpreted from seismic reflection profiles (discussed below).
2. Create a series of bathymetric profiles at locations where paleoshorelines are suspected, such as across lineaments expressed in hillshade images and slope maps, or at locations where contours indicate a gently sloping wave-cut platform (beveled bedrock) situated seaward of a relatively steeper slope.
3. Interpret shoreline angles where profiles indicate scarp-platform morphology or marked changes in slope. Points are digitized to record the interpreted elevation of the shoreline angle and bounds of uncertainty on the elevation of the shoreline angle are estimated from the relative roughness of the profile and adjacent bathymetry. Where wave-cut platforms are relatively rough and include substantial relief (i.e., erosion has scoured crevices between resistant rock outcrops) bounds of uncertainty are estimated by correlating concordant tops of outcrops and concordant bases of crevices, and projecting those correlated surfaces back to the paleosea-cliff location. Where the shoreline angle appears to be buried by sediment, elevations of shoreline angles and bounds of uncertainty are estimated by projecting potential wave-cut platforms from nearby rock outcrops (either upslope along the profile, along contour in map view, or both). General notes about the shoreline angle are recorded with each point, such as the relative strength of the scarp-platform morphology, width and roughness of the platform surface, interpreted depth of burial, etc.
4. Map a strandline where shoreline angles identified in multiple profiles indicate scarp-platform morphology and where the geomorphology of the seafloor suggests a

continuous strandline. In many locations, the scarp-platform morphology of the seafloor is sufficiently well-expressed that step 3 may be skipped, and strandlines may be mapped without digitizing shoreline angle points. The elevation of the strandline and associated uncertainties are interpreted using the same rationale as the elevations and uncertainties interpreted for the shoreline angles described above. As also described above, general notes about each strandline are recorded, such as the relative strength of the scarp-platform morphology, width and roughness of the platform surface, interpreted depth of burial, lateral continuity, etc.

5. Utilize the newly mapped strandline to guide mapping of the associated submerged wave-cut platform. Elevations and positions of the newly mapped strandlines are used in conjunction with contour maps, slope maps, and hillshade images to visually identify relatively planar areas of the seafloor consistent with the position of a previously mapped submerged strandline.
6. Generate multiple topographic profiles across previously identified planar bathymetric surfaces to determine the margins of submerged wave-cut platforms based on lateral continuity of relatively planar surfaces. Given the significant roughness of the seafloor in many locations, margins of platforms can be commonly delineated by systematic changes in the elevation of concordant peaks and or troughs. Wave-cut platforms buried by seafloor sediment are not mapped unless sufficient seismic reflection data are available to define wave-cut platform margins. In many cases, wave-cut platforms are mapped along only portions of their associated submerged strandlines as sections become eroded, or buried.
7. Document average slope of wave-cut platform and maximum width for each submerged wave-cut platform. As the surface morphology of wave-cut platforms can be highly variable, along with the elevations and positions of their associated submerged strandlines, their widths and slopes also can be highly variable. Slopes are documented for multiple profiles across each mapped polygon, usually taken at locations where the platform surface is most planar and easily identified. Slopes are averaged for all representative profiles and recorded in the shapefile. Maximum platform widths are measured orthogonal to the submerged strandline. Distinct promontories, deemed unrepresentative of the platform as a whole, are not included in the width or slope measurements. Offshore and inshore platform segment slopes in the convention of Bradley and Griggs (1976) are not delineated for this study.
8. Where potential strandlines are buried by mobile sand sheets or thicker sediments, elevations and locations of shoreline angles are interpreted from the 2008 USGS high-resolution seismic-reflection data. In most cases, shoreline angles are clearly evident at the location where relatively flat, beveled platforms meet associated paleosea cliffs underlying an acoustically transparent layer (e.g., Figure I-4-4). In some cases where the shoreline angle is buried by a relatively thin layer of sediments, the bubble pulse in the seismic reflection profile interfered with measuring the precise location and burial depth. The uncertainty in the measurements of shoreline angles from seismic reflection data is estimated to be about a meter or two, both vertically and horizontally.

4.2.1.1 Relative Confidence Assessment Levels

To aid in assessment and correlation of strandlines, a set of ranking criteria in a matrix format is used to assign a letter reflecting level of confidence (from a high level of A to a lowest level of D) to each mapped strandline (Table 4-1). The level ranking matrix was developed as a tool to allow for straightforward comparison of the mapper's confidence in assessing strandline correlations or using strandlines as potential tectonic deformation indicators. Strandlines with lower letters were generally given less weight or consideration during the analysis than those with higher letter ranks. The ranking scheme utilizes geomorphic expression of the shoreline angle and wave-cut platform, lateral continuity of the strandline, confidence in mapped shoreline angle location, and an assessment of the probability that the feature represents a paleoshoreline.

Mapping strandlines based on buried reflection picks is difficult due to the 800 m spacing of the seismic reflection survey lines. In several instances, buried shoreline angles are coincident with traces of the Hosgri fault, complicating interpretation of shoreline angles. Therefore, this study focused on unburied or partially buried shoreline angles, supplemented by seismic reflection picks of possible buried shoreline angles.

In the context of the strandline and wave-cut platform mapping, geomorphic expression is defined as the prominence, or lack thereof, of an identifiable wave-cut platform and shoreline angle. Strandlines with strong geomorphic expression display distinct breaks in slope between the wave-cut platform and paleosea cliff, have paleosea cliffs several meters in height with slopes significantly higher than the surrounding bathymetry, and are readily identifiable in multiple profiles taken along the break in slope. Strandlines displaying moderate geomorphic expression generally have an identifiable paleosea cliff up to several meters in height along most of the length of the feature, but the feature may be more diffuse or muted, possibly due to wave erosion during subsequent transgressions or regressions or partial burial by colluvium derived from the sea cliff. Strandlines with poor geomorphic expression are difficult to identify in cross section alone as their paleosea cliffs are highly degraded and usually have topographic relief of less than 4 m. As with moderate strandlines with moderate geomorphic expression, paleosea cliffs have been degraded by sequences of paleosea transgressions or regressions or are buried by colluvium and landslide debris derived from the sea cliff. The slope of the paleosea cliff is commonly only slightly higher than the slope of the surrounding seafloor.

Wave-cut platforms with strong geomorphic expression display relatively planar surfaces with slopes generally ranging from 0.5 to 4 percent (0.005 to 0.04 slope gradient) and are easily distinguished from the surrounding continental shelf. Platform roughness does not hinder identification and definition of the platform. Inshore and offshore platform segments are

commonly, but not always, distinguishable on platforms with strong geomorphic expression. Widths of these platforms are commonly in the hundreds of meters, although some narrower notches into resistant rock slopes and small seamounts also are interpreted as wave-cut platforms with strong geomorphic expression. Moderate geomorphic expression in wave-cut platforms is characterized by roughness, variable platform slope, possible platform dissection, and difficulty in defining the platform outer edge. Slopes of moderately well-expressed wave-cut platforms commonly are measured on concordant troughs, peaks, or an average of the two. Platforms having poor geomorphic expression are difficult to distinguish from the surrounding bathymetry due to their rough surface texture, variable slopes or slopes similar to the surrounding bathymetry, abundant dissection, and lack of a defined front edge. These platforms generally exhibit highly variable widths. Slopes of poor platforms can be difficult to characterize as microtopography peaks and troughs commonly are not concordant and do not necessarily show a preferred slope angle.

Continuity of the strandline refers to the consistency in elevation and lateral continuity of the mapped strandline. Strandlines displaying relatively constant elevations (± 2 m) along traces mappable for distances of several hundred meters are assigned higher-level rankings than those with inconsistent elevations and lateral discontinuities.

Location confidence can be negatively affected by sediment burial, bedrock topography, or multiple alternative interpretations where lines can be drawn in different locations and still satisfy shoreline morphologic criteria.

The probability of a mapped strandline representing a paleoshoreline formed during a period of relative sea-level stability is an assessment of the criteria described above (geomorphic expression, continuity, and location confidence) and consideration of other geomorphic explanations for the origin of the feature. For example, at locations where broad wave-cut platforms are evident but no clear strandline is observed, a strandline may be mapped with very low confidence at a break in slope. This potential strandline may not closely represent a paleoshoreline, but the broad wave-cut platform likely results from a long period of wave erosion during a relative sea-level stillstand, which should have recorded a strandline upslope. Additionally, where a topographic break-in-slope or scarp inferred to be a strandline could be related to other processes or factors, such as differential bedrock erosion resulting from lithologic variation, fault scarps, jointing, or other structural discontinuities, the probability that a mapped strandline represents a paleoshoreline is decreased.

4.2.1.2 Relationship of Submerged Strandlines to Rock Structure

In order to evaluate the possibility that some or all of the mapped strandlines were formed by differential erosion in rock, instead of wave erosion during paleosea-level stillstands, the relationship of mapped strandlines to existing bedrock structure (i.e., mapped faults, folds, joints, and bedding attitudes) as described in Appendix B and interpreted from the seafloor texture exhibited in shaded-relief images of MBES bathymetry in rocky parts of the seafloor was documented separately from the confidence assessment described above. In addition to influencing the confidence assessments (as described above), these relationships were used to assist with the correlation of paleoshorelines (described in Section 6.3 and shown on Plates I-3-a through I-3-d). Strandlines mapped parallel to prominent bedding, faults, folds, and joints are given less weight in the paleoshoreline correlations than those that clearly crosscut bedrock structures and bedding. Strandlines were assigned to one of four categories based upon their orientation with respect to surrounding bedrock structure and bedding:

1. Strandlines that crosscut bedding and bedrock structure, where evident.
2. Strandlines that crosscut bedding but parallel structure.
3. Strandlines that clearly parallel bedding and/or structure.
4. Strandlines that have no clear relationship to structure or bedding. In most cases strandlines in this group are developed in rock where bedding is unrecognizable or does not exist, and/or structure is chaotic, poorly defined, or absent.

In many cases individual strandlines were separated into multiple segments as their orientation with respect to bedrock structure and bedding varied along their length. The relationships of strandlines to rock structure and bedding are shown as colored symbols on Plates I-3-a through I-3-d.

Where strandlines are parallel to bedding, differential erosion by wave action and other nearshore and submarine erosion processes is a reasonable interpretation for their origin. Approximately one-third of the mapped strandlines are parallel to bedding or other bedrock structure (such as joints or faults). Differential erosion is a less likely explanation for the strandlines developed in rock that does not exhibit a distinct geomorphic expression of bedding or other structure (described herein as an "indistinct" relationship to structure). Approximately one-third of the mapped strandlines fall into this category. Where strandlines clearly crosscut bedding and other rock structure, differential erosion of bedrock is not a viable explanation for the origin of these geomorphic features. Approximately one-fourth of the mapped strandlines

clearly crosscut bedding and other bedrock structure, and the rest of the strandlines appear to crosscut bedding, but are parallel to joints or faults.

4.2.2 Holocene Wave-Cut Platform Mapping

To better understand processes and rates of strandline and wave-cut platform formation, the modern (mid- to late-Holocene) wave-cut platform is used as a proxy for paleoplatform development during periods of relative sea-level stability. Given that timing and elevation of the mid- to late-Holocene eustatic sea-level highstands are relatively well constrained, rates of Holocene platform development can be estimated (where sufficient bathymetric data exist) and used to better understand potential rates and timing of paleoplatform development.

Holocene platforms from the mouth of Islay Creek to Point San Luis are the primary data set used in this analysis. North of Islay Creek, the Holocene platform is difficult to define because LiDAR data terminate less than 200 m north of the creek mouth. Although LiDAR and multibeam bathymetry data sets were merged for this exercise to allow for continuous two-dimensional profiling between the offshore and onshore, at no point along the Islay Creek to Point San Luis coastal segment do the LiDAR and bathymetry data overlap to form a continuous data set. The gap between the two data sets is filled by a zone of computer-interpolated data, taken as unrepresentative of actual bathymetry. In many locations, bathymetric data do not extend near enough to shore to image platforms, should they exist. For this reason, several sections along the coast are not represented in the mapping and analysis.

The Holocene platform mapping approach consists of the following steps:

- Establish a reference line along the coastline to document locations of two-dimensional profile measurements, allowing for longitudinal profiling, correlation with geologic units, and reinterpretation/reoccupation of measurements during analysis.
- Generate coast-normal bathymetric profiles across the suspected location of a Holocene platform. Profiles are interpreted based on apparent relationships between platform slopes as projected across the gap between the LiDAR and multibeam data. The outer edge of the Holocene platform is judged to be present in the multibeam data when slopes aligned such that a continuous platform could be interpreted to cross the gap between the data sets.
- Map a wave-cut platform where multiple coast-normal profiles suggest that outer edge and inner (backedge) morphologies show the presence of a Holocene platform with a strandline that occurs near the modern mean sea level. For this study, two platform sets are mapped: one set using a more conservative approach where only contiguous platforms are included, and a second, less conservative set that includes broader areas commonly farther offshore at water depths consistent with the main platform bodies. Areas included in the less conservative set are interpreted to be platform remnants isolated from the main platform body by submarine erosional processes. Areas are not

mapped where profiles display inconsistent outer edge elevations or morphology, steep morphology, no apparent outer edge, or pinnacles with water depth unrelated to an adjacent platform.

- Use profiles to measure outer edge depths, shoreline angle elevations, and platform widths at points along the station line. Record rock type at the location of each platform measurement to generate platform statistics by rock type.

The distribution of Holocene wave-cut platforms mapped for this study using the above approach is shown on Plates I-1a through I-1d.

4.2.3 Top-of-Bedrock Contouring

Abundant sand sheets and other marine sediments in the study area are most prevalent in areas to the west of the Islay and Santa Rosa Reef shelves, in the topographic low between the two blocks, and in San Luis Bay. In addition to obscuring low-relief submerged strandlines, geologically young marine sediments have the potential to conceal significant bedrock topography that could otherwise be used to identify differing lithologies or tectonic structures. In order to evaluate the general seafloor topography beneath these broad sand sheets, the 2008 USGS high-resolution seismic-reflection profiles were interpreted to map and contour the inferred top of bedrock for approximately 215 km² of seafloor. The top-of-bedrock contours are presented in Figure I-4-5. The methodology used to define the top of bedrock in these areas consisted of following steps:

1. The top of bedrock was interpreted using 2008 high-resolution seismic-reflection profiles loaded into SMT Kingdom Suite software. The top of bedrock was mapped as a continuous horizon for each seismic line, except where bedrock was exposed at the seafloor surface. Seismic interpretation was completed for lines extending south from Estero Bay through lines terminating at the north end of Pismo Beach at the southeast margin of San Luis Bay (near the offshore extension of the Wilmar Avenue fault). The seismic reflection profiles used in this interpretation are spaced approximately 800 m apart and oriented northeast-southwest. The top of bedrock, where buried, was picked on the presence of a strong, commonly undulatory reflector located beneath a set of weaker subhorizontal reflectors. Additional reflectors beneath the strong top-of-bedrock reflection are commonly tilted and/or folded. Vertical motion of the reflection survey equipment due to waves was not corrected in the high-resolution seismic-reflection profiles, resulting in undulatory reflectors. The bedrock horizon was mapped through the vertical average of the wave peaks and troughs. The type and age of underlying bedrock commonly affects the strength of the bedrock reflection, with Monterey and Pismo Formations generally showing weaker signals than those of the Franciscan Complex and Cretaceous sandstone units.
2. The depth to bedrock was measured in milliseconds, converted to meters, and plotted on 1:15,000 scale hillshade maps. Depths to bedrock were calculated using two-way travel times in milliseconds, measured from the averaged seafloor surface to the averaged bedrock surface and converted to depth in meters based on an assumed seismic velocity

of 1,600 m/s. Sediment thickness values were calculated on 500 m spacing along each seismic line, yielding a sediment depth grid size of 800 x 500 m. Sediment depths were plotted on paper maps with 5 m bathymetric contours and converted to top-of-bedrock elevations.

3. 5 m bedrock elevation contours were generated using the top-of-bedrock elevation grid where bedrock is buried beneath sediments on 1:15,000 scale maps. These structure contours were merged with the existing 5 m seafloor contours in regions where bedrock is exposed at the to create a seamless 5 m top-of-bedrock map.

Because of the wide spacing of depth measurements and survey lines, the top-of-bedrock map shows general topographic trends, but is not detailed enough to delineate subtle or small-scale topographic features.

4.3 TYPES OF UNCERTAINTIES

Several types of uncertainties are considered in both the mapping and analysis of paleostrandlines and associated wave-cut platforms. These include uncertainties related to the accuracy and precision of the data used to identify and map features; as well as less quantifiable uncertainties broadly defined herein as “geologic context” and “interpretation” uncertainties. Geologic context uncertainty is related to geologic processes other than tectonic deformation that can influence the development and geomorphic expression of paleostrandline features in a submerged environment. Interpretation uncertainty addresses whether or not the interpretation of features as indicators of paleostrandlines is correct. Table I-4-2 outlines various types of uncertainties identified during this investigation and the possible implications of these uncertainties in our assessment of the patterns and rates of late Quaternary deformation on the continental shelf, specifically with respect to the assessment of the Shoreline fault zone as a seismic source. Further discussion of the issues related to geologic context and interpretation is provided in Sections 6.0 (Results) and 7.0 (Discussion), as noted in Table I-4-2.

At four specific locations in the study area, wave-cut platforms mapped across fault traces are used to assess potential fault displacement. Potential sources of uncertainty and specific estimates of uncertainty in these measurements are provided in Section I-7.3. Because the measurement and geologic context uncertainties are not correlated and are approximately normally distributed, the combined uncertainty in characterization of potential fault displacement is calculated as the square root of the sum of the squares. For example, given a site with a measurement uncertainty of 0.5 m and a geologic context uncertainty of 1.5 m, the combined uncertainty is $(\sqrt{0.5^2+1.5^2}) = 1.6$ m.

In this appendix, uncertainties are rounded to the nearest 0.5 m.

5.0 WORLDWIDE SEA-LEVEL CURVES

This section provides a summary of current global sea-level data used to develop a paleosea-level curve that in turn is used to evaluate ages of emergent and submerged paleoshoreline features in the study area (Section 7.2).

Changes in relative sea level result from the interplay of several processes operating at different rates and over contrasting spatial and temporal scales. Relative sea level (RSL) is defined as the height of the ocean surface relative to the solid Earth (or ocean floor) (Milne and Shennan, 2007). Changes in RSL are driven, therefore, by processes that produce a height shift in either of these two bounding surfaces.

During the Quaternary Period, the dominant mechanism responsible for sea-level change has been the progressive buildup and decay of continental-scale ice sheets in response to Milankovitch cycles (e.g., Hays et al., 1976). In addition to these global eustatic changes in sea level related to changing ice volumes, more local factors related to tectonics and glacio- and hydroisostatic responses influence the RSL curve and resulting geologic record of geomorphic features at a specific site.

The timing and amplitude of these eustatic changes have tended to conform to a consistent pattern, as indirectly indicated by the marine oxygen-isotope record and corroborated by geomorphological and stratigraphic evidence from tectonically uplifted and more stable coastal areas (Murray-Wallace, 2007b). However, as noted below, there still remain significant uncertainties in deciphering a global sea-level curve that can be used for site-specific studies in regions where sequences of terraces or paleoshoreline features are not well dated.

Normalized oxygen isotope ratios in foraminifera preserved in deep ocean sediments are a proxy record for global ice volume and are used for developing continuous reconstructions sea level over late Quaternary time (Shackleton and Opdyke, 1973, 1976; Chappell and Shackleton, 1986; Labeyrie et al., 1987, 1976; Shackleton, 1987, 2000; Chappell et al., 1996). Figure I-5-1 presents two recent interpretations of Quaternary global sea-level history for the past 450 ka derived from such studies (Shackleton, 2000; Waelbroeck et al., 2002). Both of these curves are based on oxygen isotope ratios scaled to match magnitudes of sea-level fluctuations documented by fossil data. It is important to note that oxygen isotope curves may not correlate directly with paleosea levels because oxygen isotope ratios measured from deep sea cores are not only dependent on the ratio of the volume of water in the sea relative to the volume of water stored in glaciers on land, but also other factors, such as salinity, water temperature, and diagenesis (Olson and Hearty, 2009). Invariably, many assumptions are necessary to use oxygen isotopes as a direct proxy for sea level. Both of the curves in Figure I-5-1 represent significant improvements

over previously published curves used in PG&E (1988) because of increases in the resolution of the data, timing constraints, and treatment of extraneous effects that are not caused by relative water volume.

Local observations of RSL change around the world that have been developed from interpretation of geomorphic and stratigraphic relationships and dating of features formed at or near sea level provide constraints to test sea-level curves inferred from models based on marine oxygen isotope ratios as well as quantitative geophysical models for global meltwater discharge. Far-field locations, distant from late Quaternary ice sheets, most closely resemble global eustatic sea level, but still include local effects. Attempts to fit relative sea-level observations from far-field locations with numerical models of glacial isostatic adjustment (GIA) and models of global ice distributions reveal significant misfits (see references cited in Shennan, 2007, p. 2970). These differences arise from the number of unknown parameters, including Earth-model parameters, ice-model parameters, as well as uncertainties in RSL observations. The major differences in RSL changes that are predicted by the GIA models generally are summarized by different curves for six characteristic zones (e.g., Clark et al., 1978). The existence of the zones and the position of the boundaries between them, however, are a strong function of both the Earth and deglaciation models adopted (Shennan, 2007).

Peltier (2004) presents a refined model of the global process of GIA, denoted ICE-5G (VM2) model that incorporates data available from the Bonaparte Gulf and Sunda shelf and various other lines of evidence that point to a larger, multidomed Laurentide ice sheet. Lambeck et al. (2002) present an alternative GIA model that uses alternative earth and ice models, and different calculation methods, but is calibrated using much of the same data used by Peltier (2004). Peltier and Fairbanks (2006) note that the Waelbroeck et al. (2002) curve, which attempts to carefully account for variation of the temperature of the abyssal ocean that otherwise would contaminate the $\delta^{18}\text{O}$ proxy for variation of land ice and associated sea level over time, agrees in general with sea-level data from Barbados and the Sunda shelf over the last glacial-interglacial cycle from 120 ka to the present, particularly with regard to the rise in sea level from the Last Glacial Maximum (LGM; Figure I-5-2).

The main far-field records used to calibrate sea-level curves come from studies of uplifted and submerged terraces in Barbados (Bard et al., 1990; Peltier and Fairbanks, 2006); Tahiti (Bard et al., 1996); the Huon Peninsula on the island of New Guinea (Lambeck and Chappell, 2001; Cutler et al., 2003); Bonaparte Gulf (Yokoyama et al., 2000, 2001); and the Sunda shelf (Peltier and Fairbanks, 2006). The data from Barbados, Tahiti, and the Huon Peninsula require a correction for long-term tectonic movement, usually corrected assuming a uniform tectonic uplift rate. A summary of paleosea-level data from these studies and others is provided in Table 5-1.

This table illustrates the significant variation that exists in estimates of Quaternary global sea-level history.

Figure I-5-3 shows selected interpretations of sea level fluctuations for the past 140 ka based on interpretations of data from several localities as well as the prediction from Lambeck et al. (2002) and the ICE-5G (VM2) model (Potter et al., 2004; Cutler et al. 2003; Chappell, 2002; Ramsay and Cooper, 2002; Lambeck and Chappell, 2001; Lambeck et al., 2002; Hanson et al., 1994; and Peltier, 2004). With the exception of the ICE-5G (VM2) and Lambeck et al. (2002) model curves, each of these curves are primarily reconstructed from the precise ages and elevations of fossil corals collected from elevated or submerged coral terraces. These curves and data constraints are selected to be most appropriate for the Shoreline fault zone study area because they span the range of (1) being representative of global eustatic sea-level curves, to (2) being based on local data.

Observations and new information cited in the literature reviewed for this study that bear more directly on assessments of the ages and paleosea levels for uplifted and submerged terraces in the Shoreline fault zone study region are discussed below. A general observation noted by several researchers is that sea level during lowstands is relatively consistent globally, but during highstands has more deviation (Ramsay and Cooper, 2002).

5.1 POST-GLACIAL SEA-LEVEL CHANGES

The period from the peak of the LGM (ca. 22–20 ka) to the present, the Holocene Interglacial, represents the extreme end points of eustatic sea level in glacial cycles. Recent assessments give an uncertainty of eustatic sea level at the LGM to a range from approximately 114 to 135 m (Shennan, 2007). Murray-Wallace (2007b) summarizes literature that suggests that during this time interval, sea level rose worldwide from approximately 120 to 125 m below present levels and almost attained (or in some locations exceeded) present levels by about 7 ka (Figure I-5-2). The rate and general pattern of RSL change during this period was spatially variable and differed according to geographic regions in response to glacio-hydroisostatic adjustment processes, tectonism, and localized climatic changes (i.e., steric changes accompanying changes in localized sea-surface temperatures and salinity) (Murray-Wallace, 2007b).

One of the major issues regarding RSL since the LGM has been uncertainty in the general nature of the change: Was the pattern of sea-level rise a smooth function with time or characterized by a series of well-defined oscillations superimposed on a broader pattern of changes (Murray-Wallace, 2007b, p. 3035)? High-quality RSL data from the mid-latitudes reveal spatial and temporal variations among eustatic, isostatic (glacio- and hydro-), and local factors since the LGM. Errors that are commonly ignored in sea-level analyses include (1) the uncertainty in the

relationship between a given indicator and the local to regional paleoenvironment in which it was formed (known as the indicative meaning); (2) sediment compaction and tidal range variations; and (3) calibration of radiocarbon dates, and if appropriate the application of the marine reservoir effect (Horton, 2007).

Despite these uncertainties, the general pattern of eustatic (ice-equivalent) sea-level rise since the end of the LGM, based on the study of far-field settings is as follows:

1. A slow initial rise in sea level with the onset of deglaciation.
2. A phase of relatively rapid sea-level rise with the possibility of short-term meltwater pulses characterized by even more rapid sea-level rise.
3. The attainment of an early Holocene highstand.

Selected interpretations of post-LGM sea-level rise are illustrated on Figure I-5-2.

5.1.1 Onset of Deglaciation

Most authors agree that the early post-LGM transgression was characterized by a period of relatively slow sea-level rise that continued until about 15–17 ka, during which the global eustatic sea level rose to about 100 m below modern sea level. Average rates of sea-level rise for this period are estimated to range from about 6 mm/yr (Fleming et al., 1998) to 4 mm/yr (Fairbanks, 1989). Lambeck and Chappell (2001) and Lambeck et al. (2002) suggest that the onset of deglaciation may have been punctuated by a period of accelerated sea-level rise (meltwater pulse) at about 19 ka that accounted for about 15 m of global eustatic sea-level rise over the course of 500–1,000 years, although some authors dispute the evidence for this meltwater pulse (e.g., Peltier, 2004; Peltier and Fairbanks, 2006). This meltwater pulse (shown on Figure I-5-2 as MWP 1Ao) was then followed by a period of relatively slow global melting with sea level rising at a rate of about 3.3 mm/yr (Lambeck et al., 2002).

5.1.2 Rapid Sea-Level Rise

The onset of deglaciation was followed by a phase of relatively rapid sea-level rise that extended until approximately 7 ka during which time global eustatic sea level rose to within a few meters of modern sea level (Figure I-5-2). The mean rate of sea level rise during this period was close to 10 mm/yr (IPCC, 2001; Fleming et al., 1998). Significant departures from this average rate may have occurred at the time of the Younger Dryas cold period (between about 12.5 and 11.5 ka), and possibly during potential meltwater pulses that began circa 14 ka and 11 ka (Fleming et al., 1998; Lambeck et al., 2002).

Of these departures from a linear sea-level curve, the best supported by data and the most widely accepted appears to be a reduced rate of sea-level rise associated with the Younger Dryas cold period (Fairbanks, 1989; Fleming et al., 1998; Lambeck et al., 2002). Lambeck et al. (2002) recognize only the Younger Dryas event and do not recognize meltwater pulses between 16 and 8.5 ka. Instead, they adopt a simpler, three-phase model for this period: a rapid, sustained rise from about 16 ka to 12.5 ka with an average rate of 16.7 mm/yr, followed by a short-duration plateau extending from 12.5–11.5 ka (the Younger Dryas), and a rapid, uniform, post-Younger Dryas sea-level rise of about 15.2 mm/yr. Global data from Lambeck et al. (2002) suggest that global eustatic sea level was about 60–70 m below modern sea level during the Younger Dryas. Murray-Wallace (2007b) reports a mean rate of sea-level rise of about 5.6 mm/yr for the Younger Dryas based on data from Barbados, but suggests the period lasted about 2–3 kyr, ending about 11.3 ka.

In a detailed reconstruction of post-LGM sea level based on corals collected from a series of boreholes in Barbados, Fairbanks (1989) indicates that the Younger Dryas was immediately preceded by an exceedingly rapid sea-level rise of 24 m in less than 1,000 years, which he termed meltwater pulse 1A (MWP1A), and was immediately followed by a second rapid rise in sea level of about 28 m, which he termed meltwater pulse 1B (MWP 1B). Subsequent studies indicate that the magnitude of these meltwater pulses may have been lower, and even call into question the existence of MWP 1B (e.g., Shennan, 1999; Bard et al., 1996). Fleming et al. (1998) note that evidence from Barbados points to a rapid sea-level rise of about 12–13 m at about 14 ka, which may correspond with Meltwater Pulse 1A (MWP 1A) of Fairbanks (1989) and Bard et al. (1990). However, they caution that this interpretation is based on several assumptions that may not be valid, and suggest that an alternative explanation may lie in different growth depths for the corals sampled (corals before and after this time frame come from different colonies), rates of tectonic subsidence or uplift not being constant, or lateral variation in mantle parameters that lie outside the limits imposed in the isostatic correction calculation. They indicate that this interpretation is based on few records from only one location, and that additional records from other localities would be desirable. Lambeck et al. (2002) describe a gap in their data set at about 14 ka that could be construed as corresponding to a short-duration, very rapid sea-level rise (i.e., MWP 1A), but describe evidence for a steady rate of sea-level rise following the Younger Dryas, suggesting an absence of MWP 1B.

Gornitz (2007) describes a fourth interval of rapid sea level rise 8.2–7.6 ka (shown on Figure I-5-2 as MWP 1C) inferred by a hiatus in coral growth in the Caribbean. Although less firmly established than the meltwater pulses described above, this interval is supported by stratigraphic

evidence from Chesapeake Bay, the Mississippi River delta, the Yellow River in China, coastal Lancashire in England, and Limfjord in northwestern Denmark (Gornitz, 2007).

5.1.3 Holocene Highstand

By about 7 ka ocean volumes approached their present-day level but did not attain it precisely until sometime later (Lambeck et al., 2002). Fleming et al. (1998) report that 3–5 m of water depth has been added to the oceans since that time. However, many far-field sites also record a fall in relative sea level following the attainment of the early Holocene highstand due to hydroisostatic adjustments, the amplitude of which is in part a function of the width of continental shelves. Hydroisostasy involves the subsidence of continental shelves due to the geologically “instantaneous” loading effects of water that has returned to the continental shelves from the decay of ice sheets. This is accompanied by the landward migration of viscous mantle material and results in the formation of emergent shoreline deposits but without a reduction in the water volume of the ocean basins.

Early to middle Holocene highstand features have not been reported for the central California coastline.

5.2 MIS 2 (LAST GLACIAL MAXIMUM)

The position of sea level during the LGM is relatively well defined from several independent lines of evidence, including direct stratigraphic evidence from sediment cores from continental shelves, inferences drawn from modeling the areal extent and thickness of ice sheets at the time of maximum ice-sheet development, and inferred ice volumes derived from oxygen isotopes in foraminifera from deep-sea cores. Recent estimates for full glacial sea-level lowering are less than originally predicted on the basis of model calculations of ocean-volume accommodation space and estimates of water locked up in continental ice, which had placed LGM ice-equivalent sea level at approximately –154 m (Williams et al., 1998) or the CLIMAP (1981) reconstructions of a “minimum model” with 127 m of eustatic change and a “maximum model” with 163 m of eustatic change.

Areas regarded as tectonically stable have been favored in studies attempting to define the position of sea level during glacial maxima, particularly for regions far from former ice sheets (far-field regions) such as Australia. In such regions, the effects of the glacio-isostatic adjustment process are minimized and the relative sea-level is overwhelmingly eustatic in nature (ice-equivalent sea level) (Murray-Wallace, 2007a). Studies of sedimentary successions on continental shelves and shallow marine platforms such as southeastern Australia (New South Wales), northwestern Australia (Bonaparte Gulf), South Africa, and Barbados have indicated a maximum sea-level lowering of between <130 and 121 m during the LGM 20–22 ka (Bard et al.,

1990; Ferland et al., 1995, Yokoyama et al., 2001; Ramsay and Cooper, 2002). Results from Bonaparte Gulf in northwestern Australia indicate a eustatic sea level of 125 ± 4 m below present (Murray-Wallace, 2007b). Yokoyama et al. (2001) proposed that a maximum sea-level lowering occurred before 22 ka and ended abruptly at about 19 ka. Although these findings are consistent with other independent observations such as modeling global ice-equivalent sea level between 135 and 120 m below present sea level during the LGM (Clark and Mix, 2002), Shennan and Milne (2003) suggest that the sea-level reconstruction presented by Yokoyama et al., (2001, 2002) is not consistent with the evidence in all of the cores and that this model needs to be reassessed. They question the inference of a 19 ka meltwater pulse. Peltier and Fairbanks (2006) also cite errors with the Lambeck and Chappell (2001) curve with respect to the depth of the LGM lowstand that was based on incorrect information in Yokoyama et al. (2001).

5.3 MIS 3-4

Eustatic sea levels of MIS 3 have been subject to several interpretations. A recent compilation of data constraining sea-levels for this interval included in Wright et al. (2009) indicates that there is considerable range in the estimates for the relative sea level during the multiple highstands and lowstands of MIS 3 and 4. This compilation includes estimates of sea-level highstands as high as -25 m and lowstands as low as -90 m, although no single data set includes the total magnitude of fluctuations implied by this range. As illustrated on Figure I-5-3, the best-constrained data from New Guinea suggest that eustatic sea level during MIS 3 was in the range from about -90 m to -45 m. The ICE-5G (VM2) model predicts lower sea level during this time, and stratigraphic evidence from the Atlantic coastal margin of New Jersey shows evidence for sea level at higher elevations (Wright et al., 2009). This apparent discrepancy may result from isostatic adjustment of the Atlantic coastal margin of New Jersey during MIS 3. Wright et al. (2009) made no adjustment for forebulge collapse in their analysis. Ramsay and Cooper (2002) cite evidence for sea levels between -40 and -60 m between 55 and 40 ka that are also consistent with development of a major shoreline sequence that is preserved on the continental shelf. Uranium-series dating of the shoreline suggests that these younger sea-level highstands reoccupied an older shoreline initially formed during MIS 5d.

5.4 MIS 5

Uranium-series ages for corals from emergent marine terraces obtained subsequent to the LTSP data compilation, provide additional information regarding the precise timing, duration, and paleoclimatic conditions during the last interglacial (MIS 5) in the study region. The results of these studies are summarized in a series of papers by Muhs et al. (2002a, 2002b, 2004, 2006). In the Monterey–Santa Cruz region north of the study region, where the lowest platform (the Davenport terrace) in a sequence of terraces had been previously assigned ages ranging from

approximately 65 ka (MIS 3) to approximately 140 ka (MIS6/5e) (Muhs et al., 2006), new uranium-series coral ages for the Davenport terrace at Point Año Nuevo and Point Santa Cruz indicate that the Davenport platform dates to the MIS 5a (approximately 80 ka) highstand of the sea. The multiple coral ages from the Point Año Nuevo area also demonstrate with a high degree of confidence that this sea-level highstand had a duration from approximately 84 ka to at least 77 ka, similar to that recorded in Bermuda (Muhs et al., 2006).

At Cayucos, just north of Morro Bay, a geomorphically well-expressed low terrace has a shoreline angle elevation of approximately 7-8 m, and platform exposures in the modern sea cliff as high as 5 m. Previous uranium-series analyses of corals from this terrace showed that all samples have been affected by open-system conditions, and more recent analyses by Muhs et al. (2002b) yielded similar results with ages generally in the range from 125 to 116 ka (MIS 5e). Some samples in both an earlier study (Stein et al., 1991) and the Muhs et al. (2002b) study gave apparent ages of approximately 101 ka (one sample) and 109 ka (two samples), respectively. Using an approach that corrects the age bias of samples based on a model of continuous, secondary U and Th uptake, Muhs et al. (2002b) show that despite the open-system conditions, two age groups of corals are present, probably representing the MIS 5c (approximately 105) and MIS 5e (approximately 120 ka) sea-level highstands.

Whereas most eustatic sea-level curves place the MIS 5a sea-level elevation well below present (-20 m or deeper), many records from sites in the United States show it at or above present. Uranium-series coral ages from the U.S. Atlantic Coastal Plain (Wehmiller et al., 2004), and several localities along the Pacific Coast from Oregon to Baja California (Hanson et al., 1994; Hanson and Lettis, 2000; Muhs et al., 2004) suggest sea level near (within 6 m) or above present levels at the end of MIS 5, contradicting age-elevation relations based on marine isotopic or coral reef models of ice equivalent sea level. Emergent approximately 80 ka deposits are also observed in Bermuda, at elevations virtually identical to those for approximately 125 ka deposits (Muhs et al., 2002a). Wehmiller et al. (2004) speculate that the apparent occurrence of early and late stage 5 units and/or landforms at nearly identical emergent elevations, with coral ages from MIS 5a being far more abundant than those from substage 5e, requires some mechanism (such as hydroisostatic subsidence) by which the approximately 45 kyr of flooding of the continental margin during MIS 5, coupled with forebulge collapse following MIS 6 glaciation, generated this record of coastal evolution. It is not known whether this is a viable explanation for the Pacific Coast.

Muhs et al. (2002a, 2002b) also note that uranium-series ages of last interglacial corals from the Pacific Coast overlap with, but are on average younger than, corals from Barbados, the Bahamas, and Hawaii. This age difference is explained by the nature of the geomorphic response to sea

level change. Fringing or barrier reefs on low-latitude coastlines have “keep up” corals with accretionary growth that can keep pace with rising sea level, whether on a tectonically rising or stable coastline. In contrast, mid-latitude, high-energy coastlines undergo platform cutting during the early part of a sea-level highstand. Sediment and fossil deposition in this type setting take place as sea level starts to recede. Muhs et al. (2002a, 2002b) note also that the youngest ages of corals from Pacific Coast sites (San Clemente Island and Punta Banda) overlap with intermediate-aged and younger corals in Hawaii and the Bahamas and suggest that sea level was still relatively high at approximately 116 ka. This finding conflicts with estimates of a relatively large global ice volume during MIS 5d, a time of low summer insolation at high latitudes in the Northern Hemisphere.

6.0 DATA ANALYSIS AND RESULTS

Quantitative analysis and resulting evaluations of paleoshorelines and platform development in both offshore and onshore environments of the Shoreline fault zone study area are discussed in the following sections. These evaluations provide information to constrain patterns and locations of the uplift in the study area as well as amounts of possible vertical deformation associated with mapped traces of the Shoreline fault zone and N40W fault.

6.1 HOLOCENE PLATFORM DEVELOPMENT

A detailed, rigorous, and quantitative analysis of modern shoreline angles and their associated wave-cut platforms is critical in understanding processes and rates of offshore platform development. The results of this analysis provide constraints on the duration of time needed to form broad wave-cut platforms in the study area and this in turn is used to evaluate the ages of mapped platforms (see Section 7.2).

The process of sea-cliff retreat and platform development results from a combination of the delivery of wave energy and the erosion resistance of the rock and sediment receiving that energy. The amount of wave energy delivered to the shoreline is a function of many factors including initial wave energy, orientation of the shoreline with respect to principle wave direction (obliquity to oncoming waves), and geometry of the sea floor. Factors affecting bedrock and sediment erosion include hardness, abrasion resistance, jointing/fracturing/bedding plane weaknesses impacting the efficacy of plucking and removal, resistance to mechanical weathering, and type and amount of sediment cover. These factors as well as the overall period of time during which a bedrock substrate is exposed to wave erosion influence the resulting geomorphology of a platform and its associated shoreline angle. For this analysis, it is assumed that Holocene wave-cut platform development was initiated approximately 7 ka when sea level rose approximately to the present level (Section 5.1.3, Figure I-5-2).

For this study, 21 sections of the Holocene wave-cut platform were mapped between Islay Creek and Point San Luis using the methods outlined in Section 4.2.2. A total of 56 measurements of platform width and slope in eight mapped bedrock formations were obtained for these platform sections. In general, the age of bedrock increases from northwest to southeast; i.e., from the Miocene Miguelito Member of the Pismo Formation at the mouth of Islay Creek to the Cretaceous-Jurassic ophiolite and associated rocks of the Franciscan Complex at Point San Luis (Appendix B).

Table 6.1 summarizes the Holocene platform widths, depths of outer edges, slopes, and sea-cliff retreat rates. Each of these parameters is presented as an average value for all measurements in each rock type, and also as an average of all measurements. Rates of Holocene sea-cliff retreat (and also platform development) are estimated by dividing the mapped platform width by the estimated time of exposure to marine erosion (7 kyr). The highest average retreat rate is observed in Miguelito mudstone at 95 m/kyr. The lowest retreat rate is observed in the lithologically resistant ophiolite at 30 m/kyr.

This analysis includes only those platforms wide enough and deep enough to be imaged in the multibeam bathymetry survey. In localities where no suitable candidate for a modern wave-cut platform was identified in the bathymetric data, the platform is interpreted to be too narrow or too shallow to extend offshore across the gap between data sets into the region covered by the multibeam survey. These localities are not included in our analysis or the average parameter values presented in Table 6-1. The addition of narrower platforms to the data set would lower the estimates of Holocene retreat rates as these rates are a direct function of platform width. However, given the high level of completeness of the Holocene platforms identified in the bathymetric data (Plates I-1a to I-1d), the calculated retreat rates do not significantly overestimate actual Holocene retreat rates. It is possible that the data set of mapped Holocene platforms includes only fractions of the Holocene platform, and that the geomorphic features that have been mapped are actually parts of the bathymetric signatures of potentially wider wave-cut platforms. Additional uncertainties in the analysis include the onset age, duration, and elevation of a postulated middle Holocene sea-level highstand (Section 5.1.3), and potential Holocene reoccupation of a late Pleistocene platform. A discussion of possible effects of these uncertainties is provided in Section 7.0.

Analysis of Holocene platform morphology yields several noteworthy observations. First, on the Islay shelf both the morphology and outer edge depth of Holocene wave-cut platforms between Islay Creek and approximately 1.5 km south of the mouth of Diablo Canyon vary significantly from those platforms on the Santa Rosa Reef and San Luis Bay shelves to the south. The outer edges of Holocene platforms on the Islay shelf commonly occur at elevations of between -10

and -12 m and have outer edges that commonly are subtle and difficult to differentiate from the general slope of the inner continental shelf. In contrast, Holocene platforms on the two southern shelves have outer-edge elevations generally between -6 and -8 m and their outer edges are more easily distinguished from the surrounding inner continental shelf. The morphologic boundary is roughly coincident with the contact between Mesozoic and Cenozoic bedrock (Appendix B).

Second, Holocene platforms show a general decrease in width from north to south, with the exception of platforms in the Obispo Formation. The widest platforms are formed in Miguelito Member mudstone, which is the lithologically least resistant bedrock unit along this section of coast. However, where the Holocene platforms are carved into the Miguelito Member, the shoreline also is roughly orthogonal to the predominant direction of incoming waves arriving from the northwest (Lettis and Hanson, 1992). Platforms in the Miguelito Member average approximately 670 m in width, nearly 200 m wider than the next widest set of platforms that are in the Obispo Formation. Holocene platforms in rocks of the Franciscan Complex and ophiolite at Point San Luis average approximately 210 m in width (Table 6-1). The location of the widest Holocene platforms roughly coincides with the stretch of coastline where the widest remnants of the MIS 5e terrace are mapped onshore. Although significant uncertainty exists as to the original width of the MIS 5e platform, the coincidence in locations of wide and narrow platforms associated with the MIS 5e and Holocene highstands suggests that similar conditions favorable to platform development existed during the MIS 5e and Holocene highstand.

Third, Holocene platform slopes are consistently greater than those calculated for offshore platforms (Figure I-6-1) of similar width identified in this study and commonly are near the upper values of slopes for inshore segments reported by Bradley and Griggs (1976). Given current limitations in the data available to profile complete Holocene platforms, it is not possible at this time to distinguish between inshore and offshore platform segments; therefore composite slope values are reported here.

6.2 SUMMARY OF SUBMERGED WAVE-CUT PLATFORM MORPHOLOGY

A total of 141 wave-cut platforms associated with paleoshorelines have been mapped in the study area (Plates I-1a to I-1d). Of those, 111 platforms have slopes that fall in the 0.5–4 percent slope range for wave-cut platforms as described by Bradley and Griggs (1976) (Figure I-6-1), 18 have slopes of 0.1–0.4 percent, 7 display slopes greater than 4 percent, and 5 platforms show highly variable slopes where no representative value could be determined. These last five platforms are either very irregular, narrow, or partly buried, and therefore represent the weakest geomorphic expression of all the mapped platforms. Examples of platforms associated with strandlines are

shown in Figures I-4-2a to I-4-2d. Due to the variable nature of slopes and the commonly dissected nature of platforms, slopes values are given as composites of the entire platform, as opposed to defining separate slopes for inshore and offshore segments in the convention of Bradley and Griggs (1976). Platform widths range from 13 to 1,150 m. Platform slopes follow a general asymptotic trend where slopes show a rapid decrease with increasing width between 13 and 100 m, shallowing to near zero for the widest platform at 1150 m (Figure I-6-1). As noted in Section 6.1, Holocene platforms show a similar asymptotic trend in the width/slope curve but display significantly higher slope values.

In addition to platforms that exhibit a conventional morphology (i.e., a well-defined outer edge and shoreline angle), broad platforms, greater than 850 m wide, have been identified (Figure I-6-2). These broad platforms are likely the result of erosion during multiple highstand/lowstand occupations and intervening erosion events during transgressions and regressions. Broad platforms are generally less planar than their narrower counterparts and in many cases encompass smaller mapped platforms (i.e., there is evidence for reoccupation of a preexisting platform). Bedrock benches hundreds of meters wide separated vertically by a few to several meters commonly are observed within a single broad platform. Five broad platforms on the Santa Rosa Reef shelf and one platform on the San Luis Bay shelf have been mapped. No broad platforms are observed on the Islay shelf.

Examination of the top-of-bedrock contour map suggests that additional broad platforms that are buried by sediment may exist south and south-southwest of Point San Luis at approximate elevations of -50 to 60 m and -75 to 85 m, respectively. Southwest of Islay Creek, there are potentially two more buried broad platforms at depths of 65-70 m and 80-85 m, although their existence is less certain as they are constrained by only one seismic reflection profile apiece, as opposed to multiple reflection profiles for the possible broad platforms south of Point San Luis.

6.3 CORRELATION OF SUBMERGED STRANGLINES

Correlation of individual submerged strandlines is complicated by the lack of continuity of many of the paleoshoreline features. The lack of continuity is likely due to fluvial incision and erosion during sea-level lowstands, erosion, and marine planation during younger sea-level highstands, burial of the features by younger sediment, and possible faulting or tectonic deformation.

Individual strandlines have been correlated based primarily on (1) their interpreted elevations, (2) spatial relationships with respect to adjacent strandlines, (3) similarities in widths of associated wave-cut platforms, (4) the ranking criteria outlined in Section I-4.2, and (5) the relationship of individual strandlines to bedrock structure and bedding. The preferred

interpretations correlate well-developed and widespread shoreline features at similar elevations, many strandlines of which clearly crosscut strata and structural features.

Regionally, the best expressed and most continuous strandlines occur at elevations between -18 and -50 m; additionally, more discontinuous strandline sets are mapped intermittently at elevations between -50 and -70 m (Plate I-3a). A number of buried shoreline angles also have been interpreted from seismic-reflection profiles and scattered bedrock outcrops at elevations between -50 and -90 m.

A longitudinal profile showing the relative extent and elevation of mapped submerged strandlines in the offshore area between Islay Creek (Islay shelf) and Point San Luis (Santa Rosa Reef shelf) is provided on Plate I-3a. There is both an apparent difference in the spacing and number of strandlines recorded on the two shelves and a marked geomorphic contrast between the two shelf segments. These differences suggest that the two shelves are being uplifted at differing rates (see discussion in Sections 6.3.1 and 7.1). Alternative interpretations of the continuity and correlation of specific strandlines are possible given uncertainties in the identification and mapping of the less distinct features (i.e., the possibility that some subtle strandlines might actually represent the change in slope between the outer and inner parts of the same platform, or instead may be related to differential erosion of bedrock). Similarly, there may be some localized variations in the present elevation of the paleoshorelines related to hydroisostatic adjustments, which are not considered in the analysis. Despite these uncertainties, the preferred interpretation is that the relatively uniform elevation of the strandlines as correlated on each shelf is indicative of relatively uniform uplift, and there is likely a structural boundary between the two uplifting domains that is accommodating the change in uplift.

Alternative interpretations of correlations and ages of paleoshorelines based on the mapped strandlines and associated platforms are shown on Plates I-3b, I-3c, and I-3d. The interpretations shown on Plates I-3b and I-3c and discussed in Section I-6.3.1 are both based on the assumption that the Islay and Santa Rosa Reef shelves have experienced different rates of uplift during the late Quaternary. The primary difference between the two interpretations regards the location and nature of the uplift boundary between the two zones. The third alternative, shown on Plate I-3d and discussed in Section I-6.3.2, assumes that most of the features mapped as strandlines were formed or significantly modified during the post-LGM transgression from a sea-level lowstand of about -120 to -125 m at about 20-22 ka to the present level, and that given their young age, they do not record significant vertical deformation. This third alternative interpretation, as discussed below, does not provide a reasonable fit to much of the data and therefore is not considered to be a viable interpretation.

6.3.1 Correlation Alternatives 1 and 2

A sequence of seven paleoshorelines (each composed of multiple individual strandlines) on the Islay shelf (defined in Section 2.2) have shoreline angles at elevations of -18 ± 1 m, -22 ± 1 m, -27 ± 1 m, -38 ± 1 m, -43 ± 2 m, -47 ± 1 m, and -61 ± 1 m (Plate I-3b). All the paleoshorelines are traceable to the southern margin of the Islay shelf, where bedrock becomes buried by marine sediment. Of these, the most well-developed paleoshorelines (i.e., those that include more continuous strandlines, strandlines with higher confidence assessments and/or wider platforms, and a greater number of strandlines that crosscut bedrock structure or bedding) include the paleoshorelines at elevations -22 ± 1 m, -27 ± 1 m, -38 ± 1 m, and -61 ± 1 m.

Elevations of the correlated shoreline angles are generally constrained to within ± 1 m (range of uncertainty given the assumption that the correlated strandlines all formed at the same paleosea level), and vary minimally within the majority of the Islay shelf. That is, strandlines are roughly horizontal and show no apparent tilting or internal deformation. Near the southern margin of the shelf the two shallowest paleoshorelines (elevations of -18 ± 1 m and -22 ± 1 m) are correlated with strandlines about 2 m lower than they are in the center of the shelf (about -20 ± 1 and -24 ± 1 , respectively). The paleoshoreline at -27 ± 1 m could also be interpreted to descend slightly near the southern margin of the Islay shelf, although this correlation is not well constrained, and therefore, is not shown. The elevation uncertainties in these strandlines overlap within the elevation uncertainties of the strandlines in the center of the Islay shelf, suggesting that deformation at the southern margin is not required. However, considering the consistent drop in elevation between the two (or three) paleoshorelines involved, and the relative continuity of strandlines involved, this pattern is interpreted as a slight downward warp of about 2 m at the southern margin of the Islay shelf adjacent to the boundary between the two shelves.

Eleven individual paleoshorelines (composed of multiple strandlines) across the Santa Rosa Reef shelf have shoreline angles at elevations of -16 ± 1 m, -20.5 ± 2 m, -24 ± 1 m, -29 ± 2 m, -34 ± 1 m, -40 ± 1.5 m, -45 ± 1 m, -49.5 ± 1 m, -58 ± 1 m, -62 ± 2 m, and -67 ± 1 m. Of these, the best-developed paleoshorelines include the paleoshorelines at elevations -29 ± 2 m, -40 ± 1.5 m, -45 ± 1 m, and -67 ± 1 m. In general, the distribution of paleoshorelines across the Santa Rosa Reef shelf shows that strandlines are somewhat less continuous and some have slightly greater variability than those of the Islay Creek shelf. Despite the greater vertical variability, approximately horizontal paleoshorelines are correlated across the Santa Rosa Reef shelf with little to no consistent change in elevations (tilting or warping) observed. One exception may be the strandline at -29 ± 2 m, where an alternative interpretation suggests an approximate 2 m drop from -29 m to -31 m between 2.6 and 0.4 km from its intersection with the southern segment of the Shoreline fault zone (Plates I-3b and I-3c, respectively). However,

an additional well-correlated strandline mapped at -34 m directly downslope from that strandline shows no evidence of this postulated deformation. It is therefore probable that the -31 m strandline that crosses the southern segment of the Shoreline fault zone is a separate strandline from the -29 m strandline that is mapped to the northwest.

Direct correlation of strandlines between the Islay and the Santa Rosa Reef shelves is difficult because few of the correlated strandlines maintain a consistent elevation across the boundary between the two shelves and each shelf has a distinct suite of submerged paleoshorelines. The locations of the boundary between the two shelves inferred by correlation alternatives 1 and 2 are discussed in Section 7.1.

6.3.2 Correlation Alternative 3

The submerged strandline correlations shown on Plate I-3d are based on the assumption that most of the features mapped as strandlines were formed or significantly modified during the post-LGM transgression from a sea-level lowstand of about -120 m at about 20-22 ka to the present level, and that, given their young age, they do not record significant vertical deformation. A corollary assumption is that there needs to be an uplift boundary in the offshore (see discussion in Section 7.1) and that if the strandlines and associated wave-cut platforms were older they would record this differential uplift. The primary guide, therefore, for strandline correlations in alternative 3 is elevation. Less weight is given to platform width, strandline confidence assessment, and relationship of strandlines to bedrock structure or bedding attitudes.

Twelve individual paleoshorelines (composed of multiple strandlines) across the Islay shelf have strandline elevations between -18 and -70 m. Some of these correlations are identical to the Islay shelf correlations described in alternatives 1 and 2, and these are better defined than the remainder. There are 15 individual paleoshorelines across the Santa Rosa Reef shelf between elevations -10 and -70 m. Similar to the Islay shelf, the strength of these correlations varies widely, and the stronger correlations are the same as those listed above in alternatives 1 and 2.

Direct correlation of strandlines between the Islay and Santa Rosa Reef shelves is difficult because each shelf has a distinct suite of submerged paleoshorelines. As shown on Plate I-3d, direct correlation of paleoshorelines between the two shelf segments with little change in elevation results in several weak or inconsistent correlations. For example, correlation of a paleoshoreline at -22 ± 1 m that is widespread and well defined on the Islay shelf is correlated to a very weakly developed one on the Santa Rosa Reef shelf. Similarly, the paleoshoreline at -45 ± 1 m elevation is widespread and well developed on the Santa Rosa Reef shelf, but is only intermittently preserved, and generally associated with low-confidence-level strandlines on the Islay shelf. The well-developed paleoshoreline at -40 ± 1 m elevation on the Santa Rosa Reef

shelf has no match on the Islay shelf without some amount of vertical separation. Because the geomorphic expression of the paleoshorelines (i.e., the width of the wave-cut platform and relative continuity of strandlines that are preserved across distinct rock types) are indirect indicators of characteristics of paleosea-level stillstands (most significantly, duration) well-developed paleoshorelines should correlate with each other across the two shelves. Therefore, direct correlation of paleoshorelines between the Islay and Santa Rosa Reef shelves with no vertical separation is not considered to be a viable interpretation because it would require the matching of strongly developed and well-expressed paleoshorelines with very weakly developed paleoshorelines.

A potential correlation between the two shelves is possible with as little as 2 m of down-to-the-south vertical separation. Such a correlation would match paleoshorelines on the Islay shelf at elevations of -18 ± 1 m, -22 ± 1 m, -27 ± 1 m, -38 ± 1 m, -43 ± 1 m, -47 ± 1 m, and -61 ± 1 m with paleoshorelines on the Santa Rosa Reef shelf at elevations of -20.5 ± 2 m, -24 ± 1 m, -29 ± 2 m, -40 ± 1.5 m, -45 ± 1 m, -49.5 ± 1 m, and -62 ± 2 m, respectively. While this potential correlation clearly has more merit than a correlation with no vertical separation, it is still not preferred because it matches well-developed paleoshorelines on one shelf with less well-developed paleoshorelines on the adjacent shelf. For example, one of the best-expressed paleoshorelines in the Santa Rosa Reef shelf occurs at a depth of -45 ± 1 . Correlating this well-expressed paleoshoreline with the relatively discontinuous shoreline with variable elevation centered around -43 ± 2 m is judged unlikely. Likewise, correlating the well-expressed shoreline at -22 ± 1 m elevation on the Islay shelf with the discontinuous and poorly developed shoreline at -24 ± 1 m on the Santa Rosa Reef shelf also is unlikely.

7.0 DISCUSSION

The following sections discuss the significance of paleoshoreline mapping and analysis. Section 7.1 describes the patterns of uplift inferred for the coastline and continental shelf offshore of the Irish Hills. Section 7.2 discusses the probable ages of submerged shorelines and associated uplift rates. Section 7.3 discusses the late Quaternary displacement on the Shoreline fault zone.

7.1 PATTERNS OF UPLIFT

As described in Section 2.2, the continental shelf in the study area offshore of the Irish Hills is divided into three separate shelf areas based on the seafloor morphology and correlation to onshore tectonic blocks. From northwest to southeast, these are the Islay, Santa Rosa Reef, and San Luis Bay shelves. The following discussion focuses on the two western shelves, Islay and Santa Rosa Reef, where most of the submerged strandlines are preserved. The geomorphology of these shelves is described in more detail in Appendix B.

7.1.1 Islay Shelf

Shelf geomorphology and correlation of paleoshorelines suggest that the Islay shelf is part of the Irish Hills tectonic subblock. The Islay shelf is narrower and steeper than the two southern segments. Up to seven correlated paleoshorelines are identified along this shelf segment. These paleoshorelines roughly parallel the coast, trending northwest in the southern part of the Islay shelf, wrapping around Point Buchon, and extending northeast toward Estero Bay (Figure I-1-2). As described in Section 6.3.1, strandlines maintain a relatively consistent elevation across each shelf, suggesting an absence of tectonic tilting or regional-scale folding. The consistent elevations suggest that the shelf is undergoing relatively uniform block uplift mimicking the emergent marine terraces preserved directly onshore of the Islay shelf (Lettis et al., 1994; Hanson et al., 1994). Well-constrained ages for the lower emergent terraces, which correlate to MIS 5e and 5a, indicate an uplift rate of 0.2 ± 0.03 mm/yr for the coastal region between Point Buchon and the DCP (Hanson et al., 1994). No faults are mapped between the emergent terraces and Islay shelf (Appendix B). The coincidence of flights of paleoshorelines both onshore and offshore that maintain consistent elevation and depth spacing as they change directions at Point Buchon and the lack of a throughgoing fault at the coast strongly indicates that they are developed in the same tectonic block. Therefore, the uplift rate of 0.2 ± 0.03 mm/yr is used for the Islay shelf.

7.1.2 Santa Rosa Reef Shelf

Similar to the Islay shelf, the geomorphology of the Santa Rosa Reef shelf and correlation of paleoshorelines on the shelf indicate that it also is undergoing block uplift, but at a lower rate than the Islay shelf. The Santa Rosa Reef shelf is notably broader and slopes more gently than the Islay shelf. Up to 11 correlated paleoshorelines are mapped along this shelf segment. Also similar to the Islay shelf, the strandlines maintain a relatively consistent elevation across the shelf, indicating that the shelf is undergoing relatively uniform block uplift. Wave-cut platforms on the Santa Rosa Reef shelf are generally broader than those on the Islay shelf. For example, five broad wave-cut platforms, wider than 850 m, are observed within this shelf segment, whereas none this wide are observed on the Islay shelf (Figure I-6-2). This broad, gently sloping morphology and the presence of very broad platforms suggest that the Santa Rosa Reef shelf has experienced more episodes of marine erosion than the Islay shelf. This difference could be explained as the result of a lower uplift rate that would expose the Santa Rosa Reef shelf to more sea-level highstands and lowstands than the Islay shelf over its late Quaternary history.

The following analysis is used to establish the uplift rate of the Santa Rosa Reef shelf. Most of the submerged strandlines observed in the Santa Rosa Reef shelf are located west of the Shoreline fault zone. However, a suite of five strandlines are evident in a section of rocky

seafloor south of Point San Luis on the east side of the southern Shoreline fault zone (Plates I-1c and I-2c; Figure I-6-6). These strandlines occur at elevations of -8 ± 0.5 m, -11 ± 0.5 m, -17 ± 1 m, -25 ± 1 m, and -31 ± 1 m. The strandline at elevation -25 ± 1 m correlates well with a strandline preserved at a similar elevation at several locations along the Santa Rosa Reef shelf (Plate I-3a). The strandline at -31 ± 1 m, although not widespread, is well preserved (confidence level A and B) and is evident on both sides of the fault as a nearly continuous feature for a distance of about 3 km south of Point San Luis (Figure I-6-6; Plate I-2c). The uplift of the onshore part of the tectonic subblock at San Luis Hill, which is calculated to be 0.06 ± 0.2 mm/yr, is well constrained by the elevation and age of the MIS 5e emergent marine terrace, which is continuous along the lower flank of San Luis Hill (Hanson et al., 1994). Therefore, the same uplift rate is appropriate to use for the Santa Rosa Reef shelf.

7.1.3 MIS 5a Wave-Cut Platform

Assuming that the Santa Rosa Reef shelf is being uplifted at a rate of 0.06 mm/yr, the possibility is investigated that a broad eroded platform that extends out to a depth of approximately -14 to -18 m (shown in light blue on Figure I-7-1a, and also on Plates 1b, 1c, and 1d) represents the MIS 5a wave-cut platform modified by erosion during the post-5a regression and most recently during the Holocene (Figures I-7-1a and I-7-1b). Based on relative terrace spacing and ages of the emergent marine terraces in the Irish Hills, the paleosea level for the approximately 80 ka (MIS 5a) highstand is estimated to be -4 ± 1 m (Hanson et al., 1994). At an uplift rate of 0.06 mm/yr, the MIS 5a shoreline would approximately coincide with the present shoreline. The general morphology of this broad platform, which is characterized by a flatter, more planar offshore segment (0.8 to 1 percent slope, 0.008 to 0.01 gradient) and a slightly concave inshore segment, is consistent with the platform morphologies reported by Bradley and Griggs (1976). As noted in Section 6.1, the innermost part of this platform is interpreted to be more heavily influenced by late Holocene erosion and ongoing wave erosion. This broad platform is mapped along the coast north from Point San Luis to near the mouths of Rattlesnake and Pecho Creeks. Remnants of older paleostrandlines and wave-cut platforms, such as the paleostrandline at -11 m elevation directly west of San Luis Hill, are entirely encompassed by this broad platform. These older paleoshoreline features apparently did not get completely removed during development of this wave-cut platform.

At the approximate location of the projected trend of the Rattlesnake trace of the San Luis Bay fault in the offshore, a similar broad platform, which can be mapped as far north as about Olson Hill, is identified at a higher elevation of approximately -10 ± 2 m (shown in dark blue on Figure I-7-1a). If both platforms are correlative, then the inferred vertical separation between the two platforms is on the order of 5–8 m. The apparent vertical separation boundary between the two

platforms, which appears to coincide with the projected trend of the San Luis Bay fault, continues to the west of the Shoreline fault zone (Figure I-7-1a). Assuming that the -10 ± 2 m platform is an eroded offshore remnant of the approximately 80 ka terrace, which is consistent with the overall morphology of the platform and onshore elevation of the Q1 (MIS 5a) terrace (7 ± 1 m shoreline angle), this platform would represent an offshore continuation of the approximately 0.12–0.14 mm/yr uplift zone recorded onshore between the Rattlesnake Trace of the San Luis Bay fault and Olson Hill.

A similar broad offshore platform is not present in the near offshore north of Olson Hill. To the north of Olson Hill the onshore remnant of the Q1 (MIS 5a) terrace is higher (11 ± 1 m shoreline angle) and does not project to any offshore platform. Erosion during the development of the Holocene platform appears to have completely eroded the offshore portions of the MIS 5a terrace north of Olson Hill. Sections of the Holocene wave-cut platform that are wide enough to extend offshore into the region covered by the MBES bathymetry north of Olson Hill are shown on Figure 7-1a.

7.1.4 Location of Uplift Boundary

In correlation alternative 1, the San Luis Bay fault is the uplift boundary between the Islay and Santa Rosa Reef shelves. In the offshore, this boundary is interpreted to be approximately coincident with a west-trending magnetic lineament (discussed in Appendices B and D) and a west-trending sediment-filled trough located west of Olson Hill (Plate I-2b). South of this general location, numerous discontinuous submerged strandlines and broad wave-cut platforms occur, characteristic of the Santa Rosa Reef shelf. North of this general location, a group of poorly expressed strandlines (chiefly confidence levels C and D) are preserved in a region of partially buried rocky seafloor. This group of poorly expressed strandlines does not correlate well with sequences on either the Islay or Santa Rosa Reef shelves.

This location of the uplift boundary is consistent with the interpretation of possible remnants of the MIS 5a platform in the offshore that appear to be displaced across an offshore extension of the Rattlesnake fault (Figure I-7-3). Near the shore, the southern margin of the uplift boundary is approximately coincident with the offshore extension of the Rattlesnake trace, and the northern margin of the boundary is approximately coincident with the Olson Deformation Zone. This boundary also coincides with a distinct change in slope of the inner continental shelf, from relatively gently sloped (to the south) to relatively steep (north of the boundary; Figure 7-1a).

Correlation alternative 2 (Plate I-3c) is much the same as alternative 1, except that the uplift boundary between the Islay and Santa Rosa Reef shelves is interpreted to underlie the sand sheets west of the DCP, slightly to the north of where it is interpreted in alternative 1. The

suites of paleoshorelines interpreted for the two shelf segments are identical to those described above in alternative 1.

The northern location of the uplift boundary in alternative 2 is based on the presence of a well-expressed submerged strandline at -20.5 ± 1 m directly south of the DCP (Plate I-2b). In alternative 1, this strandline, which is interpreted to be part of the Islay shelf, has been warped downward about 2 m. In alternative 2, this strandline is correlated directly with the -20.5 ± 2 m paleoshoreline on the Santa Rosa Reef shelf. Likewise, strandlines at elevations of -24 to -25 m south of the DCP are correlated directly with the 24 ± 1 paleoshoreline on the Santa Rosa Reef shelf in alternative 2, rather than inferred to be warped downward from the -22 ± 1 m paleoshoreline on the Islay shelf. Consequently, no warping of the Islay shelf is interpreted in alternative 2. The northern location of the uplift boundary coincides with a broad geomorphic boundary between the two shelves.

The position of the uplift boundary in alternative 2 indicates that the vertical separation across the San Luis Bay fault onshore (represented by a change in uplift rate between the Irish Hills and Point San Luis) does not extend directly offshore. Instead, it must extend northwestward from the vicinity of the Rattlesnake fault and Olson Hill at least as far as the submerged strandline at -20.5 ± 1 m directly south of the DCP. This correlation indicates that the boundary between the Irish Hills and the Santa Rosa Reef shelf is located in a narrow zone between the submerged strandline at -20.5 ± 1 m and the MIS 5a and 5e marine terraces preserved in the vicinity of the DCP. Given this constraint, a reasonable interpretation of the location of the uplift boundary is the Shoreline fault zone itself. Considering that the ages of these strandlines and marine terraces are interpreted to be MIS 5 or earlier (discussed in Section 7.2) and the vertical separation rate constrained by the emergent marine terraces (on the order of 0.14 mm/yr), the cumulative vertical separation across this narrow zone is anticipated to exceed 10 m. The bathymetric data in the vicinity of the DCP is sufficiently detailed and the coastline is sufficiently complex (with embayments, points, and seastacks), to rule out the potential presence of a 10 m scarp between the strandline at -20.5 ± 1 m and the MIS 5a and 5e marine terraces. Therefore, the uplift boundary shown in alternative 1 (Plate I-3b) is the more strongly supported alternative.

7.2 AGE ASSESSMENTS

Age estimates for submerged paleoshorelines in the Shoreline fault zone study area are based on correlation with current late Quaternary global eustatic sea-level curves because no direct age constraints are available. Uncertainty in uplift rates affecting the Islay and Santa Rosa Reef shelves, uncertainty in sea-level curves for marine oxygen isotope stages 3 and 4 (MIS 3 and 4), uncertainty in correlation caused by potential reoccupation of paleostrandlines, and potential

effects of hydroisostatic loading of the continental shelf (which is not addressed in this appendix) permit only tentative age estimates for individual paleoshorelines. Despite these uncertainties, paleosea-level curves are understood well enough that clear constraints on the ages of submerged paleoshorelines can be established. Based on the range of potential uplift rates affecting the Santa Rosa Reef and Islay shelves, and correlation with well-constrained paleosea-level curves from MIS 3 and 4, shallower submerged paleoshorelines, higher than about -30 m on the Islay shelf and about -35 m on the Santa Rosa Reef shelf, are concluded to have developed during MIS 5 or earlier (i.e., older than about 75 ka). Deeper paleoshorelines were likely most recently occupied during one of several highstands or lowstands between MIS 5 and the LGM (i.e., between 75 and 22 ka). Additionally, one paleoshoreline (preserved at an elevation of about -61 to -62 m on the two shelf segments) may have been developed during the Younger Dryas (about 12.5-11.5 ka).

7.2.1 Post-LGM Erosion

Wave erosion during the Holocene sea-level rise has modified the seafloor geomorphology in the study area. Evidence of this erosion abounds: differential erosion of rock has facilitated the interpretation of bedding and rock structure, and even lithology from the texture of rocky parts of the seafloor (Appendix B). The discontinuous and commonly subdued character of submerged strandlines also likely results, in part, from post-LGM erosion.

However, a fundamental question that relates to the assessment of ages of submerged shoreline features is whether erosion during the post-LGM transgression modified the landscape sufficiently to remove all traces of older wave-cut platforms and strandlines. A few lines of evidence suggest that it did not. Paleostream channels carved into bedrock of the continental shelf are preserved. This indicates that the post-LGM transgression did not strip all Pleistocene geomorphic signals. These channels (most clearly evident offshore of Islay and Coon Creeks on Plate I-1a, and offshore of Pecho and Rattlesnake Creeks on Plate I-1c) clearly were carved by subaerial streams that flowed across the inner continental shelf during Pleistocene sea-level lowstands. The shallowest parts are missing from the offshore channels associated with many creeks in the study area, such as Pecho and Rattlesnake Creeks (Figure I-4-6, parts a and b). The presence of a gap between the onshore and offshore parts of the creek channels suggests that more marine erosion has occurred near the coastline (i.e., between about 0 and -15 m elevation) than farther offshore. It is likely that this zone of increased erosion is a result of wave erosion during the Holocene highstand.

7.2.1.1 Potential Post-LGM Strandlines

If erosion during the post-LGM transgression was sufficient to remove the geomorphic signature of preexisting shorelines, then the strandlines and wave-cut platforms documented in this appendix would necessarily have been developed during the transgression. As described in Section 5.1, sea level rose quite rapidly during the post-LGM transgression, particularly in the depth interval where these strandlines and wave-cut platforms are preserved. Estimates of the rate of sea level rise for this part of the transgression range from 10 mm/yr (the average rate from 16 to 7 ka) to 24 mm/yr (during MWP 1A) (IPCC, 2001; Fleming et al., 1998; Fairbanks, 1989). The most significant reduction in the rate of sea-level rise during the post-LGM transgression occurred during the Younger Dryas cold period (Section 5.1). This event had a greater potential to have developed a shoreline than any other period between 16 ka (when sea level was at about -100 m) and 7 ka (when sea level reached about -10 m) (Figure I-5-2). Data from Lambeck et al. (2002) indicate that global eustatic sea level during the Younger Dryas was between about -60 and -70 m elevation.

Notably, strandlines and wave-cut platforms are preserved in the study area within that depth range, but they are significantly less well developed than the widespread strandlines and wave-cut platforms between -20 and -50 m elevations. That is, correlated strandlines between -60 and -70 m, which could potentially have been developed during the Younger Dryas, have wider gaps between them, are associated with narrower wave-cut platforms, and have slightly lower confidence levels than the shallower strandlines. This is particularly true on the Santa Rosa Reef shelf, where bedrock exposure commonly extends below this depth.

7.2.1.2 Duration of Relative Sea-Level Stability Required to Carve Wave-Cut Platforms

It is instructive to evaluate the duration of wave erosion required to develop wave-cut platforms of the dimensions observed in the study area. Based on the mapping of active (Holocene) wave-cut platforms, the mean widths of platforms and an estimated sea-level residence time of about 7,000 years for the Holocene sea-level highstand yields an average platform widening rate of about 50 mm/yr for the coastline between Estero Bay and Point San Luis (Section 6.1). This rate suggests that about 2,000 years of relative sea-level stability are required to develop a wave-cut platform 100 m in width. More than half of the submerged wave-cut platforms mapped for this project are wider than 100 m.

As described in Section 5.1, only the Holocene highstand and the Younger Dryas could have produced a stillstand of 2,000 years. Therefore, it is highly likely that submerged wave-cut platforms in the study area wider than 100 m were developed prior to the LGM.

Uncertainty in estimates of the duration of relative sea-level stability during the Holocene highstand affects the rates of wave-cut platform widening, but does not change the fundamental conclusion that the wider wave-cut platforms mapped in the study predate the LGM. If onset of the Holocene highstand occurred at 8 ka, calculated retreat rates decrease by 20 percent. If the Holocene highstand has reoccupied a platform developed during a significantly older highstand, lowstand, or stillstand, the platform widths reported here would be too high, and the corresponding retreat rates would be too high, resulting in a greater length of time required to develop a given wave-cut platform. As noted in Section 5.2, some far-field locations record evidence for sea levels higher than the present sea level during the middle Holocene (Murray-Wallace 2007b). No evidence for a middle-Holocene highstand has been described for the central California coast. However, if such a highstand did occur, it could be part of the cause of the steeper platform slopes measured from the Holocene wave-cut platform (Figure I-6-1). A potential middle-Holocene sea-level highstand is unlikely to have a significant effect on platform development rates because the highstand recorded in far-field sites is on the order of a few meters (Murray-Wallace, 2007b).

7.2.1.3 Estimates of Downcutting

The amount of bedrock lowering that occurred at a point on the seafloor during the post-LGM transgression may be estimated if both the the period of time that a point was subjected to significant wave erosion and the rate of downcutting are known. This estimate is important for evaluating uncertainty in the amount of offset (or lack thereof) of a wave-cut platform where it crosses a potentially active fault trace.

Rates of downcutting are estimated by examination of bathymetric profiles at two locations in the study area: offshore of Islay Creek and offshore of Olson Hill. At Islay Creek, an onshore-offshore longitudinal profile of the channel thalweg shows a smooth, concave-up profile for most of its length, typical of well-developed fluvial systems, suggesting that this channel gradient developed while the channel was exposed subaerially during Pleistocene sea-level lowstands (refer to discussion in Appendix B, and also Figure B-3-4). Offshore, approximately 7–8 m of marine sediment partly fill the channel, as indicated by interpretation of high-resolution seismic-reflection profiles. The profile from the deeper part of the offshore channel, below elevation of about –13 to –15 m, approximately aligns with the projection of the onshore part of the channel profile. In shallower water, however, the channel profile is markedly lower. Instead of sloping gradually upward as it does both onshore and farther offshore, the channel profile is nearly horizontal, remaining between about –10 and –15 m, elevation for about a kilometer. This departure from a smoothly sloping channel profile suggests that up to about 6 or 7 m of the seafloor has been removed since the channel was developed. The most likely cause of this

erosion is wave erosion during the Holocene highstand. Considering the duration of the Holocene highstand (about 7,000 years; e.g., Lambeck et al., 2002), the amount of missing section suggests that bedrock in this region was lowered by about 1 m per thousand years. Because this region is underlain by mudstone of the Miguelito Member of the Pismo Formation, one of the less resistant rock units in the study area, this estimate is probably higher than the mean rate of bedrock lowering by wave erosion in the study area.

A similar estimate of downcutting results from examination of bathymetry offshore of Olson Hill. A northeast-southwest trending profile of this site is shown on Profile C on Figure I-7-1b. On the southwest side of this profile, numerous accordant outcrop tops define a gently west-sloping surface, which is interpreted as a remnant of the wave-cut platform developed during the MIS 5a sea-level highstand (approximately 80 ka; Section 7.1). The relatively narrow and shallow crevices between these outcrop tops suggest that bedrock at that location is relatively resistant to erosion, and that erosion during the Holocene highstand was relatively limited. In contrast, the seafloor on the east side of the profile is significantly more eroded. Between profile station 950 and the modern shoreline, the seafloor is about 8 m below the projected surface of the MIS 5a wave-cut platform, suggesting that slightly over 1 m per thousand years of downcutting occurred at this site over the duration of the Holocene highstand. The difference in amount of rock downcutting evident on opposite sides of this profile illustrates the variability in resistance to erosion, amount of erosion, and rates of erosion in the study area.

The duration of time that a wave-cut platform may be subjected to significant erosion during the post-LGM transgression is the other key variable for estimating how much it may have been modified since it was carved. This duration is estimated by evaluating the depth to which significant bedrock erosion has occurred in the study area during the Holocene highstand, and comparison to the rate of sea level rise during the post-LGM transgression.

The bulk of marine erosion of bedrock that occurred within the study area during the post-LGM transgression is thought to have occurred either at the sea cliff or near the coastline in the zone of breaking waves during intense winter storms. The maximum depth of significant bedrock erosion by waves in the study area may be estimated by three independent measures:

1. The depth to which onshore-offshore channels are interrupted, which is best constrained at Islay Creek to be about -10 to -15 m (see discussion above, this section).
2. The depth of scour into the MIS 5a wave-cut platform south of Olson Hill, which is estimated to reach about -12 to -14 m elevation (see Profile C on Figure 7-1b and also discussion above, this section).

3. The offshore limit of the Holocene wave-cut platform (i.e., the deepest part of the platform) along the coastline. As described in Section 6.1, the mean depth of the outer edge of the platform varies by rock type and by position along the coastline, ranging from about 12 m in areas in the northwest where bedrock at the sea floor is the Miguelito Member of the Pismo Formation, to about 6 m in the south where bedrock at the seafloor is ophiolite, Cretaceous sandstone, and the Franciscan Complex. The mean depth of the outer edge of the Holocene platform developed from all measurements in the study area is 8.7 m.

This range of estimates compares favorably with the approximate depth of the transition between inshore and offshore segments of wave-cut platforms (about 13 m) documented by Bradley and Griggs (1976), and also water depths of 7–12 m estimated for breaking waves during intense winter storms in the Santa Cruz area reported by Bradley and Griggs (1976). The low end of this estimate corresponds with sets of deep-water wave heights of 4.5 m, expected to occur about five times per year, whereas the high end of this estimate corresponds with deep-water wave heights of 7.5 m, the greatest known in the Santa Cruz area.

Assuming significant bedrock erosion by wave energy is limited to water depths shallow enough to produce breaking waves, the length of time any particular part of the seafloor is exposed to wave erosion depends on the rate of sea level rise. Using conservative estimates for the rate of post-LGM sea level rise (about 10 mm/yr) and the depth of significant erosion by strong winter storm waves (about 10–15 m) any particular point on the seafloor would be expected to be subjected to wave erosion for about 1,000–1,500 years (with erosion becoming less frequent and less significant with depth).

Because the platforms used to constrain fault displacements are quite flat (slopes are on the order of 0.1–0.2 percent, gradients on the order of 0.001–0.002), it is unlikely that a “knickpoint” migrated across the platform due to sea level rise. Rather, it is likely that sea level rose past the platforms over the span of one to two hundred years, and the bulk of platform erosion occurred at the wave base while the platform was submerged. This type of erosion likely lowers the wave-cut platform relatively uniformly, except in places where there is a significant change in resistance to erosion (such as lithologic contacts). An average of up to about 1.5 m of bedrock lowering is predicted on these wave-cut platforms during the post-LGM transgression, based on a mean rate of bedrock lowering (for less resistant rock) of 1 m per thousand years, and an estimated erosion duration of up to 1,500 years. As applied to fault offset estimation, this erosion should act equally on both sides of the fault.

7.2.2 Potential Ages of Selected Paleoshorelines on the Islay Shelf

The best-constrained global eustatic sea-level curves for the past 140 ka indicate significant variability in sea level on time scales ranging from about 5 to 20 thousand years (Figure I-5-3). However, a general trend of gradual, but persistent, decrease in sea level from MIS 5e (approximately 120–125 ka) to the LGM during MIS 2 (approximately 20–22 ka) is evident in the curves. This observation suggests an inverse relationship between the age of the most recent pre-Holocene occupation of submerged wave-cut platforms/associated strandlines and water depth. This relationship suggests that the deeper strandlines in the study region are expected to be younger than the shallower strandlines.

Figure I-7-1 shows preliminary age estimates for well-developed and well-correlated strandlines on the Islay shelf. Submerged strandlines are correlated to the late-Quaternary global eustatic sea-level curve using an inferred uplift rate of 0.2 mm/yr based on the well-constrained uplift rate of the Irish Hills subblock from dated emergent marine terraces (discussed in Section 7.1). The most recent occupation of a well-developed strandline at -22 ± 1 m elevation on the Islay shelf appears to be a stillstand (period of relative sea-level stability) during MIS 5d (approximately 90–95 ka). Restoration of the inferred 0.2 mm/yr uplift rate suggests that the strandline at -22 ± 1 m elevation was at an elevation of about -40 to -45 m during MIS 5d (approximately 110–115 ka). This elevation is similar to the elevation of a well-developed paleoshoreline feature preserved on the tectonically stable continental shelf of South Africa. Uranium-series dating of beach rock collected from this paleoshoreline yields an age of 117 ± 7 ka (Ramsay and Cooper, 2002). The -22 ± 1 m strandline on the Islay shelf is shown in green on Plates I-3b and c.

Restoration of uplift suggests that the most recent stillstand at -27 ± 1 m could have been as recent as MIS 5b, based on a weak correlation with a well-constrained sea-level lowstand documented by Cutler et al. (2003). However, the weakness of the correlation suggests that this strandline, shown in gray on Plates I-3b and I-3c, may be even older. A better correlation with the MIS 5b lowstand may be the well-developed strandline at -38 ± 1 m, shown in red/yellow on Plates I-3b and I-3c. Restoration of uplift suggests that this strandline may have been reoccupied during MIS 3 highstands between about 49 and 61 ka at elevations of about -45 to -50 m documented by Chappell (2002). A well-developed shoreline preserved at -61 ± 1 m on the Islay shelf, shown in blue/beige on Plates I-3b and I-3c, was probably occupied during a late-MIS3 highstand about 30 to 40 ka at about -70 m elevation (documented by Cutler et al., 2003). This shoreline may also have been partly developed during an earlier MIS 4 sea-level lowstand at about -75 m between 60 and 70 ka. Furthermore, the elevation of the shoreline (slightly below

–60 m) suggests that it may have been occupied during the Younger Dryas cold period between 12.5 and 11.5 ka (Lambeck et al., 2002).

7.2.3 Potential Ages of Selected Paleoshorelines on the Santa Rosa Reef Shelf

Figure I-7-2 shows preliminary age estimates for well-developed and well-correlated paleoshorelines developed on the Santa Rosa Reef shelf. Submerged strandlines are correlated to the late-Quaternary global eustatic sea-level curve using an inferred uplift rate of 0.06 mm/yr based on correlation with well-dated marine terraces on Point San Luis (discussed in Section 7.1). The most recent occupation of a well-developed paleoshoreline at -40 ± 1.5 m (shown in green on Plates I-3b and I-3c) elevation in the Santa Rosa Reef shelf appears to be during MIS 5d (approximately 110–115 ka). Restoration of the inferred 0.06 mm/yr uplift rate suggests that this paleoshoreline was located at about –46 m during MIS 5d, the approximate elevation of a well-developed shoreline feature on the continental shelf of South Africa developed during MIS 5d (Ramsay and Cooper, 2002). An additional well-correlated paleoshoreline at -45 ± 1 m, shown in yellow on Plates I-3b and I-3c, probably was most recently occupied during one or more of a series of MIS 3 highstands between about 49 and 61 ka documented by Chappell (2002) based on coral data from New Guinea. Restoration of uplift suggests that this paleoshoreline was located at elevations of about –47 to –49 m during that period. Additional restoration of uplift suggests that a slightly lower paleoshoreline at an elevation of -50 ± 3 m (shown in red on Plates I-3b and I-3c) may also have been occupied during an earlier MIS 5b (approximately 90–95 ka) lowstand documented by Cutler (2003).

A deeper strandline at -67 ± 1 m, shown in blue on Plates I-3b and I-3c), is locally well expressed on the Santa Rosa Reef shelf. The most recent occupation of this paleoshoreline was likely during a late-MIS 3 highstand about 30 to 40 ka at about –70 m elevation. If a shoreline was developed in the DCPD region during the Younger Dryas at about –63 m (as suggested by the occurrence of a paleoshorelines at -61 ± 1 m on the Islay shelf) it would be predicted at about its original elevation (i.e., –63 m) because of the lower uplift rate of the Santa Rosa Reef shelf. Only two strandlines and one seismic reflection pick are recorded on the Santa Rosa Reef shelf close to this elevation. Although these strandlines are spatially distant, they are correlated on Plates I-3b and I-3c in beige to facilitate comparison between a potential Younger Dryas shoreline and other, shallower paleoshorelines.

7.2.4 General Age Constraints

The tentative correlations to late-Quaternary sea-level highstands and lowstands described above do not represent unique age assessments or correlations for the paleoshorelines preserved on the Islay and Santa Rosa Reef shelves (see Section 6.3.1). Uncertainty in global eustatic sea levels

and selection of alternative paleosea-level curves allow for alternative age correlations. Similarly, variations in uplift rates assumed for the Islay and Santa Rosa Reef shelves would result in different correlations or combinations of shoreline reoccupations during various late Quaternary highstands and lowstands. The potential effects of hydroisostatic loading of the continental shelf by flooding during the most recent transgression have not been investigated as part of this study. This effect, if significant in the project area, is likely to depress the shelf, reducing the effective uplift rates of the Islay and Santa Rosa Reef shelves.

Each of the well-developed paleoshorelines described above (and shown in color on Plates I-3b and c) include broad wave-cut platforms and more than one strandline that crosscuts bedding and/or other rock structure; consequently, they are interpreted to be older than the LGM (i.e., >22 ka). Furthermore, the strandlines preserved at elevations higher than about -30 m on the Islay shelf and about -35 m on the Santa Rosa Reef shelf are interpreted to have been developed during MIS 5 or earlier (i.e., greater than 75 ka).

7.3 CONSTRAINTS ON FAULT DISPLACEMENT

At three locations in the study area, wide wave-cut platforms cross the Shoreline fault zone, and at a fourth location a wave-cut platform crosses the N40W fault. The faults are discussed in detail in Appendix B. These relationships provide constraints on the timing and rates of potential fault deformation, and also limit potential differences in uplift rate on opposite sides of the faults. These locations include (from northwest to southeast):

- The platform associated with the -38 m strandline crossing the N40W fault.
- The platform associated with the -25 m strandline crossing the C-1 strand of the Central segment of the Shoreline fault zone.
- The platform associated with the -21 m strandline crossing the C-2 strand of the Central segment of the Shoreline fault zone.
- The platform associated with the -31 m strandline crossing the South segment of the Shoreline fault zone.

At each location, possible vertical separation across the fault since platform development is constrained based on projection of the wave-cut platform from opposite sides of the fault trace. The greatest credible vertical separation at each location is based on the amount of uncertainty in this projection. Uncertainty in vertical separation across the fault trace includes measurement uncertainty, geologic context uncertainty, and interpretation uncertainty. Measurement uncertainty is estimated from roughness, continuity, and general shape of the wave-cut platform that intersects the fault. Geologic context uncertainty stems primarily from consideration of the amount of erosion that likely occurred since the platform was developed (i.e., during the post-

LGM transgression), which is estimated to range up to 1.5 m for the study area, as described in Section 7.2.1.3. Other types of geologic context uncertainty (such as uncertainty in uplift rates, potential effects of hydroisostatic loading of the continental shelf, and precise relationship of the wave-cut platform to paleosea level) are less important for these measurements. Therefore, a geologic context uncertainty of ± 1.5 m is assumed for each of the sites described below.

Interpretation uncertainty is mainly epistemic, and addresses questions related to the quality of the mapping and interpretations. Such questions include whether or not the wave-cut platform actually crosses the fault trace in question (i.e., are both features mapped accurately enough to use the wave-cut platforms as a strain gauge), and whether or not the wave-cut platform was indeed carved during a paleosea-level stillstand. The interpretation uncertainties are addressed in other parts of this appendix, and are not included in the ranges of uncertainty included with the vertical separation measurements provided in the following subsections.

7.3.1 N40W Fault

The -38 m strandline roughly parallels the trace of the N40W fault for about 1.4 km and its wave-cut platform is mapped across multiple traces of the fault (Figure I-7-4a). Locally, sections of mapped fault traces are buried by 1–2 m of sediment as inferred from bathymetric profiling and evaluation of one seismic-reflection profile. Where exposed in rock, some traces of the N40W fault are associated with bedrock troughs or low bedrock scarps up to about 1–2 m high, such as the eastern trace shown on Profile A on Figure I-7-4, parts a and b. Elsewhere, bedrock traces of the N40W fault are not associated with scarps in the wave-cut platform, such as in profile B on Figure I-7-4, parts a and b. Consideration of numerous profiles provides evidence for no systematic vertical separation of the wave-cut platform across the N40W fault, with a measurement uncertainty of ± 1 m based on the natural variability of the platform. Therefore, the estimated vertical separation across the N40W fault is zero, with a combined uncertainty of approximately 2 m.

The probable timing of the most recent sea-level occupation (and associated significant geomorphic modification) of the -38 m paleostrandline and adjacent wave-cut platform on the Islay shelf was between 49 and 60 ka (Section 7.2). Given these age estimates, the estimated vertical separation rate for the N40W fault is 0 ± 0.04 mm/yr.

7.3.2 Central Segment, Shoreline Fault Zone

The -25 m strandline is mapped near the intersection between the C-1 and C-2 subsegments of the Shoreline fault zone, less than 100 m south of the north-trending jetty of Intake Cove (Figure I-7-5). At this location, the Shoreline fault zone is mapped as a series of west-northwest-trending, discontinuous strands with, en echelon right stopovers. Two seismic-reflection profiles

(Lines PBS 25 and PBS 25T) oriented nearly perpendicular to each other show that the strandline and platform are buried by about 3–5 m of sediment. These seismic-reflection profiles were used to develop 1 m elevation contours on the top of bedrock in this region (shown in black on Figure I-7-5). The seismic-reflection profiles suggest that a small northwest-trending trough up to about 2 m deep is located along the northwestward projection of the C-2 subsegment of the Shoreline fault zone. Farther to the northwest, an escarpment 1–2 m in height extends across the wave-cut platform along the northwestward projection of the C-2 subsegment of the Shoreline fault zone. Northeast of this escarpment the wave-cut platform surface is consistently about 1 m higher than it is southwest of the escarpment, suggesting that the scarp represents a persistent offset of the wave-cut platform. The measurement uncertainty for this site is estimated to be ± 2 m because measurement of the scarp is based on interpretation of seismic-reflection profiles.

Seismic-reflection profiles at this site, therefore, suggest a 1 m high scarp (with northeast side up) coincident with the C-2 subsegment of the Shoreline fault zone, with a combined uncertainty of 2.5 m. The preferred interpretation is that this scarp is a fault-line scarp from differential erosion that was not completely removed during development of the -25 m wave-cut platform. The basis for the preferred interpretation is the presence of fault-line scarps northwest and southeast of the -25 m wave-cut platform and the lack of evidence for vertical separation on the C-2 subsegment where it crosses the -21 m wave-cut platform as discussed below. However, it cannot be precluded that the scarp represents vertical separation on the fault and is caused by late Quaternary tectonic deformation. Therefore, the vertical separation across the C-2 subsegment of the Shoreline fault zone at this site is concluded to be either zero or one, with a combined uncertainty of 2.5 m.

The -25 m strandline is moderately well developed (confidence level B) and is tentatively correlated with shallower strandlines at -22 ± 1 m farther to the north on the Islay shelf. Because it is sufficiently shallow (i.e., higher than elevation -30 m on the Islay shelf), it is constrained to be older than 75 ka (Section 7.2.4). Therefore, the vertical separation rate across the C-2 subsegment of the Shoreline fault zone at this site is concluded to be either 0 ± 0.03 mm/yr or 0.01 ± 0.03 mm/yr.

Approximately 1.3 km to the southeast offshore of the entrance to DCP, the wave-cut platform associated with the -21 m strandline is mapped across the C-2 subsegment of the Shoreline fault zone (Figure I-7-6a). Here, the platform and strandline show evidence of no vertical deformation where the strandline bends 90 degrees to the northeast and the wave-cut platform extends across the mapped fault trace. Portions of the -21.5 m platform are mapped on exposed bedrock, whereas other areas are covered by shallow sediment, likely less than 1 m deep, as suggested by bathymetric profiles (Figure I-7-6b). Consideration of numerous profiles provides evidence for

no vertical separation of the wave-cut platform across the Shoreline fault zone, with a measurement uncertainty of ± 0.5 m based on the natural variability of the platform. Therefore, the estimated vertical separation across the C-2 subsegment of the Shoreline fault zone is zero, with a combined uncertainty of approximately 1.5 m.

This strandline is relatively continuous and moderately well-developed (confidence levels B and C) and is correlated either with well-developed shallower strandlines at -22 ± 1 m to the north on the Islay shelf (in correlation alternative 1, Section 6.3.1) or with moderately well-developed strandlines at -20.5 ± 2 m on the Santa Rosa Reef shelf to the south (in correlation alternative 2, Section 6.3.1). Because it is sufficiently shallow (i.e., higher than elevation -30 m on the Islay shelf or higher than -35 m on the Santa Rosa Reef shelf), it is constrained to be older than 75 ka (Section 7.2.4). Given these age estimates, the estimated vertical separation rate for the C-2 subsegment of the Shoreline fault zone is 0 ± 0.02 mm/yr.

7.3.3 South Segment, Shoreline Fault Zone

South of Point San Luis, a well-expressed strandline and associated wave-cut platform occur at an elevation of -31 m across the South segment of the Shoreline fault zone (Figure I-7-7a). The platform is buried by a thin mantle of sediment likely less than 1–2 m as suggested by the similarity in elevation between the strandline and the outer edge of the wave-cut platform as shown on bathymetric profiles, and the presence of small bedrock islands protruding above the sediment. A seismic reflection profile on the southeast margin of the platform also shows relatively thin sediment cover within the resolution of the data (estimated to be ± 2 m).

Consideration of numerous bathymetric profiles across the wave-cut platform provides evidence for no vertical separation of the wave-cut platform, with a measurement uncertainty of approximately 0.5 m based on the slope, thickness of sediment cover, and natural variability of the platform. In the near vicinity, well-expressed strandlines at elevations of -31 m and -34 m northeast and southwest of the fault zone are correlated across the fault zone. These correlations suggest no vertical deformation of the platform or strandlines has occurred since they were developed. Therefore, the estimated vertical separation across the South segment of the Shoreline fault zone is zero, with a combined uncertainty of approximately 1.5 m.

As with the wave-cut platforms that cross the Central segment of the Shoreline fault zone, no unique age is estimated for this wave-cut platform based on correlation with global eustatic sea-level curves. Because they are sufficiently shallow (i.e., higher than -35 m on the Santa Rosa Reef shelf), the paleostrandline and wave-cut platform are constrained to be older than 75 ka (Section 7.2.4). Given these age estimates, the estimated vertical separation rate for the South segment of the Shoreline fault zone is 0 ± 0.02 mm/yr.

8.0 CONCLUSIONS

Numerous submerged wave-cut platforms, strandlines, and paleosea cliffs are preserved on the inner continental shelf between Morro Bay and Pismo Beach. These features are imaged as gently sloping platforms backed by steeper scarps (paleosea cliffs), both as geomorphic features evident in detailed multibeam bathymetry data from rocky parts of the shelf and also buried beneath marine sediment evident in seismic reflection profiles. These features are generally discontinuous and vary widely in the strength of their geomorphic expression. Possible explanations for the origin of these wave-cut platforms, strandlines, and paleosea cliffs include (1) wave erosion during stillstands within the transgression that followed the LGM about 20–22 ka; (2) differential erosion during late Pleistocene transgressions and regressions, including the post-LGM transgression, caused by variability in bedrock resistance; and (3) wave erosion during relatively long-lived paleosea-level highstands, stillstands, and lowstands. As explained in the following paragraphs, the third alternative is the most credible for well-developed and correlated paleoshorelines.

Analysis of the Holocene wave-cut platform demonstrates that a wave-cut platform wider than 100 m would take an average of 2,000 years of relative sea level stability to develop. Detailed studies of sea-level rise during the post-LGM transgression indicate that no such period of global eustatic sea-level stability occurred, with the possible exception of the Younger Dryas cold period, which occurred between about 11,500 and 12,500 years ago. Therefore wave-cut platforms wider than 100 m are judged to have been carved prior to the post-LGM transgression.

Approximately one-third of the mapped strandlines clearly crosscut bedding in rock, indicating that differential erosion of bedrock is not a viable explanation for the origin of these geomorphic features.

A sequence of seven paleoshorelines (each composed of multiple individual strandlines) were identified on the Islay shelf. Of these, the most well-developed paleoshorelines include the paleoshorelines at elevations -22 ± 1 m, -27 ± 1 m, -38 ± 1 m, and -61 ± 1 m. Eleven individual paleoshorelines (also composed of multiple strandlines) were mapped on the Santa Rosa Reef shelf. Of these, the best-developed paleoshorelines include the paleoshorelines at elevations -29 ± 2 m, -40 ± 1.5 m, -45 ± 1 m, and -67 ± 1 m. Based on the widths of their wave-cut platforms, the close correlation with strandlines that clearly crosscut bedding, and the strength of the geomorphic expression, these well-expressed and well-correlated paleoshorelines are interpreted to result from late Quaternary paleosea-level lowstands, stillstands, or highstands.

Based on the current correlation with late Quaternary global eustatic sea-level curves, shallower submerged paleoshorelines, higher than about -30 m on the Islay shelf and about -35 m on the

Santa Rosa Reef shelf, are concluded to have developed during MIS 5 or earlier (i.e., older than about 75 ka; Figures I-7-2 and I-7-3). Deeper paleoshorelines were likely most recently occupied during one of several highstands or lowstands between MIS 5 and the LGM (75–22 ka). Additionally, one paleoshoreline (preserved at an elevation of about –61 to –62 m on the two shelf segments) may have been developed during the Younger Dryas (about 12.5–11.5 ka).

Geomorphic distinctions, correlation of paleoshorelines, and comparison to uplift blocks onshore, suggest that the Santa Rosa Reef shelf and Islay shelf represent separate blocks that are uplifting at different rates. Correlation with emergent marine terraces of the Irish Hills subblock suggests that the Islay shelf appears to be uniformly uplifting at a rate of 0.2 mm/yr. Correlation of paleoshorelines across the South segment of the Shoreline fault zone suggests that the Santa Rosa Reef shelf is uniformly uplifting at a rate of 0.06 mm/yr, together with the Point San Luis subblock. The boundary between these two uplift blocks is constrained to be along an offshore extension of the onshore San Luis Bay fault zone (preferred interpretation shown on Plate I-3b) or possibly along the Central and North segments of the Shoreline fault zone (Plate I-3c). The preferred location is based on an interpretation of broad offshore platforms correlated to MIS 5a that extend from near the coastline to elevations of approximately -16 ± 2 m off Point San Luis and -10 ± 2 m between Rattlesnake Creek and Olson Hill as submerged MIS 5a platforms (Figure I-7-1 and I-7-1a). The apparent north-side-up step of approximately 5–8 m between the two platforms coincides with the projected offshore extension of the Rattlesnake fault of the San Luis Bay fault zone. The northern edge of the inferred MIS 5a platform is truncated offshore of Olson Hill, consistent with a westward extension of the Olson deformation zone.

This interpretation suggests that (1) the platform in the offshore region between the Rattlesnake fault and the Olson deformation zone is being uplifted at a rate (approximately 0.14 mm/yr) similar to that recorded by emergent marine terraces onshore, and (2) the boundary between the Santa Rosa Reef shelf and Islay shelf is not localized along the Central segment of the Shoreline fault zone, but rather extends across the mapped traces of the Shoreline fault zone. This interpretation supports a model whereby the San Luis Bay fault zone (bounded to the south by the Rattlesnake trace and to the north by the Olson zone of deformation) crosses the Shoreline fault zone and extends westward to an intersection with the Hosgri fault zone.

Three wave-cut platforms probably older than 75 ka cross traces of the Shoreline fault zone, and one, less than 75 ka, crosses the N40W fault. Analysis of each of these platforms constrains the total vertical separation across the fault trace. Vertical separation across the C-2 strand of the Central segment of the Shoreline fault zone is estimated at two locations. Directly south of Intake Cove, the vertical separation is estimated to be 0 or 1 m, east side up, with a combined uncertainty of 2.5 m (Figure I-7-5). About 1.3 km to the southeast, the vertical separation across

the same trace is estimated to be 0 m, with a combined uncertainty of 1.5 m (Figure I-7-6, parts a and b). The estimated vertical separation rate for the C-2 subsegment of the Shoreline fault zone is therefore 0 ± 0.02 mm/yr. Vertical separation across the South segment of the Shoreline fault zone is estimated to be 0 m, with a combined uncertainty of 1.5 m (Figure I-7-7, parts a and b). The estimated vertical separation rate for the South segment of the Shoreline fault zone is therefore 0 ± 0.02 mm/yr. The estimated vertical separation across the N40W fault is zero, with a combined uncertainty of approximately 2 m (Figure I-7-4, parts a and b). The estimated vertical separation rate for the N40W fault is 0 ± 0.04 mm/yr.

9.0 REFERENCES

- Bard, E., Hamelin, B., Fairbanks, R. G., and Zindler, A., 1990, Calibration of the ^{14}C timescale over the past 30,000 years using mass spectrometric U-Th ages from Barbados corals: *Nature*, v. 345, pp. 241-244.
- Bard, E., Hamelin, B., Arnold, M., Montaggioni, L., Cabioch, G., Faure, G., and Rougerie, F., 1996, Deglacial sea-level record from Tahiti corals and the timing of global meltwater discharge: *Nature*, v. 382, pp. 241-244.
- Bateman, M.D., Holmes, P.J., Carr, A.S., Horton, B.P., and Jaiswal, M.K., 2004. Aeolianite and barrier dune construction spanning the last two glacial-interglacial cycles from the southern Cape coast, South Africa: *Quaternary Science Reviews*, v. 23, pp. 1681-1698.
- Bowen, D.Q., 2010, Sea level ~400,000 years ago (MIS 11): Analogue for present and future sea-level? *Climate of the Past*, v. 6, pp. 19-29.
- Bradley, W.C., and Griggs, G.B., 1976, Form, genesis, and deformation of central California wave-cut platforms: *Geological Society of America Bulletin*, v. 87, pp. 433-449.
- Chappell, J., 2002, Sea level changes forced ice breakouts in the Last Glacial cycle: new results from coral terraces: *Quaternary Science Reviews*, v. 21, pp. 1229-1240.
- Chappell, J., and Shackleton, N.J., 1986, Oxygen isotopes and sea level: *Nature* v. 324, pp. 137-140.
- Chappell, J., Omura, A., Esat, T., McCulloch, M., Pandolfi, J., Ota, Y., and Pillans, B., 1996, Reconciliation of late Quaternary sea levels derived from coral terraces at Huon Peninsula with deep sea oxygen isotope records: *Earth and Planetary Science Letters*, v. 141, pp. 227-236.
- Clark, P.U., and Mix, A.C., 2002, Ice sheets and sea level of the Last Glacial Maximum: *Quaternary Science Reviews*, v. 21, pp. 1-7.
- Clark, J.A., Farrell, W.E., and Peltier, W.R., 1978, Global changes in postglacial sea level a numerical calculation: *Quaternary Research*, v. 9, pp. 265-287.
- CLIMAP, 1981, Seasonal Reconstruction of the Earth's Surface at the Last Glacial Maximum: Geological Society of America, Map and Chart Series C36.

- Cutler, K.B., Edwards, R.L., Taylor, F.W., Cheng, H., Adkins, J., Gallup, C.D., Cutler, P.M., Burr, G.S., and Bloom, A.L., 2003, Rapid sea-level fall and deep-ocean temperature change since the last interglacial period: *Earth and Planetary Science Letters*, v. 206, pp. 253-271.
- Ferland, M.A., Roy, P.S., and Murray-Wallace, C.V., 1995, Sea-level studies-Glacial lowstand deposits on the outer continental shelf of southeastern Australia: *Quaternary Research*, v. 44, pp. 294-299.
- Fairbanks, R.G., 1989, A 17,000-year glacio-eustatic sea level record: influence of glacial melting dates on the Younger Dryas event and deep ocean circulation: *Nature*, v. 342, pp. 637-642.
- Fleming, K., Johnston, P., Zwartz, D., Yokoyama, Y., Lambeck, K., and Chappell, J., 1998, Refining the eustatic sea-level curve since the Last Glacial Maximum using far- and intermediate-field sites: *Earth and Planetary Science Letters*, v. 163, pp. 327-342.
- Gornitz, V., 2007, Sea level rise, after the ice melted and today: National Aeronautics and Space Administration, Goddard Institute for Space Studies, Science Briefs, available online at http://www.giss.nasa.gov/research/briefs/gornitz_09/, downloaded 7 November 2010.
- Griggs, G.B., and Trenhaile, 1994, Coastal cliffs and platforms: in Carter, R.W., and Woodroffe, C.D. (ed.), *Coastal Evolution: Late Quaternary Shoreline Morphodynamics*, Cambridge University Press, pp. 425-450.
- Hall, C.A., 1973a, Geologic Map of the Morro Bay South and Port San Luis Quadrangles, San Luis Obispo County, California: U.S. Geological Survey Miscellaneous Field Studies Map MF-511, scale 1:24,000.
- Hall, C.A., 1973b, Geologic Map of the Arroyo Grande Quadrangle, San Luis Obispo County, California: California Division of Mines and Geology Map Sheet 24, scale 1:48,000.
- Hall, C.A., Ernst, W.G., Prior, S.W., and Wiese, J.W., 1979, Geologic Map of the San Luis Obispo-San Simeon Region, California: U.S. Geological Survey Miscellaneous Investigations Series Map I-1097, scale 1:48,000.
- Hanson, K.L., Lettis, W.R., Wesling, J.R., Kelson, K.I., and Mezger, L., 1992, Quaternary marine terraces, south-central coastal California: Implications for crustal deformation and coastal evolution: in Fletcher, C.H., III and Wehmler, J.F. (eds.), *Quaternary coasts of the United States: Marine and lacustrine systems: SEPM (Society for Sedimentary Geology) Special Publication*, 48, pp. 323-332.
- Hanson, K.L., Wesling, J.R., Lettis, W.R., Kelson, K.I., and Mezger, L., 1994, Correlation, ages, and uplift rates of Quaternary marine terraces, south-central California: in Alterman, I.B., McMullen, R.B., Cluff, L.S., and Slemmons, D.B. (eds.), *Seismotectonics of the Central California Coast Range*, Geological Society of America Special Paper 292, pp. 45-72.
- Hanson, K.L., and Lettis, W.R., 2000, Application of multiple geochronologic methods to the dating of marine terraces in south-central California: in Noller, J.S., Sowars, J.M., and Lettis, W.R. (eds.), *Quaternary Geochronology: Methods and Applications*, AGU Reference Shelf 4, American Geophysical Union, Washington, D.C., pp. 527-535.

- Hays, J.D., Imbrie, J., and Shackleton, N.J., 1976, Variations in the earth's orbit: Pacemaker of the ice ages: *Science*, v. 194, no. 4270, pp. 1121-1132.
- Horton, B.P., 2007, Sea-level studies: Mid-latitudes: in Elias, S.A. (ed.), *Encyclopedia of Quaternary Science*, Elsevier, four-volume set, pp. 3064-3072.
- IPCC, 2001, *Climate Change 2001: The scientific basis: Third Assessment Report by the Intergovernmental Panel on Climate Change*, Cambridge University Press, Oxford. See especially Chapter 11: Changes in sea level, pp. 641-693. Available online at http://www.grida.no/climate/ipcc_tar/.
- Labeyrie, L., Duplessy, J.-Cl., and Blanc, P.L., 1987, Variations in mode of formation and temperature of oceanic deep waters over the past 125,000 years: *Nature*, v. 327, pp. 477-482.
- Labeyrie, L., Labracherie, M., Gorfti, N., Pichon, J. J., Vautravers, M., Arnold, M., Duplessy, J.C., Paterne, M., Michel, E., Duprat, J., Caralp, M., and Turon, J.L., 1996, Hydrographic changes of the Southern Ocean (Southeast Indian sector) over the last 230 kyr: *Paleoceanography*, v. 11, no. 1, pp. 57-76.
- Lambeck, K., and Chappell, J., 2001, Sea-level change through the last glacial cycle: *Science*, v. 292, pp. 679-686.
- Lambeck, K., Yokoyama, Y., and Purcell, T., 2002, Into and out of the Last Glacial Maximum: sea-level change during Oxygen Isotope Stages 3 and 2: *Quaternary Science Reviews*, v. 21, pp. 343-360.
- Lettis, W. R., and Hanson, K.L., 1992, Quaternary tectonic influences on coastal morphology, South-Central California: *Quaternary International*, v. 15/16, pp. 135-148.
- Lettis, W.R., and Hall, N.T., 1994, Los Osos fault zone, San Luis Obispo County, California: in Alterman, I.B., McMullen, R.B., Cluff, L.S., and Slemmons, D.B. (eds.), *Seismotectonics of the Central California Coast Ranges*, Geological Society of America Special Paper 292, pp. 73-102.
- Lettis, W.R., Kelson, K.I., Wesling, J.R., Angell, M., Hanson, K.L., and Hall, N.T., 1994, Quaternary deformation of the San Luis Range, San Luis Obispo County, California, in Alterman, I.B., McMullen, R.B., Cluff, L.S., and Slemmons, D.B., eds., *Seismotectonics of the central California Coast Ranges: Geological Society of America Special Paper 292*, pp. 111-132.
- Lettis, W.R., Hanson, K.L., Unruh, J.R., McLaren, M., and Savage, W.U., 2004, Quaternary tectonic setting of south-central coastal California: in Keller, M.A. (ed.), *Evolution of Sedimentary Basins/Offshore Oil and Gas Investigations—Santa Maria Province: U.S. Geological Bulletin 1995 AA*, 21 pp., 1 plate (1:250,000). Available at <http://pubs.usgs.gov/bul/1995/aa/>.
- Ludwig, K.R., Szabo, B.J., Moore, J.G., and Simmons, K.R., 1991, Crustal subsidence rate off Hawaii determined by $^{234}\text{U}/^{238}\text{U}$ ages of drowned coral reefs: *Geology*, v. 19, pp. 171-174.

- Ludwig, K.R., Muhs, D.R., Simmons, K.R., Halley, R.B., and Shinn, E.A., 1996, Sea level records at ~80 ka from tectonically stable platforms: Florida and Bermuda: *Geology*, v. 24, pp. 211-214.
- Milne, G., and Shennan, I., 2007, Sea level studies-Isostasy: in Elias, S. A. (ed.), *Encyclopedia of Quaternary Science*, four-volume set, pp. 3043-3051.
- Muhs, D.R., Simmons, K.R., Kennedy, G.L., and Rockwell, T.K., 2002a, The last interglacial period on the Pacific Coast of North America: Timing and paleoclimate: *Geological Society of America Bulletin* 114, pp. 569-592.
- Muhs, D.R., Simmons, K.R., and Steinke, B., 2002b, Timing and warmth of the Last Interglacial period: new U-series evidence from Hawaii and Bermuda and a new fossil compilation for North America: *Quaternary Science Reviews* 21, pp. 1355-1383.
- Muhs, D.R., Wehmiller, J.F., Simmons, K.R., and York, L.L., 2004, Quaternary sea-level history of the United States: in Gillespie, A.R., Porter, S.C., and Atwater, B.F. (eds.), *The Quaternary Period in the United States*. Elsevier, Amsterdam, pp. 147-183.
- Muhs, D.R., Simmons, K.R., Kennedy, G.L., Ludwig K.R., and Groves, L.T., 2006, A cool eastern Pacific Ocean at the close of the Last Interglacial complex: *Quaternary Science Reviews*, v. 25, pp. 235-262.
- Murray-Wallace, C.V., 2007a, Sea-level studies: Eustatic sea-level changes, glacial-interglacial cycles: in Elias, S.A. (ed.), *Encyclopedia of Quaternary Science*, Elsevier, four-volume set, pp. 3024-3034.
- Murray-Wallace, C.V., 2007b, Sea-level studies- Eustatic sea-level changes since the last glaciation: in Elias, S.A. (ed.), *Encyclopedia of Quaternary Science*, Elsevier, four-volume set, pp. 3034-3043.
- Niemi, T.M., Branch, C.N., Hall, N.T., and Shiller, G.I., 1987, Seafloor scarps along the central reach of the Hosgri fault, Southern Coast Ranges, California: Poster presentation, Geological Society of America Annual Meeting.
- Olson, S.L., and Hearty, P.J., 2009, A sustained +21 m sea-level highstand during MIS 11 (400 ka): Direct fossil and sedimentary evidence from Bermuda: *Quaternary Science Reviews*, v. 28, pp. 271-285.
- Pacific Gas and Electric Company (PG&E), 1988, Final report of the Diablo Canyon Long-Term Seismic Program for the Diablo Canyon Power Plant: San Francisco, California, U.S. Nuclear Regulatory Commission, Docket Nos. 50-275, 50-323.
- Pacific Gas and Electric Company (PG&E), 1989, Long Term Seismic Program: Plate Q43i-2-4, Model B longitudinal profile of marine terrace shoreline angles from Morro Bay to the Santa Maria Valley, south-central California.
- Pacific Gas and Electric Company, 1990, Attachment GSG Q16-5, Map and Longitudinal Profile of Submerged Shoreline Features West and South of the San Luis/Pismo Structural Block, Response to Question GSG Q16, Diablo Canyon Long Term Seismic Program: U.S. Nuclear Regulatory Commission Docket Nos. 50-275 and 50-323.

- Pacific Gas and Electric Company (PG&E), 2004, Diablo Canyon Interim Spent Fuel Storage Installation FSAR Update.
- Peltier, W.R., 2004, Global glacial isostasy and the surface of the ice-age earth: The ICE-5G (VM2) Model and GRACE: *Annual Review of Earth and Planetary Science*, v. 32, pp. 111-149; doi: 10.1146/annurev.earth.32.082503.144359.
- Peltier, W.R., and Fairbanks, R.G., 2006, Global glacial ice volume and Last Glacial Maximum duration from an extended Barbados sea-level record: *Quaternary Science Review*, v. 25, pp. 3322-3337.
- Potter, E-K., Esat, T.M., Schellmann, G., Radtke, U., Lambeck, K., and McCulloch, M.T., 2004, Suborbital-period sea-level oscillations during marine isotope substages 5a and 5c: *Earth and Planetary Science Letters*, v. 225, pp. 191-204.
- Ramsay, P.J., and Cooper, J.A.G., 2002, Late Quaternary sea-level change in South Africa: *Quaternary Research*, v. 57, pp. 82-90.
- Ringor, C.L., Omura, A., and Maeda, Y., 2004, Last Interglacial sea-level changes deduced from coral reef terraces in southwest Bohol, central Philippines: *Quaternary Research*, v. 43, pp. 401-416.
- Roberts, D.L., Jacobs, Z., Karkanis, P., and Marean, C.W., 2007, Onshore Expression of Multiple Orbitally Influenced Late Quaternary Marine Incursions on the Ultra Stable Southern South African Coast, poster presented at 17th Inqua Congress, Cairns, Australia.
- Shackleton, N.J., 1987, Oxygen isotopes, ice volume and sea level: *Quaternary Science Review*, v. 6, pp. 183-190.
- Shackleton, N., 2000, The 100,000-year ice-age cycle identified and found to lag temperature, carbon dioxide, and orbital eccentricity: *Science*, v. 289, pp. 1897-1902.
- Shackleton, N.J., and Opdyke, N.D., 1973, Oxygen isotope and paleomagnetic stratigraphy of equatorial Pacific core V28-238: Oxygen isotope temperatures and ice volumes on a 10^5 and 10^6 year scale: *Quaternary Research*, v. 3, pp. 39-55.
- Shackleton, N.J., and Opdyke, N.D., 1976, Oxygen-isotope and paleomagnetic stratigraphy of Pacific core V28-239, late Pliocene to latest Pleistocene: *Geological Society of America Memoir* 145, pp. 449-464.
- Shennan, I., 1999, Global meltwater discharge and the deglacial sea-level record from northwest Scotland: *Journal of Quaternary Science*, v. 14, pp. 715-719.
- Shennan, I., 2007, Sea-level studies: Overview: in Elias, S.A. (ed.), *Encyclopedia of Quaternary Science*, Elsevier, four-volume set, pp. 2967-2974.
- Shennan, I., and Milne, G., 2003, Sea-level observations around the Last Glacial Maximum from the Bonaparte Gulf, NW Australia: *Quaternary Science Reviews*, v. 22, pp. 1543-1547.
- Stein, M., Wasserburg, G. J., Lajoie, K.R., and Chen, J.H., 1991, U-series ages of solitary corals from the California coast by mass spectrometry: *Geochimica et Cosmochimica Acta*, v. 57, pp. 2541-2554.

- Thompson, W.G., and Goldstein, S.L., 2005, Open-system coral ages reveal persistent suborbital sea-level cycles: *Science* 308, pp. 401-404.
- Trenhaile, A.S., 2002, Rock coasts with particular emphasis on shore platforms: *Geomorphology*, v. 48, pp. 7-22.
- Trenhaile, A.S., and Layzell, M.G.J., 1981, Shore platform morphology and the tidal duration factor: *Transactions of the Institute of British Geographers, New Series*, v. 6, no. 1, pp. 82-102.
- Waelbroeck, C., Labeyrie, L., Michel, E., Duplessy, J.C., McManus J.F., Lambeck, K., Balbon, E., and Labracherie, M., 2002, Sea-level and deep water temperature changes derived from benthic foraminifera isotopic records: *Quaternary Science Reviews*, v. 21, pp. 295-305.
- Weber, G.E., 1983, Geologic investigation of the marine terraces of the San Simeon region and Pleistocene activity of the San Simeon fault zone, San Luis Obispo County, California: U.S. Geological Survey Technical Report, 66 pp.
- Wemiller, J.F., Simmons, K.R., Cheng, H., Edwards, R.L., Martin-McNaughton, J., York, L.L., Krantz, D.E., and Shen, C.C., 2004, Uranium-series coral ages from the US Atlantic Coastal Plain—The “80 ka problem” revisited: *Quaternary International*, v. 120, pp. 3-14.
- Williams, M.; Dunkerley, D., De Deckker, P., Kershaw, P., and Chappell, J., 1998, *Quaternary Environments*, 2nd ed.: Arnold, London.
- Wright, J.D., Sheridan, R.E., Miller, K.G., Uptegrove, J., Kramer, B.S., and Browning, J.V., 2009, Late Pleistocene sea-level on the New Jersey Margin: Implications to eustasy and deep-sea temperature: *Global and Planetary Change*, v. 66, pp. 93-99.
- Yokoyama, Y., Lambeck, K., De Dekkar, P., Johnston, P., and Fifield, L.K., 2000, Timing of Last Glacial Maximum from observed sea level minima: *Nature*, v. 406, pp. 713-716.
- Yokoyama, Y., Lambeck, K., De Dekkar, P., Johnston, P., and Fifield, L.K., 2001, Correction to Yokoyama et al. (2000): *Nature*, v. 412, p. 99.
- Zong, Y., 2007. Sea-levels, Late Quaternary Tropics: in Elias, S.A. (ed.), *Encyclopedia of Quaternary Science*, Elsevier, four-volume set, pp. 3087-3094.

Table I-1-1. Definitions

Coastline	A broad region in the vicinity of a shoreline that includes coastal landforms, such as beaches, wave-cut platforms, sea cliffs, marine terraces, and seaward-facing hillslopes.
Continental Shelf	The gently westward-sloping sea floor that lies between the coastline and the break in slope to the steeper (1.0–2.0 degrees) continental slope at water depths of 100–225 m.
DCPP	Diablo Canyon Power Plant, the area includes the power block, where the reactors and generators are located, and the adjuvant support facilities.
Elevation	The vertical distance from a datum (usually mean sea level) to a point or object on the Earth's surface, especially the height of a ground point above the level of the sea. The term is used synonymously with altitude in referring to distance above sea level, but in modern surveying practice the term "elevation" is preferred to indicate heights on the Earth's surface; "altitude" is used to indicate the heights of points in space above the Earth's surface.
Islay shelf	The rocky portion of the inner continental shelf that lies offshore of Point Buchon. It extends from the coastline to the continental slope on the west and from Estero Bay on the north to the general latitude of the DCPP on the south. It is generally characterized by wide, gently sloping subsea exposures of rock, but also includes limited areas of thin late Quaternary marine deposits and sand waves.
Mean sea level (MSL)	Sea level measured at the mean of all tides in the region. This is approximately coincident with NAVD 88. The reference datum for all topographic surveys and all maps in Appendix I is NAVD 88.
Outer edge	The downslope edge of a remnant of a wave-cut platform.
Paleo-	A combining form denoting the attribute of great age or remoteness in regard to time (Paleozoic), or involving ancient conditions (paleoclimate), ancestral origin, or fossil forms (paleoanthropic). Sometimes given as <i>paleo-</i> before vowels (paleoceanography).
Paleoshoreline	A preserved remnant of an ancient shoreline. In the study area, these are discontinuous features related to sea-level high stands onshore and high and low stands offshore. Paleoshorelines are typically associated with wave-cut platforms and paleosea cliffs and/or paleobeaches. Locally,

	multiple closely spaced strandlines are grouped with a single paleoshoreline.
Project DEM	A composite digital elevation model (DEM) developed from various sources of bathymetric and topographic data in which the most accurate and detailed data sets supersede less detailed or regional data sets. Figures and plates presented in this appendix are based on version 6 of the composite DEM data, which was compiled in August 2010 at 1 m raster resolution. The projection system for the data set is Universal Transverse Mercator (UTM), zone 10 North, NAD83 with NAVD88 vertical datum.
San Luis Bay shelf	The rocky portion of the inner continental shelf within San Luis Obispo Bay. It extends from the coastline to the southern and western limit of bedrock outcrops and from Mallagh Landing on the north to Pismo Beach on the south. It is generally characterized by subhorizontal subsea exposures of rock that are intermittently buried by thin late Quaternary marine deposits.
Santa Rosa Reef shelf	The rocky portion of the inner continental shelf that lies offshore of Point San Luis. It extends from the coastline to the continental slope on the west and from the general latitude of Lion Rock on the north to the limit of bedrock outcrops south and southeast of Point San Luis. It is generally characterized by the wide, gently sloping and flat subsea exposures of rock, but also includes limited areas of thin late Quaternary marine deposits and sand waves.
Sea cliff	A cliff or slope produced by wave erosion, situated at the seaward edge of the coast or the landward side of the wave-cut platform, and marking the inner limit of erosion. It may vary from an inconspicuous slope to a high, steep escarpment.
Shoreline	The location where sea surface meets the land; this can include an entire tidal range.
Shoreline angle	A shoreline angle is the point (typically in profile) where a wave-cut platform meets a sea cliff. Because of natural variation in wave-cut platform surfaces, shoreline angles can be formed at a variety of elevations with respect to the tidal range, ranging from as low as MSL (approximate elevation of 0 relative to NAVD 88) to a few meters above MSL. In the study area, the most common elevation of shoreline angles on the modern coastline is 2 m, approximately coincident with MHHW. An ancient shoreline angle provides an approximate record of the relative sea level at the time when the paleoshoreline formed.

Shoreline fault zone study area	The area of detailed paleostrandline and wave-cut platform mapping described in Appendix I. This area is shown on Figure I-1-1.
Strandline	The two-dimensional geomorphic record of sea level. On an erosional coastline (such as the Irish Hills coastline), it is marked by the intersection of a sea cliff and a wave-cut platform. On a depositional coastline, it is marked (less precisely) by a beach berm. As with shoreline angles, modern strandlines in the study area typically occur at elevations of about 2 m, but may range from 0 to a few meters elevation. An ancient strandline provides an approximate record of the relative sea level at the time the paleoshoreline formed
Wave-cut platform	A broad bedrock platform that slopes gently seaward from a sea cliff. The term "wave-cut platform" is used in this report because wave erosion is the dominant erosional process for platform development. Some authors (e.g., Trenhaile, 2000, 2002; Trenhaile and Layzell, 1981) prefer the term "shore platform" because wave erosion is not the only process responsible for platform development. Other erosive processes acting on these platforms include chemical and salt weathering, bioerosion, and expansion-contraction of clays and/or ice (Griggs and Trenhaile, 1994).
Width	The width of the platform is the distance measured orthogonally to the strandline from the paleosea cliff or inner (coastward) to the outer (seaward) limit of the mapped extent of the platform.

Table I-4-1. Submerged Strandline Confidence Assessment

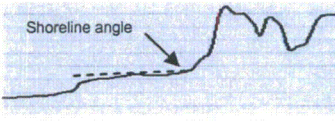
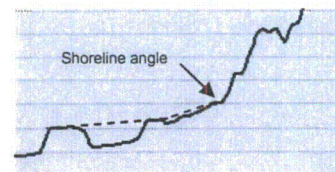
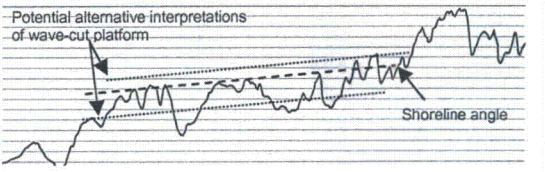
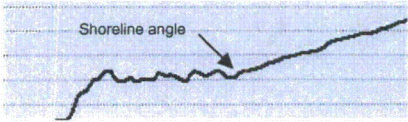
Rank	Geomorphic Expression (with data example)	Continuity	Location Confidence	Probability of Representing Paleoshoreline
Level A	<p>Strong geomorphic expression in bedrock with a well-defined wave-cut platform and prominent shoreline angle; strandline is mappable and relatively continuous.</p> 	<p>Consistent elevation over distances of a few hundred meters, excepting embayments.</p>	<p>High; map with a solid line.</p>	<p>Highly likely; closely approximates paleosea level.</p>
Level B	<p>Good geomorphic expression in bedrock with a generally well-defined platform and readily identifiable shoreline angle; strandline is mappable, but discontinuous.</p> 	<p>Mostly laterally continuous but may contain breaks in the shoreline angle or platform.</p>	<p>Moderately high; map with a solid line where well located on bedrock and a dashed line where approximately located on bedrock or inferred; dotted line where buried.</p>	<p>Likely; closely approximates paleosea level.</p>
Level C	<p>Moderate geomorphic expression; Strandlines are mappable but are highly degraded. Platforms may be mappable, but commonly are too degraded (i.e., rough, incised, or irregularly sloping) to map.</p> 	<p>Elevation generally is consistent, but may vary by 2-4 m. The shoreline angle becomes difficult to define along some portions of the mapped strandline.</p>	<p>Low; dashed line where approximately located on bedrock or inferred; dotted line where buried.</p>	<p>Moderately likely; provides limiting minimum for paleosea level, possibly incorrectly interpreted to be strandline.</p>
Level D	<p>Subtle geomorphic expression; platform and shoreline angle are difficult to identify and may consist of a simple break in slope.</p> 	<p>Platforms and shoreline angles are frequently degraded and difficult to map. Elevation of the mapped strandline may vary up to 4 m.</p>	<p>Low; questionably inferred. Dashed and queried line on bedrock; dotted and queried line where buried.</p>	<p>Possible; probably located within approximately 9 m below paleosea level, possibly incorrectly interpreted to be strandline.</p>

Table I-4-2. Uncertainties in Assessing Elevations and Ages of Paleostrandlines

Description	Resolution or Estimated Uncertainty	Comments
Data Accuracy and Measurement		
DEM from MBES bathymetry data and LiDAR data	<p>Vertical precision of MBES data is ± 10 cm. Vertical accuracy is estimated to be ± 50 cm.</p> <p>RMSE for absolute vertical accuracy of the LiDAR data is 4–5 cm.</p>	<p>In general, relative vertical accuracy is higher than the absolute vertical accuracy of a specific point. This means that while the actual elevation of a specific point (i.e., the shoreline angle elevation) may be accurate to within only 50 cm, the elevation difference between adjacent points on the seafloor inferred from profiles derived from these data is much more accurate.</p>
High-resolution seismic-reflection profile data	Vertical accuracy is estimated to be ± 2 m.	<p>The estimated elevation of shoreline angle mapped from high-resolution seismic-reflection profile data is calculated by subtracting the depth of the shoreline angle below the seafloor from the MBES data using an assumed velocity of water and subbottom sediments of 1,600 m/sec. Given the limited depth (generally less than 15 ms TWTT) of the features below the seafloor, modest changes to the assumed velocity of the sediments are not expected to have a net effect greater than about 0.5–1.0 m. The primary uncertainty stems from the variability in the quality of the images and the expression of the features. The latter uncertainty is considered to be primarily interpretative in nature.</p>
Measurement of the continuity and slope of an individual wave-cut platform.	Approximately the same as the natural variability of the platform, as characterized by numerous closely spaced profiles.	<p>The confidence in mapping individual wave-cut platforms depends on the natural variability (or roughness) of the platform, which in turn is related to bedrock lithology and structure. Sediment burial locally may complicate the assessment of the variability in the wave-cut platform. The confidence in measurement of wave-cut platform</p>

Description	Resolution or Estimated Uncertainty	Comments
		characteristics is increased by evaluating numerous closely spaced profiles.
Measurement of elevation of the shoreline angle	Measurement uncertainty ranges from less than 1 m for well-defined shoreline angles to as much as 4 m for poorly expressed features (see Table I-4-1 for data examples).	The uncertainty in the elevation of a specific point measured on profiles generated from the MBES data is a function of the width and natural variability of the associated platform, the height and expression of the paleosea cliff, and the amount of sediment cover on the platform. The uncertainty in the elevation of individual paleostrandlines shown on Plate I-3a accounts for the variability in the point measurements from numerous profiles evaluated for this study.
Geologic Context		
Influence of shoreline morphology on the development and expression of paleostrandlines and associated wave-cut platforms	Variable. Accounted for in the uncertainty in the elevation of individual paleostrandlines (see Plate I-3a).	Various factors, such as the shape of the coastline relative to the direction of major storm waves and the effect of headlands and bays on erosion and sedimentation, influence the location and amount of erosion that may occur. Examination of the elevations of the shoreline angle for some well-developed paleostrandlines mapped around a paleoheadland/paleobay or paleisland localities suggests that there could be up to 3 m of variability between the headland and bay or lee sides of paleislands. Localized deeper erosion at a headland may give rise to an anomalously low shoreline angle elevation that does not appear to be correlative with a specific paleostrandline. The mapping criteria used to correlate and map individual paleostrandlines addresses these possible outliers.
Influence of bedrock lithology and structure on interpretation of paleostrandline features	Uncertainty is reduced by using the most confident interpretations as a basis for	The possibility that some or all of the mapped paleostrandlines were formed by differential erosion in rock, instead of wave erosion during paleosea-level stillstands, was

Description	Resolution or Estimated Uncertainty	Comments
	paleoshoreline correlations.	explicitly considered in the confidence assessment of various postulated paleostrandlines (Section 4.2.1). The paleostrandlines with the highest confidence crosscut bedrock structures. The relationship of mapped paleostrandlines to existing bedrock structure (i.e., mapped faults, folds, joints, and bedding attitudes) was documented on the longitudinal profiles and used to inform paleoshoreline correlations (see Plates I-3a through I-3d).
Hydroisostatic loading of the continental shelf	N/A Estimated to be less than and included in other measurement uncertainties.	It is recognized that hydroisostatic processes, especially on wide continental shelf regions, could result in spatial and temporal differences in patterns of uplift that would influence development of submerged shoreline features and their present elevation. Modeling of such processes has not been conducted as part of this study. Due to the limited differences in the width of the shelf areas within the study area, it is not expected that there have been isostatic adjustments that would significantly affect the general conclusions regarding the apparent differences in the number and spacing of paleostrandlines between the Islay and Santa Rosa Reef shelves. The likely long-term effect of any hydroisostatic adjustments to differential loading of the broader shelf areas (e.g., San Luis Obispo Bay) relative to the narrower shelf areas on the margins of the San Luis Range would be to lower paleostrandline features that may have initially formed on isostatically uplifted areas marginal to the broader parts of the shelf during the initial stages of relative sea-level highstands. At this time, we cannot preclude minor warping of individual paleostrandlines. However, it is judged likely that, based on estimates of the location and elevation of measured shoreline

Description	Resolution or Estimated Uncertainty	Comments
		<p>angles, such warping would be within the uncertainty bounds assigned to the various paleostrandlines.</p> <p>Given the general broad waveform pattern of such deformation that stems from flow in the mantle, this process is not considered to be a likely explanation for the differential uplift between the Islay and Santa Rosa Reef shelves.</p>
<p>The degree to which erosion since development of the platform could have removed evidence for fault displacement</p>	<p>Approximately 0.5–1.5 m, depending on lithology, duration of exposure to erosion (on older [>75 ka] platforms)</p>	<p>This is difficult to quantify. Platforms formed above water depths of about 30–35 m that are assumed to have formed before about 75 ka (Section 7.2) were either exposed or buried in subaerial conditions for at least 65 thousand years. During that time they likely experienced some weathering. After that, sea level rose across the platforms, exposing them to wave erosion. Many of these platforms are flat enough, however, that sea level would have passed them quite rapidly (an estimated rate of 10 mm/yr sea level rise for the last transgression indicates that mean sea level would have passed the entire platform in less than 100–200 years), and wave erosion likely would have acted on the entire platform in a similar fashion (Section 7.2.1.3).</p> <p>For such flat platforms, it is unlikely that a “knickpoint” migrated across the platform due to sea level rise. Rather, the platforms were probably lowered relatively uniformly, or differential erosion enhanced preexisting fault-line scarps or other features with contrasting erodability. There is uncertainty in how much lowering of the platform surface would be required to remove a systematic offset (as would be expected from a brittle rupture on the fault traces that are</p>

Description	Resolution or Estimated Uncertainty	Comments
		<p>crossed by the platform) of 1 or 2 m within a platform that is currently relatively flat.</p> <p>Comparison to the paleosea cliffs is informative. While degraded, these submerged sea cliffs are still recognizable, even in locations where they are only 1 or 2 m high. The persistence of the paleosea cliffs and wave-cut platforms through this cycle of erosion suggests that the amount of rock lowering was not great enough to completely remove scarps of similar size. It seems unlikely that erosion would have removed a systematic offset of more than 1–2 m while still preserving the signature of a relatively flat platform and a paleosea cliff.</p> <p>Estimates of bedrock lowering due to post–Late Glacial Maximum erosion, based on analysis of the Holocene wave-cut platform at Islay Creek and offshore of Olson Hill (Figure I-7-1b), are about 1 m per thousand years in relatively less resistant rock (Section 7.2.1.3)</p>
Reoccupation of wave-cut platforms	N/A Uncertainty included in estimates of other uncertainties.	The potential for reoccupation of preexisting wave-cut platforms is more likely for low uplift areas. This is explicitly considered in evaluating the expected rate of sea-cliff retreat from Holocene wave erosion and the ages of submerged wave-cut platforms. Reoccupation of wave-cut platforms tends to widen the platforms and decrease their gradients, which may reduce their surface roughness and thereby reduce uncertainties associated with measuring vertical offsets that cross the platforms.

Description	Resolution or Estimated Uncertainty	Comments
Interpretative		
Interpretations of the continuity and correlation of specific paleostrandlines	Alternative correlations are considered. Correlations that match paleostrandlines with high confidence levels are preferred.	Alternative interpretations are possible given uncertainties in the identification and mapping of the less distinct features (i.e., the possibility that some subtle paleostrandlines might actually represent the change in slope between the outer and inner parts of the same platform, or instead may be related to differential erosion of bedrock). Paleostrandlines with the highest confidence levels are given the greatest weight in the preferred correlations presented in Section 6.3.
Interpretation of the preferred elevation of a mapped strandline	Elevations of the correlated shoreline angles are generally constrained to within $\pm 1-1.5$ m (This range of uncertainty is based on the assumption that the correlated strandlines all formed at the same paleosea level).	The uncertainty in the elevation of a strandline based on the assumed correlation of a number of shoreline angles measurements may be less than the elevation of specific measured shoreline angles used to define the strandline.
Inferred paleostrandline(s) formed during a period of relative sea-level stability	Groupings of paleostrandlines are considered in identifying and correlating prominent paleoshorelines.	The probability of a mapped paleostrandline representing a former shoreline formed during a period of relative sea-level stability is based on the criteria used to map features (i.e., geomorphic expression, continuity, and location confidence) and consideration of other geomorphic explanations for the origin of the feature. Multiple paleostrandlines spaced within a few meters of elevation may be associated with a period of relative sea-level stability (i.e., slight variations may reflect minor fluctuations or related storm platforms).
Estimated ages of the paleostrandlines and related wave-	Uncertainties in the timing and elevations of minor	Where they are used to constrain fault offset, inferred ages of paleostrandlines and wave-cut platforms are not specifically

Description	Resolution or Estimated Uncertainty	Comments
cut platforms	<p>fluctuations in paleosea level are on the order of tens of meters and several thousands of years for poorly constrained highstands and lowstands during MIS 3 and 4 (between about 75 and 25 ka), and for MIS 5b and 5d lowstands. These uncertainties are estimated from the range of interpretations of paleosea-level curves presented on Figure I-5-3.</p>	<p>tied to minor fluctuations in paleosea levels. Instead, age assessments are based on two primary interpretations:</p> <ol style="list-style-type: none"> 1. Paleostrandlines associated with wave-cut platforms greater than 100 m in width did not form during the post-Late Glacial Maximum transgression (see Section 7.2.1). It is assumed that the prominent paleoshoreline features (strandlines and associated wave-cut platforms) formed during periods of relative sea-level stability and that these periods are indicated by global sea-level curves (Sections 7.2.2 and 7.2.3). 2. Correlations to paleosea-level curves that pass outside of the range of interpretations for MIS 3 and 4 highstands and lowstands are used to constrain ages as MIS 5 or older (i.e., greater than 75 ka) and younger than MIS 5 (i.e., between about 25 and 75 ka).

Table I-5-1. Elevation and Age of Paleosea-Level Highstands and Lowstands

Stage	Age (ka)	Elevation (m)	Location	Source
2	14	-113.6	Hawaii	Ludwig et al., 1991
	15.8	-108.9	Hawaii	Ludwig et al., 1991
	17	-105.8	Hawaii	Ludwig et al., 1991
	19	-100.6	Hawaii	Ludwig et al., 1991
	17	-130	South Africa	Ramsay and Cooper, 2002
	23.7	-107	Huon Peninsula, Papua New Guinea, Barbados	Cutler et al., 2003
	28.6	-111	Huon Peninsula, Papua New Guinea, Barbados	Cutler et al., 2003
	19-22	-125	Bonaparte	Zong, 2007
	19-21	-115	Sunda Shelf	Zong, 2007
	21	-120 ± 5	New Jersey	Wright et al., 2009
3	38	-71	Huon Peninsula	Chappell, 2002
	about 35-50	-15	Gulf Coast	Muhs et al., 2004
		-74 to -85	Huon Peninsula, Papua New Guinea, Barbados	Cutler et al., 2003
	27.4 ± 440 ¹	-46	South Africa	Ramsay and Cooper, 2002
	39.1 ± 1530 ¹	-46	South Africa	Ramsay and Cooper, 2002
	3a	44.5	-56	Huon Peninsula
	35 ± 7	-30 ± 5	New Jersey	Wright et al., 2009
3b	52	-46	Huon Peninsula	Chappell, 2002
	45 ± 10	-60 ± 5	New Jersey	Wright et al., 2009
3c	58 to 60	-50	Huon Peninsula	Chappell, 2002
	55 ± 10	-20 ± 5	New Jersey	Wright et al., 2009
4	70.6 to 75	-37 to -54	Huon Peninsula	Chappell, 2002
	70.82	-81	Huon Peninsula, Papua New Guinea, Barbados	Cutler et al., 2003
	70 ± 10	-75 ± 5	New Jersey	Wright et al., 2009
5a	about 80	-5 ± 2	Central California	Hanson et al., 1994
	about 77 to 83	-9 to +2	Florida & Bermuda	Ludwig et al., 1996
		about -10 to -15	Bahamas	Muhs et al., 2002b
		-20	Barbados	Muhs et al., 2002a
		-16	New Guinea	Muhs et al., 2002a
		about -3 to -4	Punta Banda	Muhs et al., 2002a
	76.2 ± 4	-24	Huon Peninsula, Papua New Guinea, Barbados	Cutler et al., 2003

Stage	Age (ka)	Elevation (m)	Location	Source
	about 86–84 to 76	-6 to +6	Pacific Coast	Muhs et al., 2004
		<+7	Atlantic Coast	Muhs et al., 2004
	about 85–92	>-20	Florida Keys	Muhs et al., 2004
	79–83	-6 to -9	Phillipines	Ringor et al., 2004
	about 80	0 to about +6	Atlantic Coast	Wehmiller et al., 2004
	76–84		Pacific Coast	Muhs et al., 2006
	73.9 ± 1 to 85.3 ± 1.2	-15 ± 1	Barbados	Thompson and Goldstein, 2005
5b	92.6 ± .5	-57	Huon Peninsula, Papua New Guinea, Barbados	Cutler et al., 2003
	90 ± 10	-20 ± 5	New Jersey	Wright et al., 2009
5c		-2 ± 2	Central California	Hanson et al., 1994
		-20	Barbados	Muhs et al., 2002a
		-18	New Guinea	Muhs et al., 2002a
		about -2	Punta Banda	Muhs et al., 2002a
	101–108	-9 to -11	Phillipines	Ringor et al., 2004
	about 100	about 0	Pacific Coast	Muhs et al., 2004
	98.7 ± 1.1 to 106.9 ± 1.6	-13 ± 1	Barbados	Thompson and Goldstein, 2005
5d	113.1 ± .7	-19	Huon Peninsula, Papua New Guinea, Barbados	Cutler et al., 2003
	117 ± .7	44	South Africa	Ramsay and Cooper, 2002
5e	about 125	about +6 ± 2	Central California	Hanson et al., 1994
	about 115–136		Hawaii	Muhs et al., 2002b
	about 113–125		Bermuda	Muhs et al., 2002b
	about 114–123		Pacific Coast	Muhs et al., 2002a
	113–134		Hawaii	Muhs et al., 2004
	about 120	<10	Alaska	Muhs et al., 2004
		5–8	Florida Keys	Muhs et al., 2004
	122–131	3–6	Phillipines	Ringor et al., 2004
	107.2 ± 1 to 129.3 ± 1	7 ± 2	Barbados	Thompson and Goldstein, 2005
	125 ± 5	6 ± 5	New Jersey	Wright et al., 2009
	119	about 4	South Africa	Ramsay and Cooper, 2002
6	122–142	-122	Hawaii	Ludwig et al., 1991
	130 ± 20	-120 ± 5	New Jersey	Wright et al., 2009
7	about 210	about -3 ± 4	Central California	Hanson et al., 1994
	182 ± 18	about -3	South Africa	Ramsay and Cooper, 2002

Stage	Age (ka)	Elevation (m)	Location	Source
	about 220–230	about 0	Florida Keys	Muhs et al., 2004
	220–240	>–10	Hawaii	Muhs et al., 2004
	189.9 ± 1.2 to 248.2 ± 2	6 ± 2	Barbados	Thompson and Goldstein, 2005
8				
9	about 330	+4 ± 4	Central California	Hanson et al., 1994
	300–340	about 0	Florida Keys	Muhs et al., 2004
	300–350	–3	Atlantic Coast	Muhs et al., 2004
10				
11	400	~22	Alaska	Muhs et al., 2004
	400	>20	Bermuda	Olson and Hearty, 2009
	430	15.3	South Africa	Roberts et al., 2007
12				
13				
14				
15	500–600	–5 to +5	Hawaii	Muhs et al., 2004

Note

1. Late Pleistocene and Holocene ages from Ramsay and Cooper (2002) are ¹⁴C yr BP.

Table I-6-1. Summary of Holocene Platform Parameters

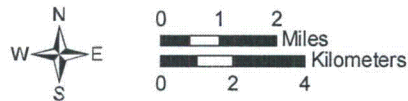
Geologic Unit (No. measurements)	Mean Width (m)	Mean Depth (m) at platform outer edge	Mean Slope (%)	Holocene Shoreline Angle Retreat Rate (m/kyr) 7 ka
Ophiolite (4)	208.3	5.7	3.7	29.3
Cretaceous sandstone (19)	274.0	6.9	3.5	39.1
Obispo Fm., resistant tuff (8)	353.5	9.5	3.5	50.5
Franciscan Complex (5)	325.8	6.2	2.7	46.5
Obispo Fm. (4)	473.8	10.7	2.8	73.3
Obispo Fm., diabase (4)	370.0	11.6	3.5	49.0
Monterey Fm. (8)	421.1	11.9	3.5	60.2
Pismo Fm., Miguelito Mem. (4)	668.0	11.6	2.0	95.4
Total (56)	338.2	8.7	3.3	50.5

File path: S:\13800\13838\13838\002\Figures\20101112_Report\Appendix_I\Figure_I-1-1.mxd; Date: [12/2/2010]; User: S. Bozkurt



LEGEND

- Study area
- Shoreline, Hosgri, San Luis Bay, and Wilmar Avenue faults, dashed where approximate, dotted where concealed



Map projection and scale: NAD 1983, UTM Zone 10N, 1:200,000

Map of Shoreline fault zone study area

SHORELINE FAULT ZONE STUDY

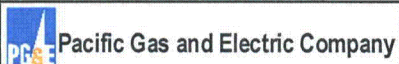
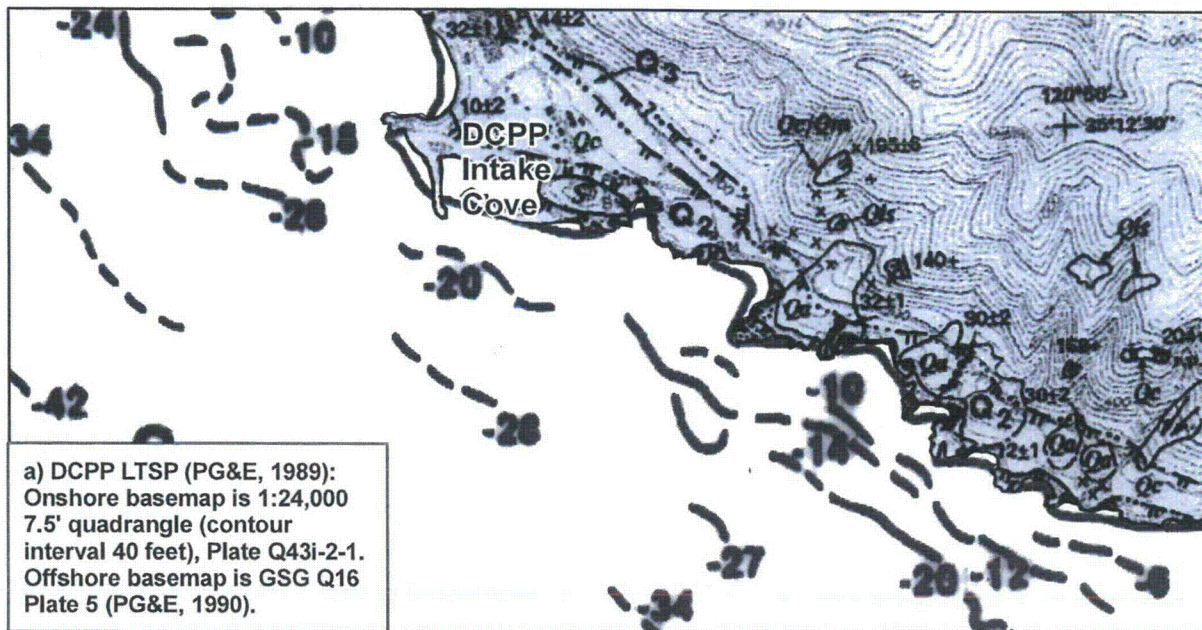
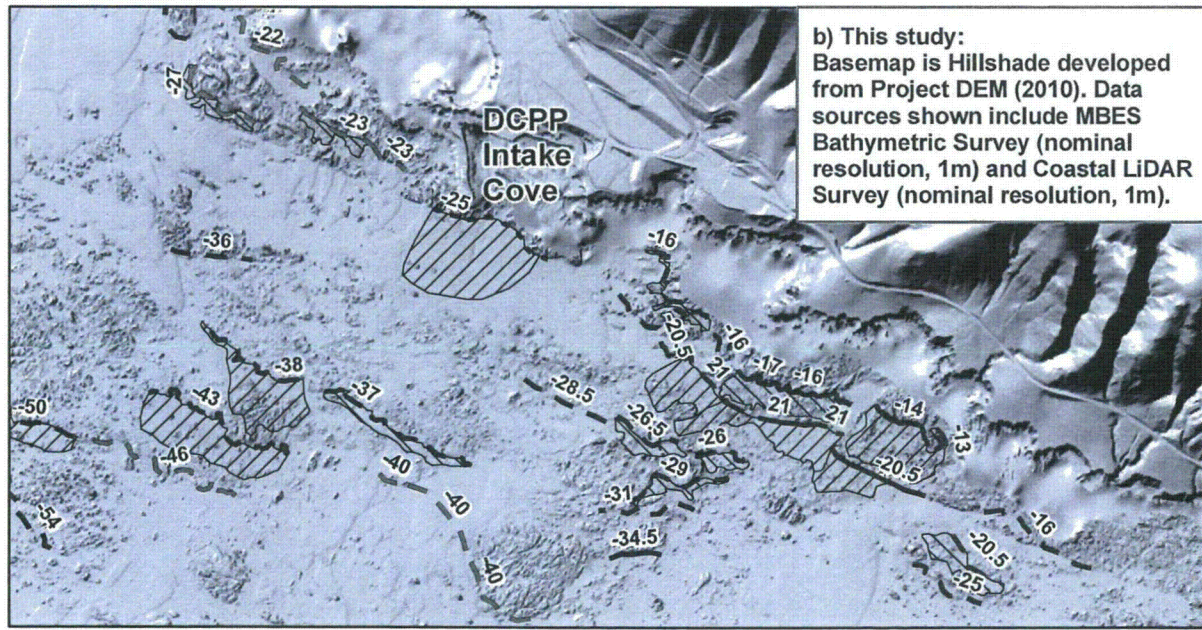


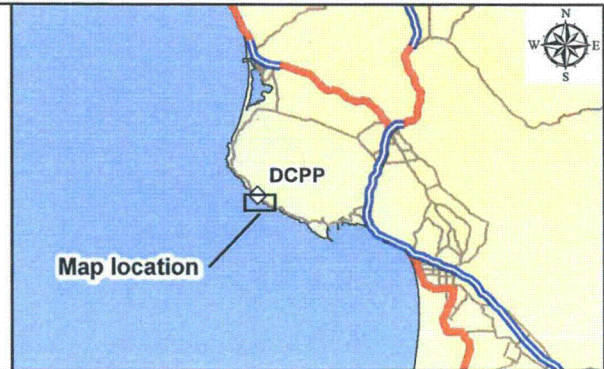
Figure **I-1-1**



a) DCPD LTSP (PG&E, 1989): Onshore basemap is 1:24,000 7.5' quadrangle (contour interval 40 feet), Plate Q43i-2-1. Offshore basemap is GSG Q16 Plate 5 (PG&E, 1990).



b) This study: Basemap is Hillshade developed from Project DEM (2010). Data sources shown include MBES Bathymetric Survey (nominal resolution, 1m) and Coastal LiDAR Survey (nominal resolution, 1m).



LEGEND

- · · · · · Emergent marine terrace shoreline angle (m), dashed where buried or less well constrained, dotted where eroded
- · · · · · Submerged strandline, dashed where approximately located, dotted where buried
- Borehole
- ▨ Submerged wave-cut platform (< 100 m wide)
- ▨ Submerged wave-cut platform (>100 m wide)

Note: Improved bathymetric data for this study has allowed for more detailed mapping of submerged shoreline angles.

Map scale: 1:24,000
 Map projection: NAD 1983, UTM Zone 10 North
 0 1,000 2,000 Feet
 0 200 400 600 800 1,000 Meters

Comparison of LTSP paleoshoreline mapping with current mapping

SHORELINE FAULT ZONE STUDY

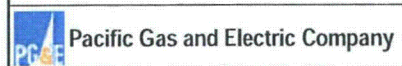
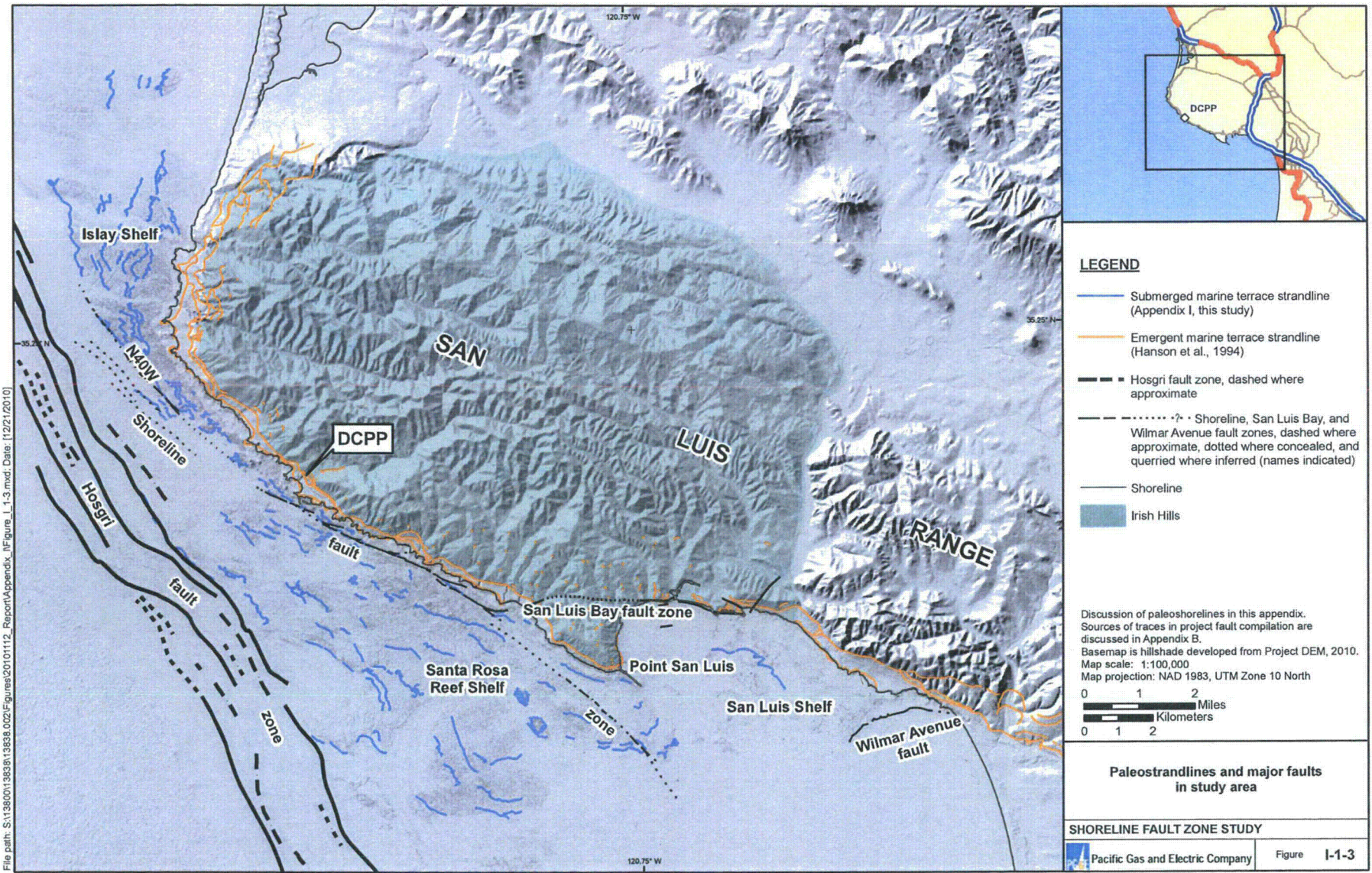
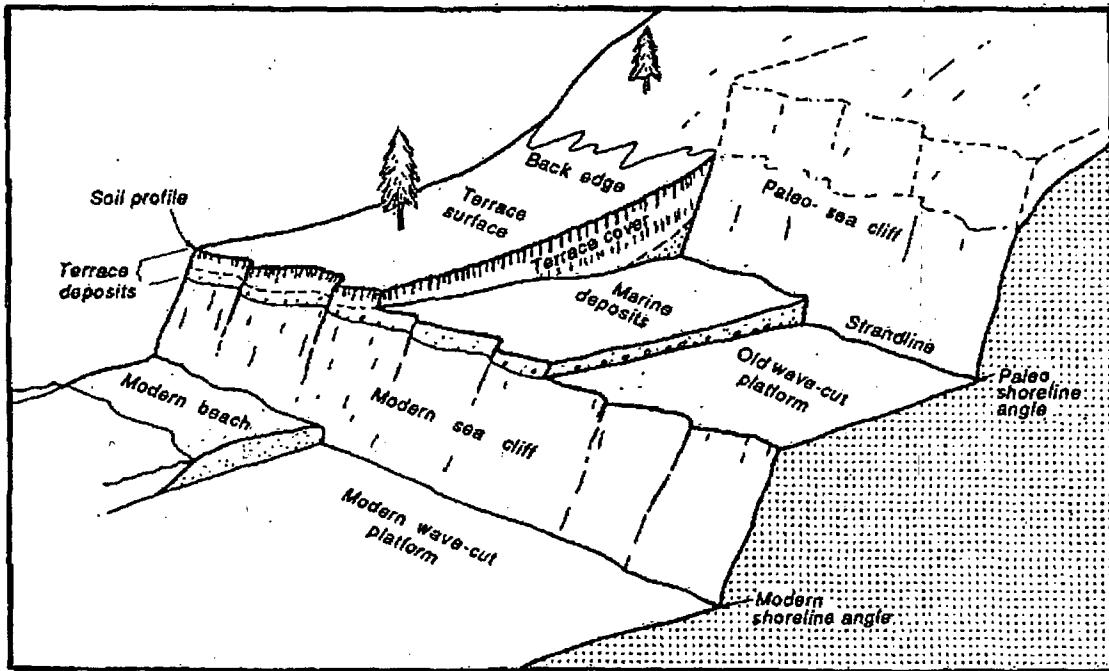


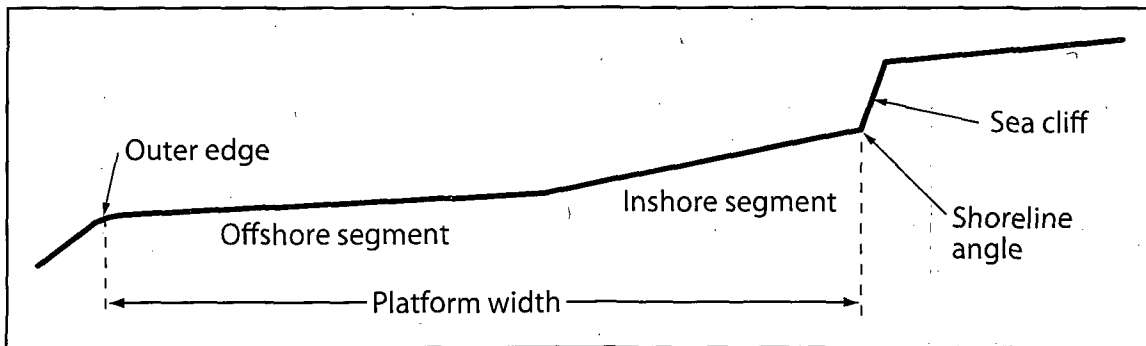
Figure I-1-2



File path: S:\1360013838\002\Figures\20101112_Report\Appendix_I\Figure_I-1-3.mxd; Date: [12/21/2010]



A. Schematic diagram illustrating the spatial relationships of major elements of marine terraces. (from Weber, 1983).



B. Sketch profile of generalized sea cliff and wave cut platform

Note:
Refer to Table I-1-1 for definitions of key terms.

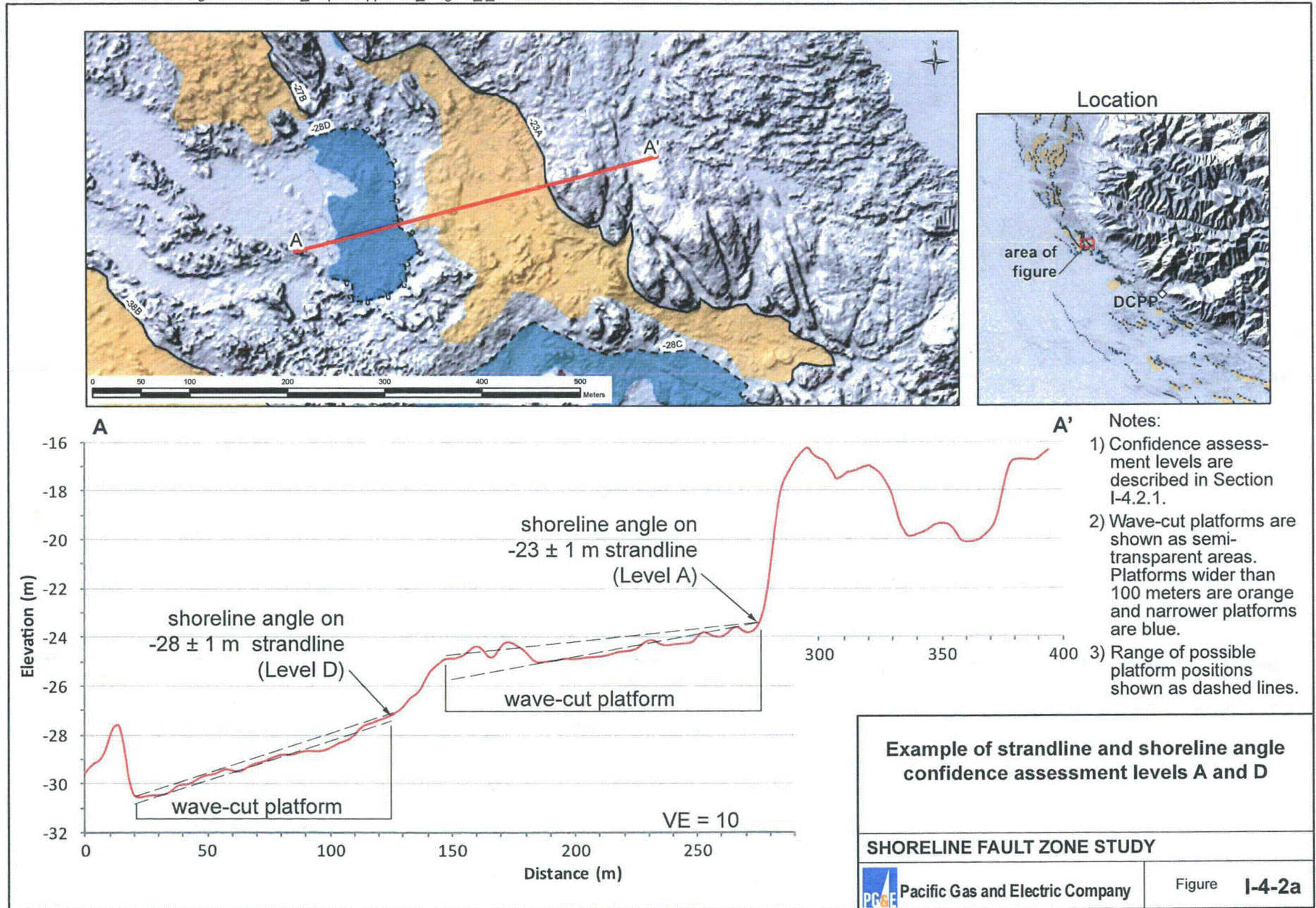
**Schematic diagrams illustrating
the coastal geomorphic features
formed by marine erosion and
their preservation in marine terraces**

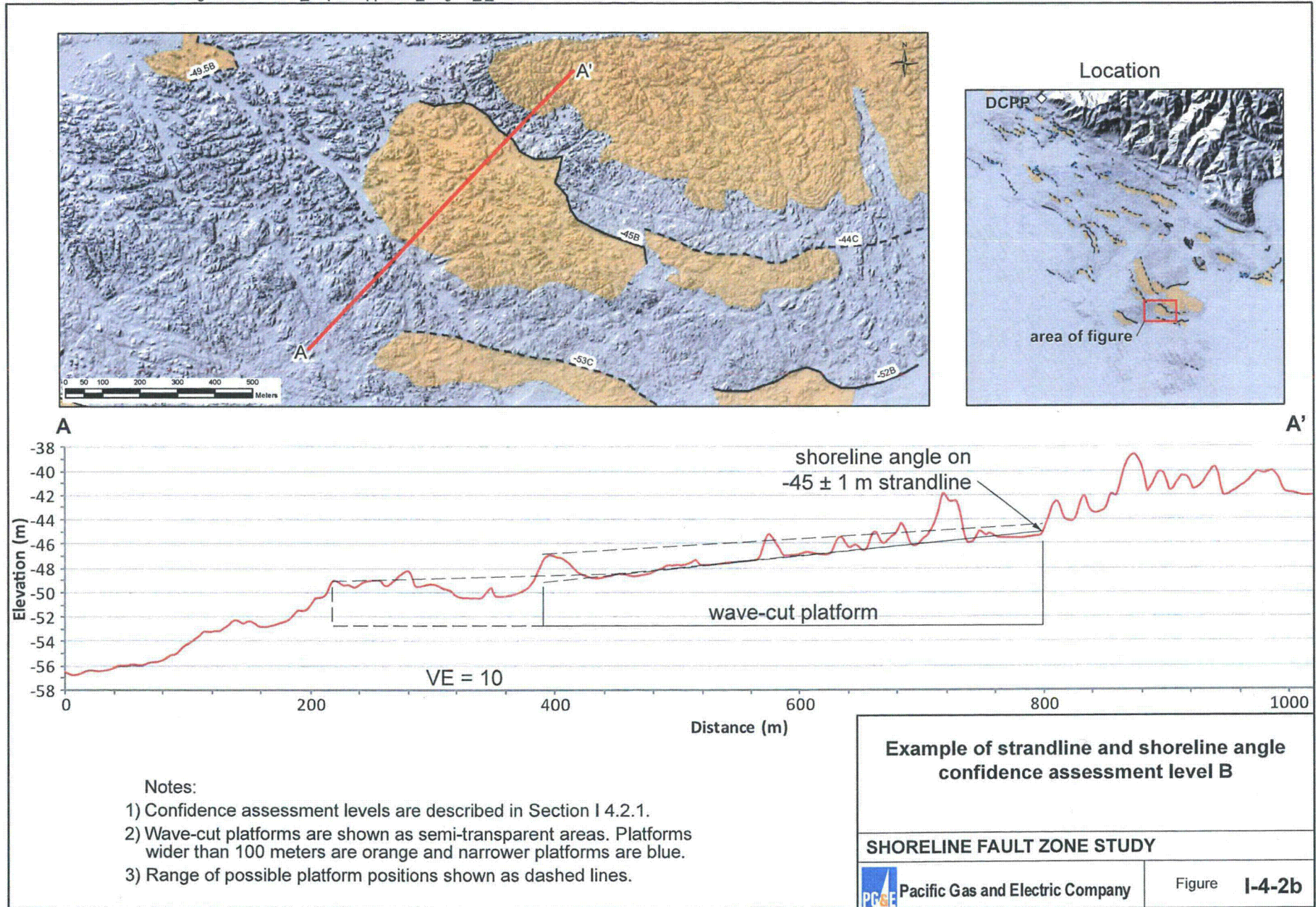
SHORELINE FAULT ZONE STUDY

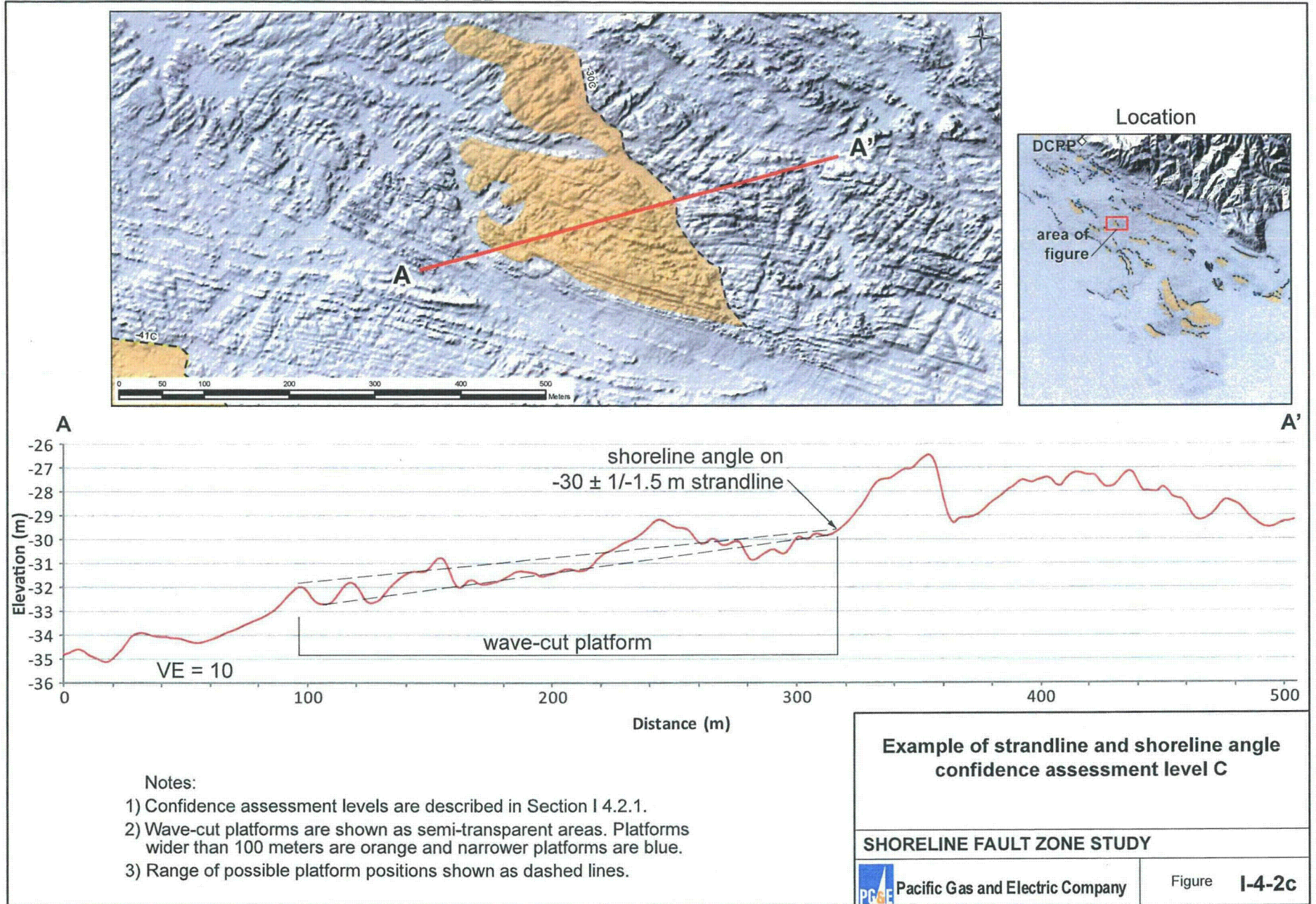
 Pacific Gas and Electric Company

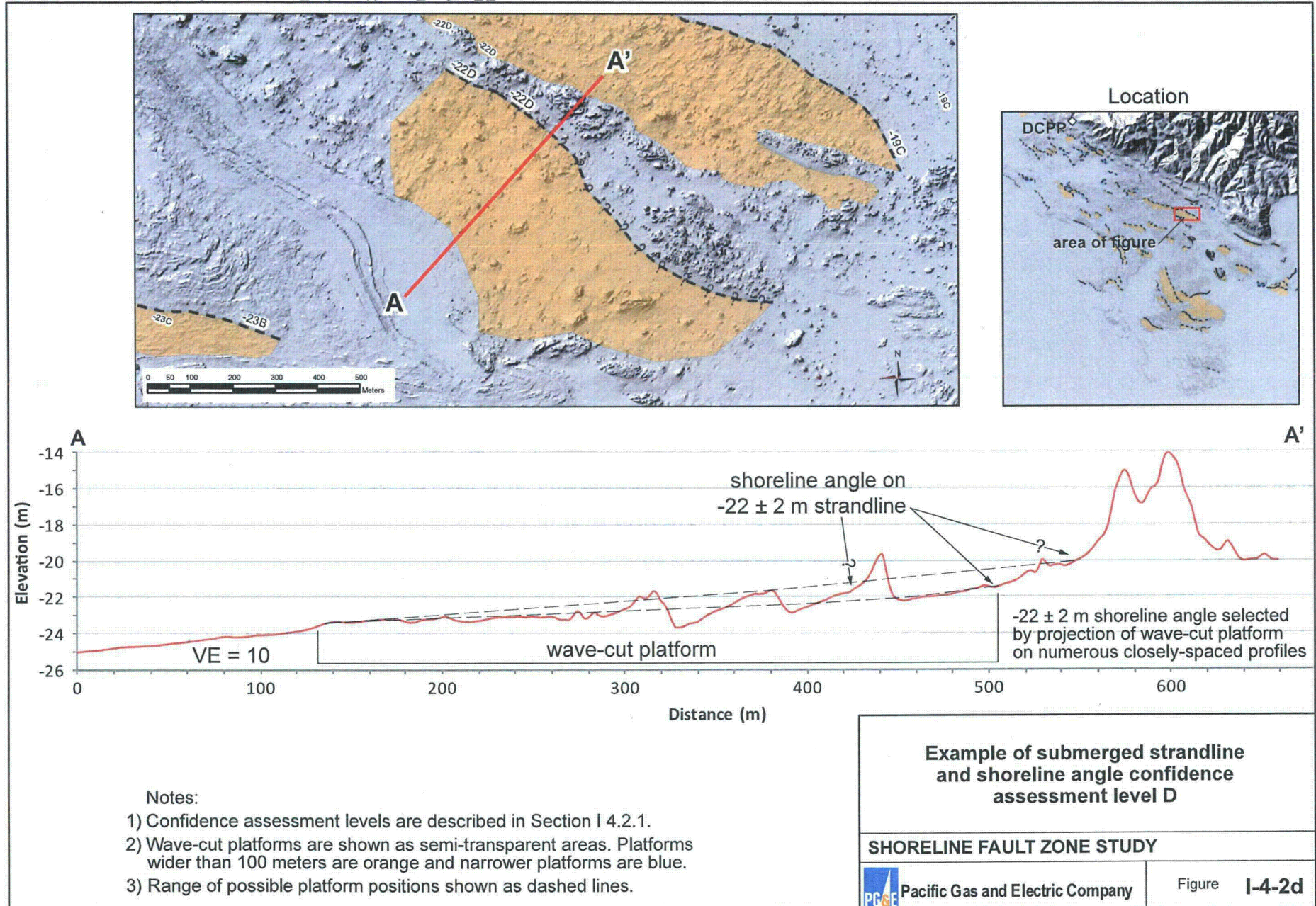
Figure **I-4-1**

S:\13800\13838\13838.002\Figures\20101112_Report\Appendix_I\Figure_I_4-1.ai

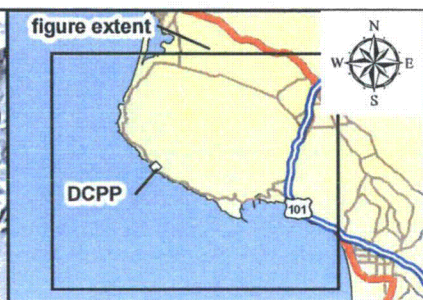
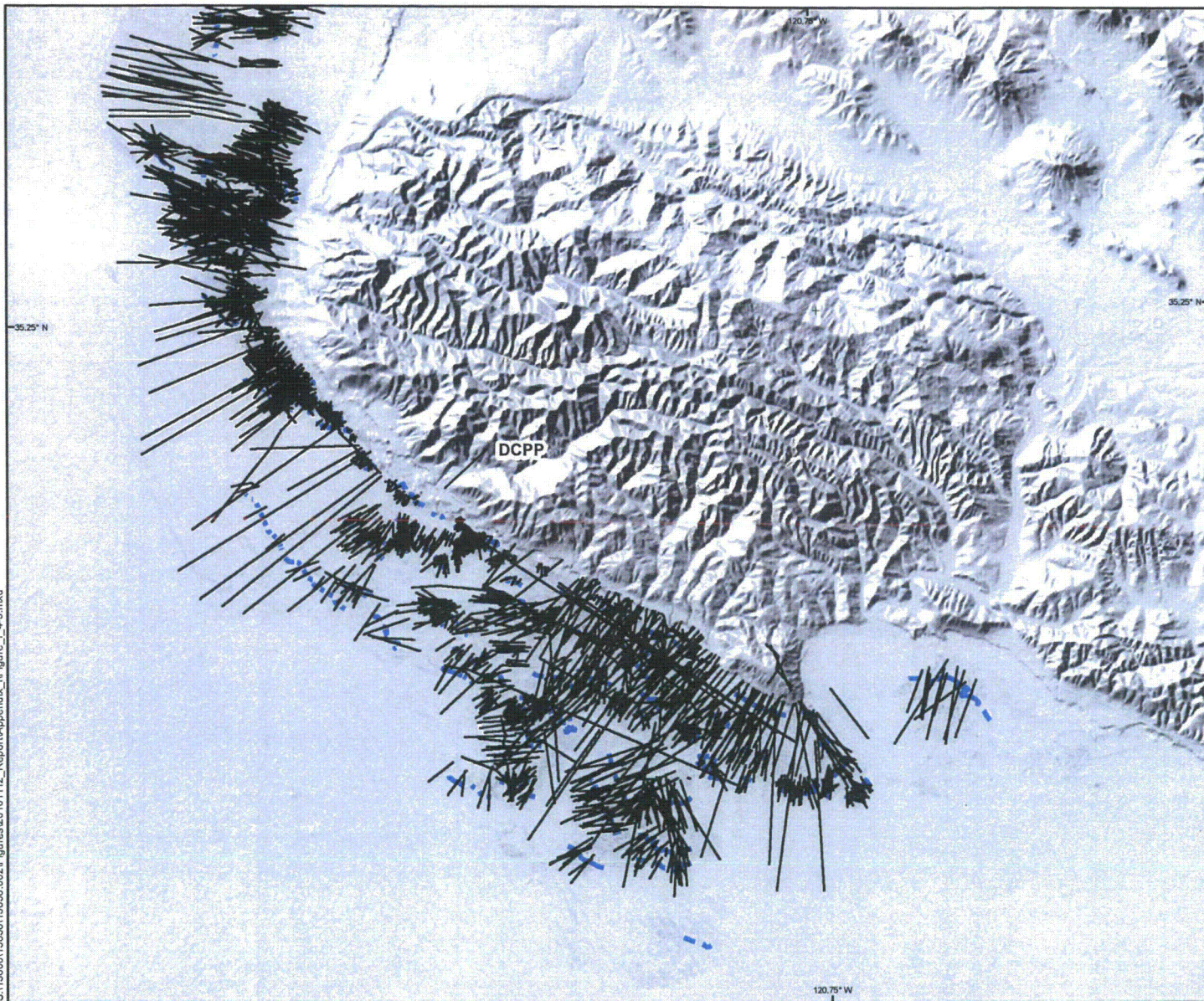








S:\138001\138381\138381002\Figures20101112_Report\Appendix_I\Figure_I_4-3.mxd



LEGEND

Submerged Strandlines
 ——— Dashed where approximately located; dotted where buried.

————— Location of bathymetric profile line

Note: Map displays some, but not all of the profiles generated during submerged shoreline angle analysis.

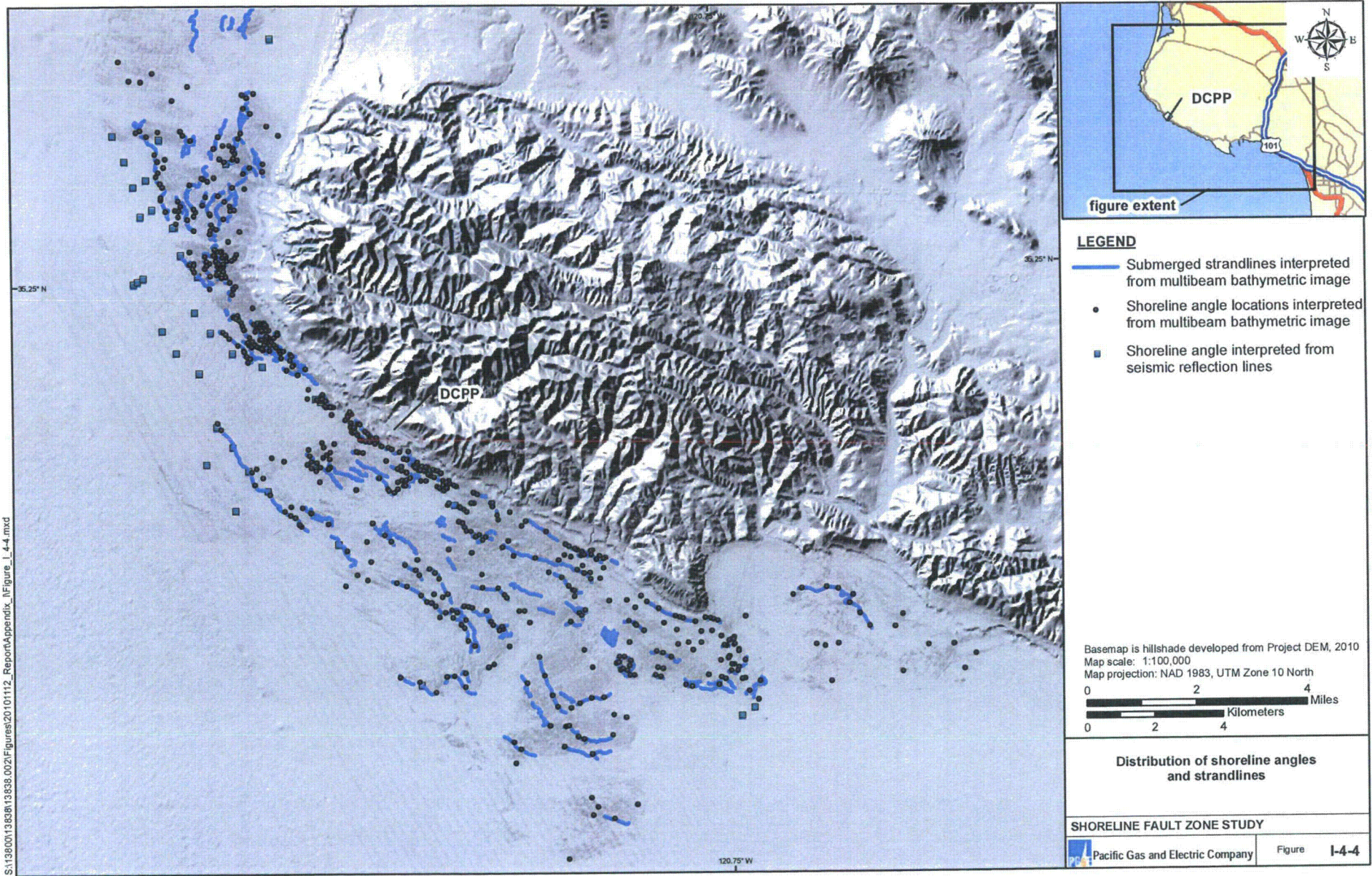
Basemap is hillshade developed from Project DEM, 2010
 Map scale: 1:100,000
 Map projection: NAD 1983, UTM Zone 10 North

0 1 2 Miles
 0 1 2 Kilometers

Bathymetric profile location for analysis of submerged strandlines and wave-cut platforms

SHORELINE FAULT ZONE STUDY

Pacific Gas and Electric Company Figure I-4-3



S:\138001\138001\138001\Figures\20101112_Report\Appendix_I\Figure_I_4-4.mxd

- LEGEND**
- Submerged strandlines interpreted from multibeam bathymetric image
 - Shoreline angle locations interpreted from multibeam bathymetric image
 - Shoreline angle interpreted from seismic reflection lines

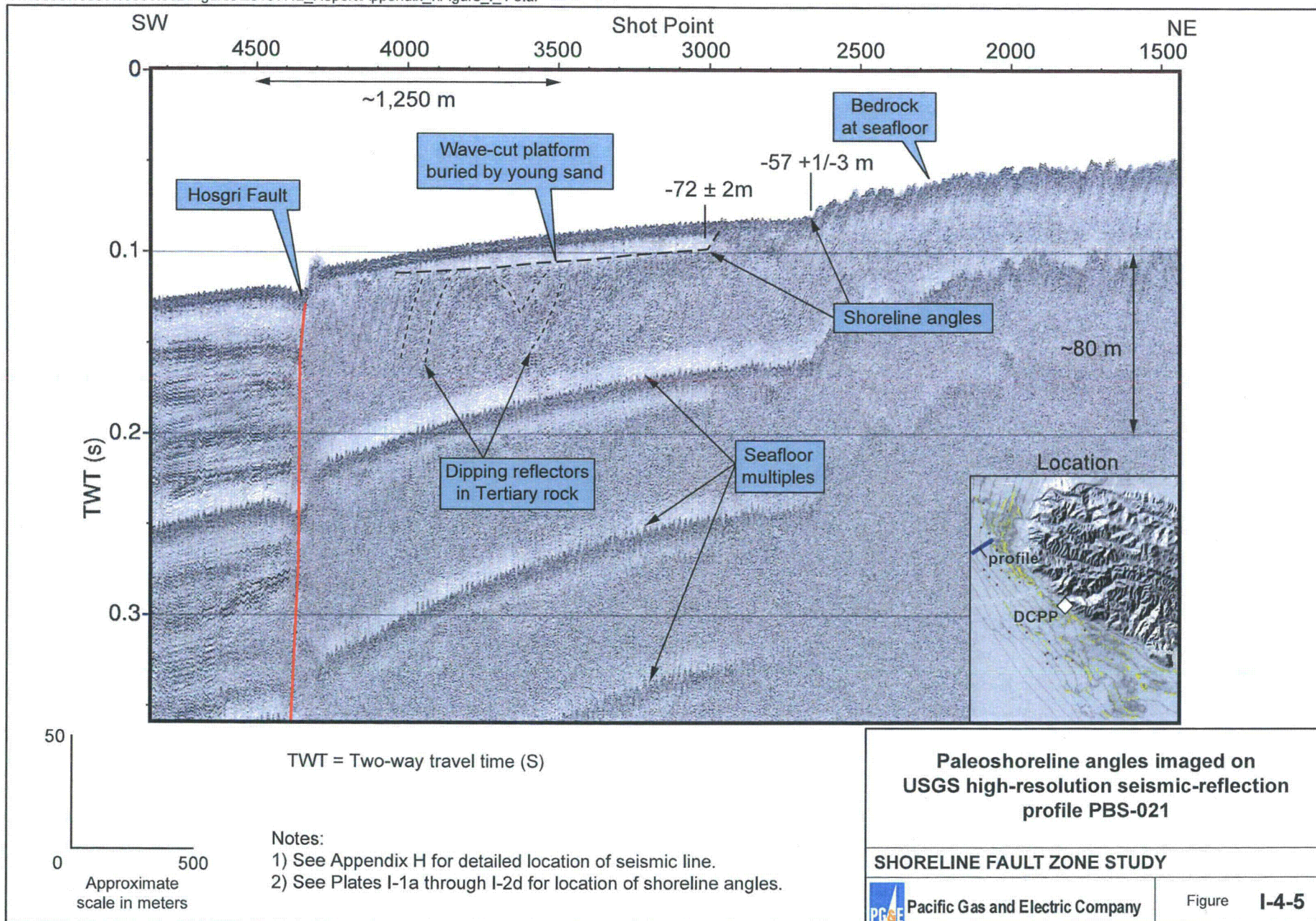
Basemap is hillshade developed from Project DEM, 2010
 Map scale: 1:100,000
 Map projection: NAD 1983, UTM Zone 10 North

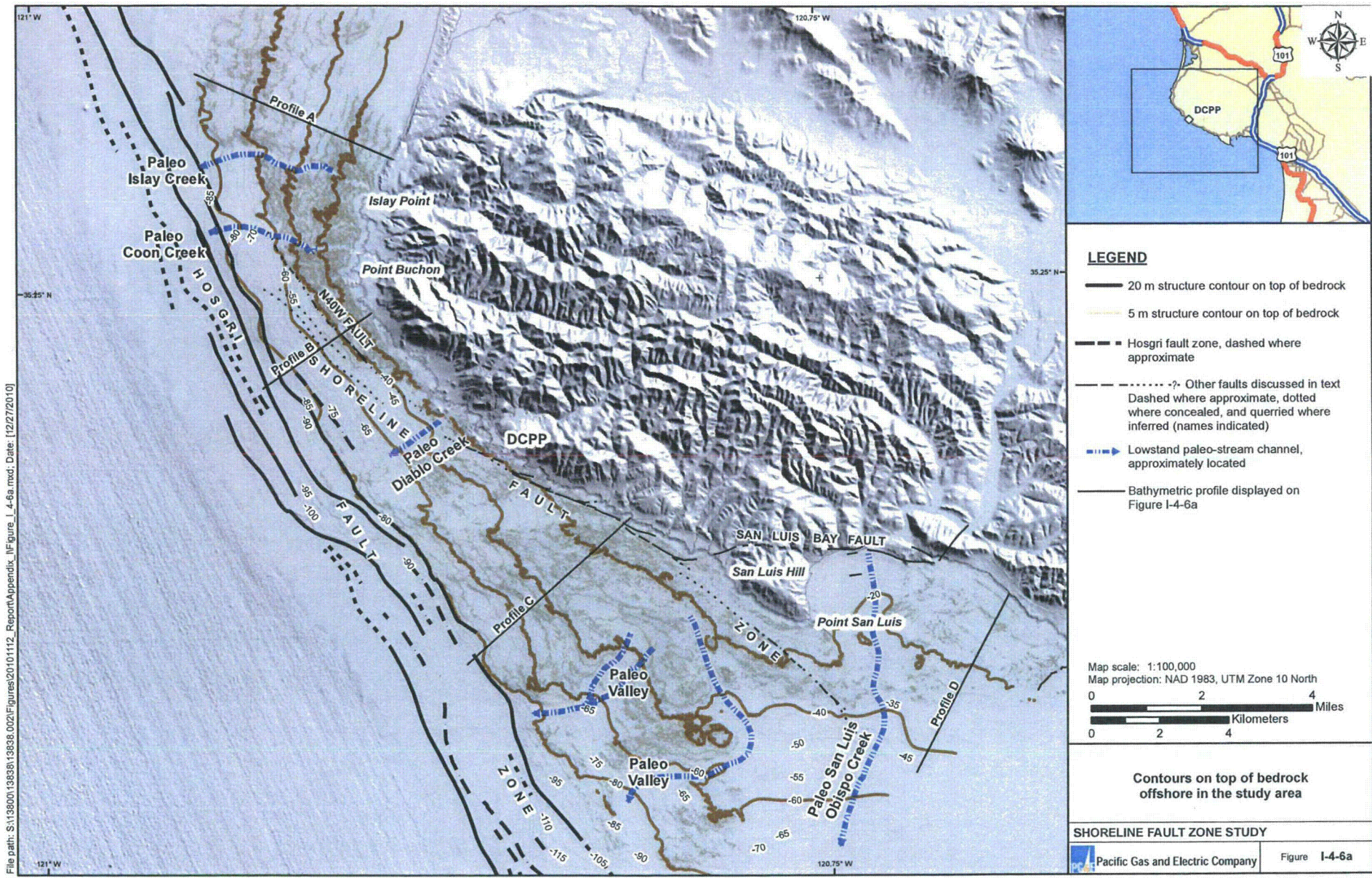
0 2 4 Miles
 0 2 4 Kilometers

Distribution of shoreline angles and strandlines

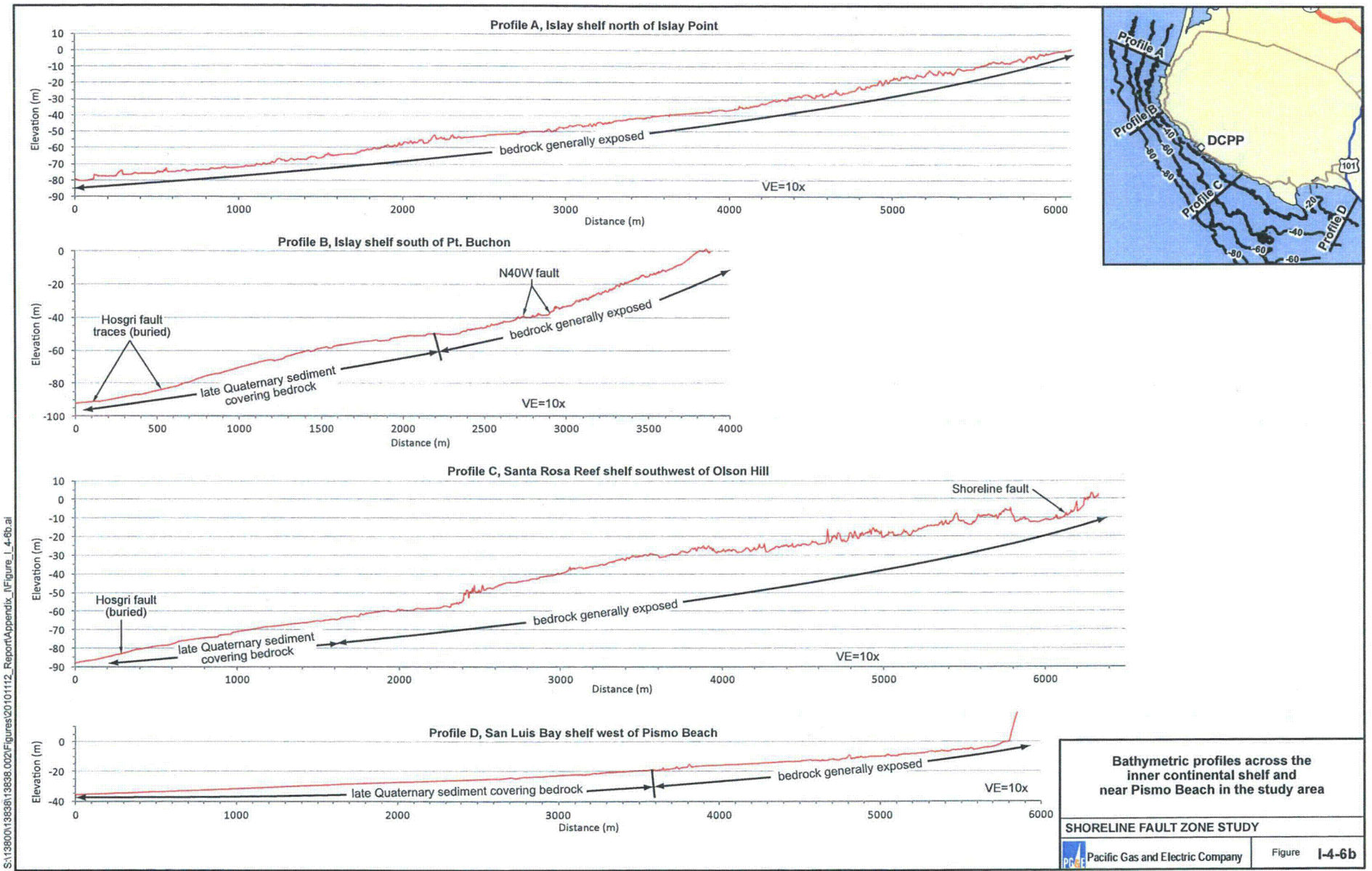
SHORELINE FAULT ZONE STUDY

PGE Pacific Gas and Electric Company Figure **I-4-4**



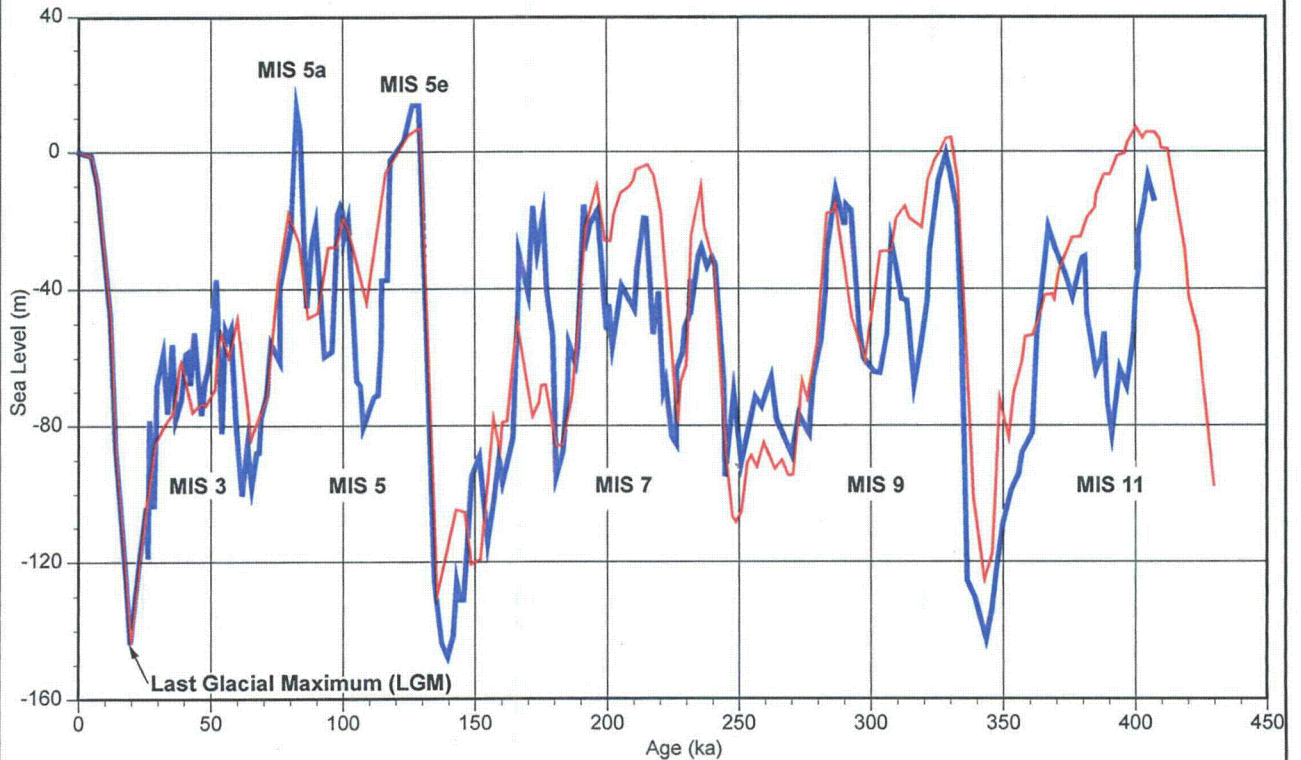


File path: S:\138001\13838\13838_002\Figures\20101112_Report\Appendix_I\Figure_I-4-6a.mxd; Date: [12/27/2010]



S:\13860013838\02\Figures\20101112_Report\Appendix_I\Figure_I_4-6b.ai

S:\13800\13838\13838.002\Figures\20101112_Report\Appendix_I\Figure_I-5-1.ai



— Shackleton (2000)*
— Waelbroeck et al. (2002)**
MIS Marine oxygen isotope stage

Notes:

* Shackleton (2000); Late Quaternary marine oxygen isotope ($\delta^{18}\text{O}$) record attributable to ice volume and sea level changes. This record is based on $\delta^{18}\text{O}$ ratios measured in benthic foraminifera and corrected using $\delta^{18}\text{O}$ ratios of atmospheric oxygen trapped in arctic ice at Vostok. In this way, contamination from the effect of deep-water temperature variability was eliminated. Curve is scaled to fit paleosea-level observations.

** Waelbroeck et al. (2002); uses regressions established from relative sea-level (RSL) coral terrace data and benthic foraminifera oxygen isotope data calibrated to sea temperature data from the north Atlantic and equatorial Pacific to create a composite RSL curve for past climatic cycles.

Comparison of late Quaternary sea-level curves from oxygen isotope data

SHORELINE FAULT ZONE STUDY

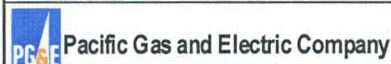
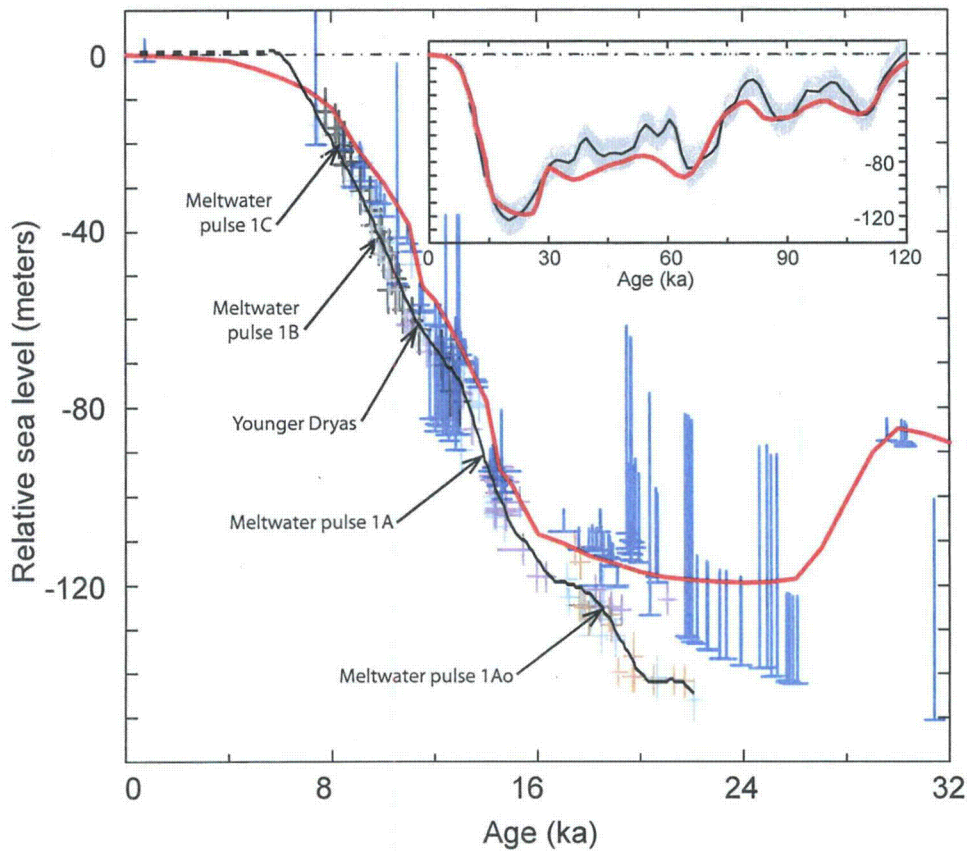


Figure I-5-1



EXPLANATION

- Linearly interpolated curve utilizing Lambeck et al. (2002) and Lambeck and Chappell (2001) data (This study).
- + Coral-based estimates of relative sea level, color indicates source of sample (Lambeck and Chappell; 2001):
 - + Cyan - Barbados*
 - + Orange - Bonaparte Gulf
 - + Black - Huon Peninsula
 - Gray - Tahiti
 - + Purple - Sunda Shelf
- Relative sea level for Barbados predicted by the ICE-5G (VM2) model (Peltier and Fairbanks, 2006)
- Coral-based estimates of relative sea level from Barbados. Horizontal bar denotes depth of sample (corrected for tectonic uplift of 0.34 mm/yr). The length of the vertical bar denotes the range with respect to sea level the coral species could be found (Peltier and Fairbanks, 2006)
- Waelbroeck et. al. (2002). Ice equivalent eustatic sea level. Gray shading indicates uncertainty band

* Note that data from Barbados are plotted at different elevations by Peltier and Fairbanks (2006) and Lambeck and Chappell (2001) and Lambeck et al. (2002) to account for differences in characterization of the viscous response of the mantle to changes in surface loads by the two groups.

Sea-level rise since the Last Glacial Maximum

SHORELINE FAULT ZONE STUDY

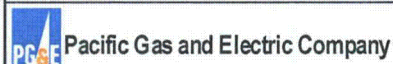
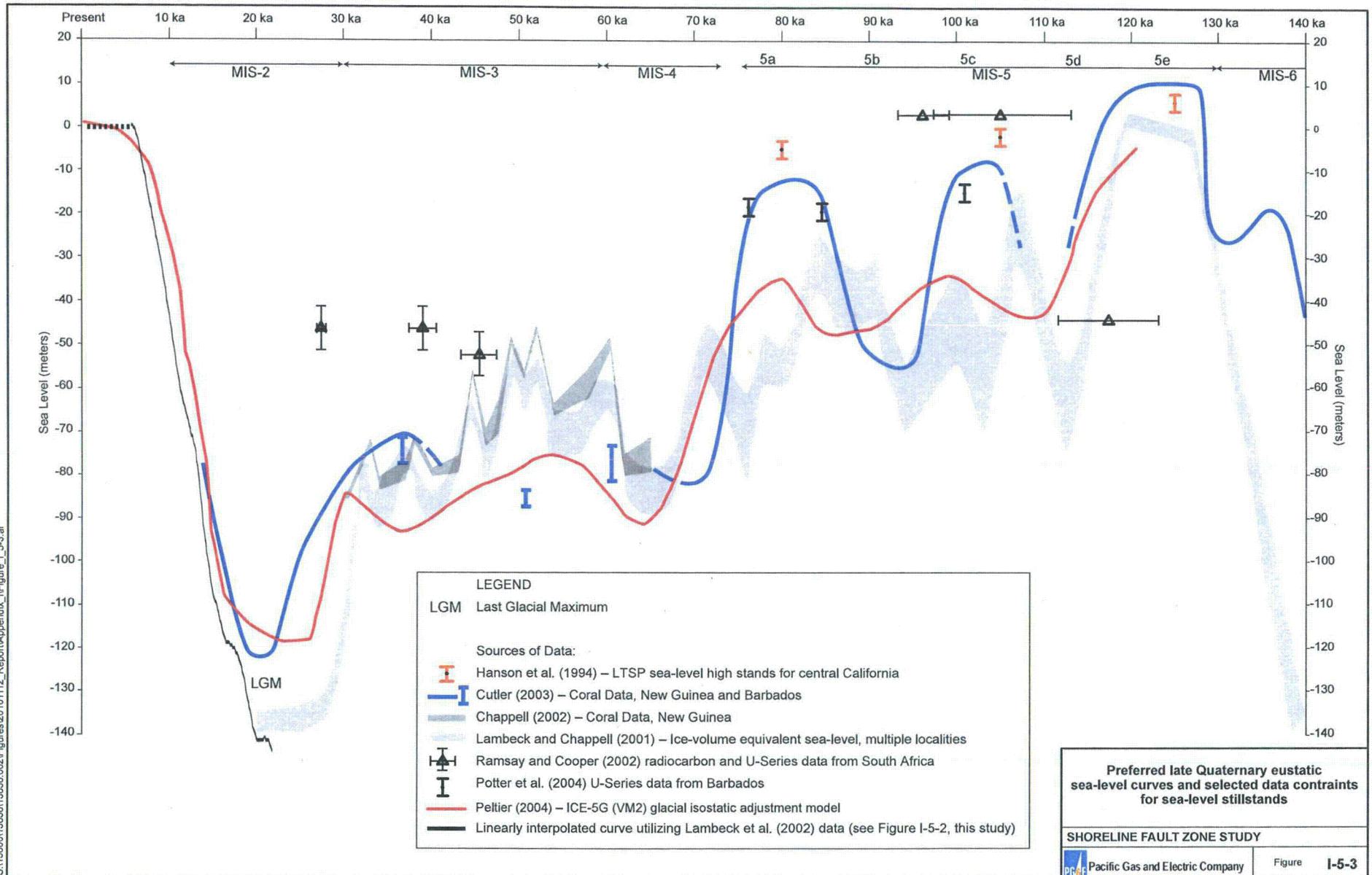


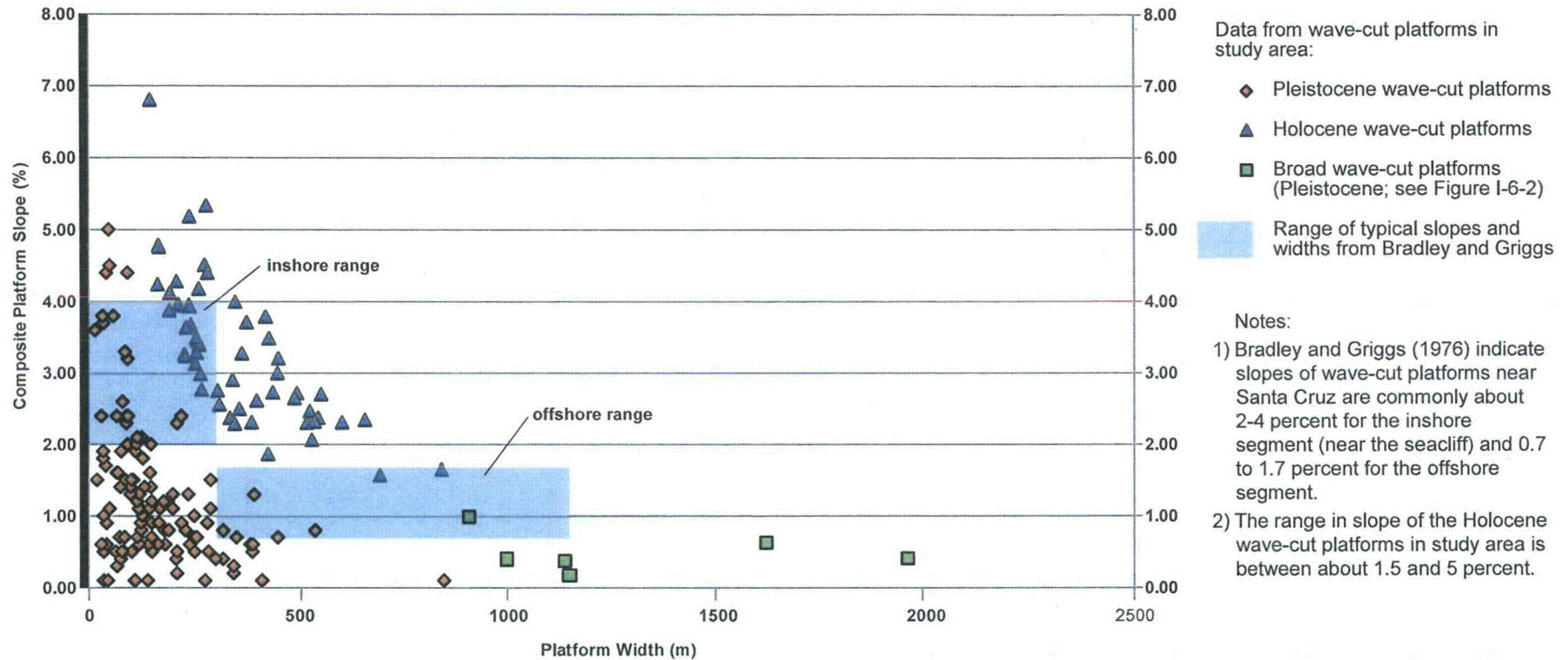
Figure **I-5-2**

S:\13800\13838\13838.002\Figures\20101112_Report\Appendix_I\Figure_I_5-2.ai

S:\138001\385381\38538_002\Figures\20101112_Report\Appendix_I\Figure_I-5-3.ai



Wave-Cut Platform Morphology



Mean slopes and maximum widths of submerged wave-cut platforms

SHORELINE FAULT ZONE STUDY

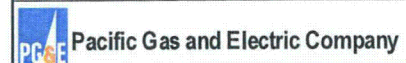
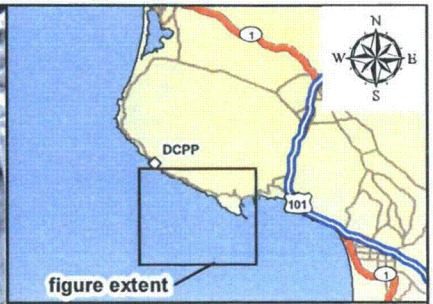
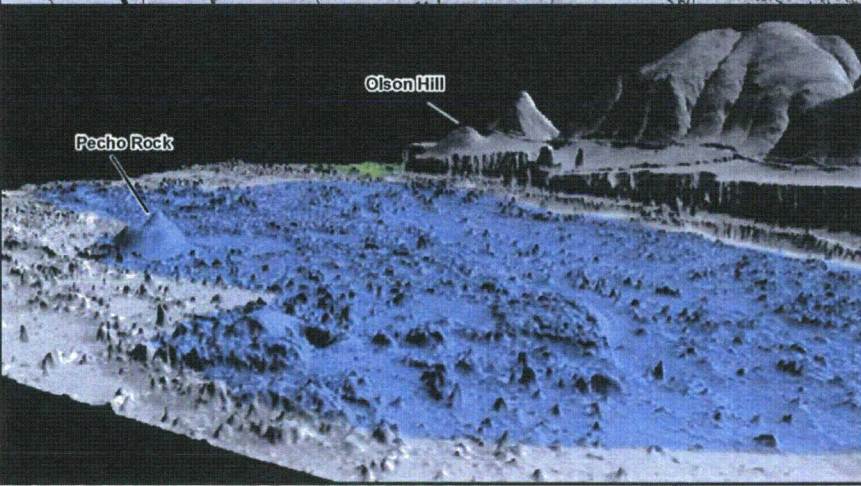
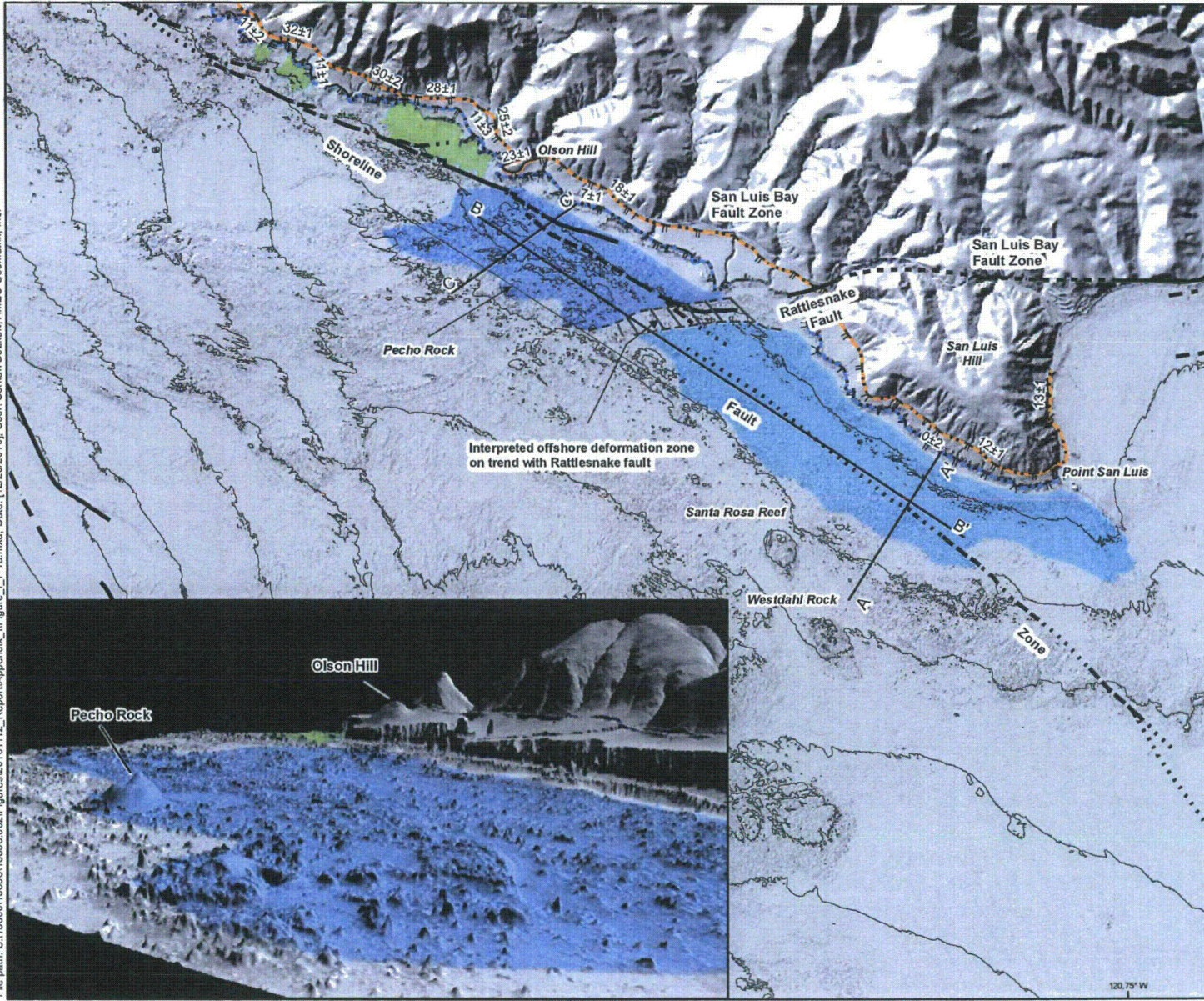


Figure I-6-1

File path: S:\13800\13838\02\Figures\20101112_Report\Appendix_I\Figure_I-7-1a.mxd; Date: [12/20/2010]; User: Sarkis Bozkurt, AMEC Geomatics, Inc.



LEGEND

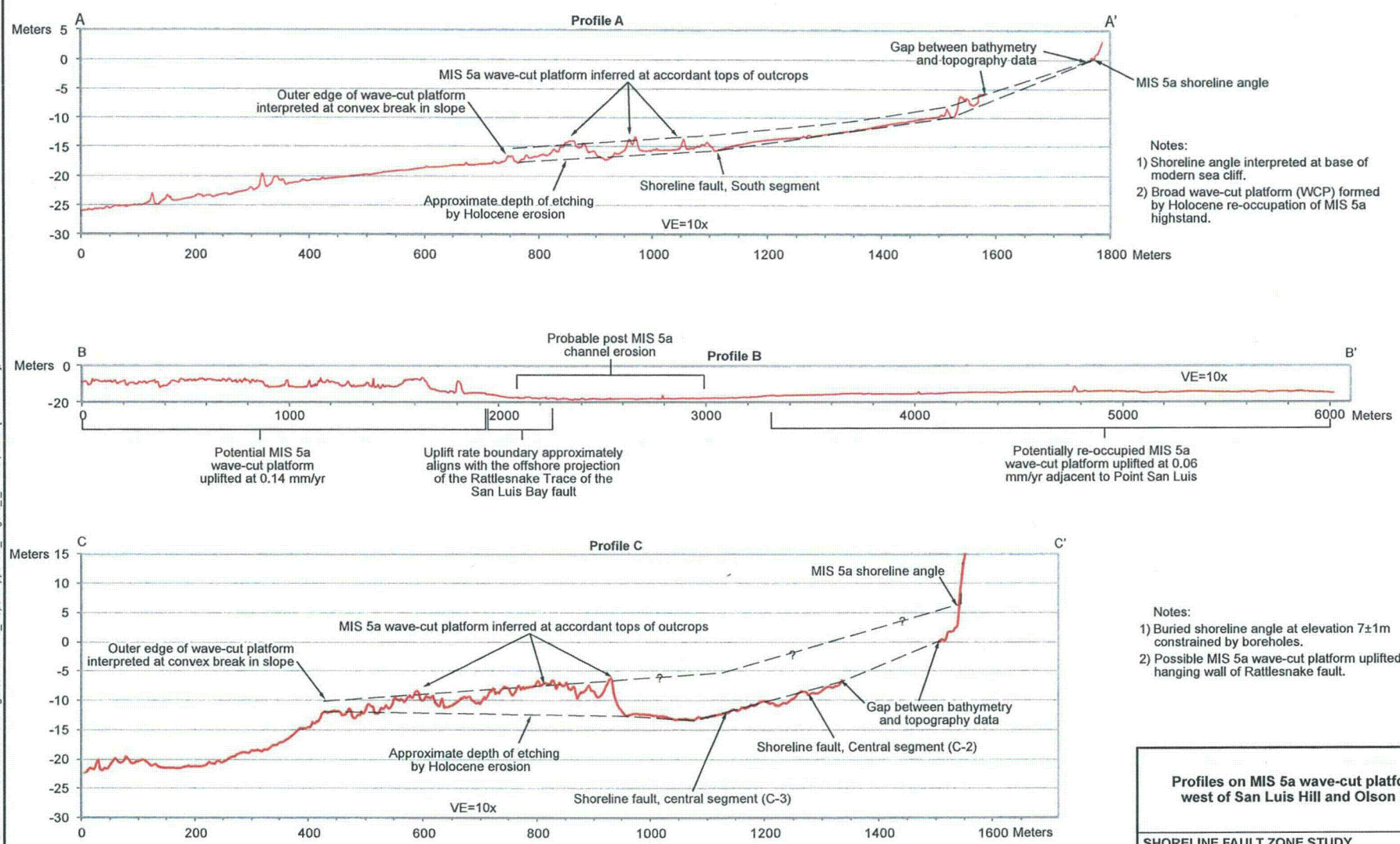
- Wave-cut Platforms**
- Holocene wave-cut platform, north of Olson Hill
 - MIS 5a wave-cut platform, south of Olson Hill, etched by Holocene erosion
 - MIS 5a wave-cut platform, west of San Luis Hill, reoccupied by Holocene high stand
 - 10m bathymetric contour
 - Emergent marine terrace strandline, dashed where buried or not well constrained, dotted where eroded (elevations labeled in meters). Orange correlation line is MIS 5e shoreline. Blue correlation line is MIS 5a shoreline
 - Fault, dashed where approximate, dotted where concealed, and queried where inferred (names indicated)

Basemap is hillshade developed from Project DEM, 2010
 Map scale: 1:40,000
 Map projection: NAD 1983, UTM Zone 10 North

0 0.5 1 Miles
 0 0.5 1 Kilometers

Map of submerged MIS 5a wave-cut platforms west of San Luis Hill

File path: S:\138001\383381\3838_002\Figures\20101112_Report\Appendix_I\Figure_I-7-1b.ai; Date: [12/20/2010]; User: Serkan Bozkurt, AMEC Geomatrix, Inc.



Notes:
1) Shoreline angle interpreted at base of modern sea cliff.
2) Broad wave-cut platform (WCP) formed by Holocene re-occupation of MIS 5a highstand.

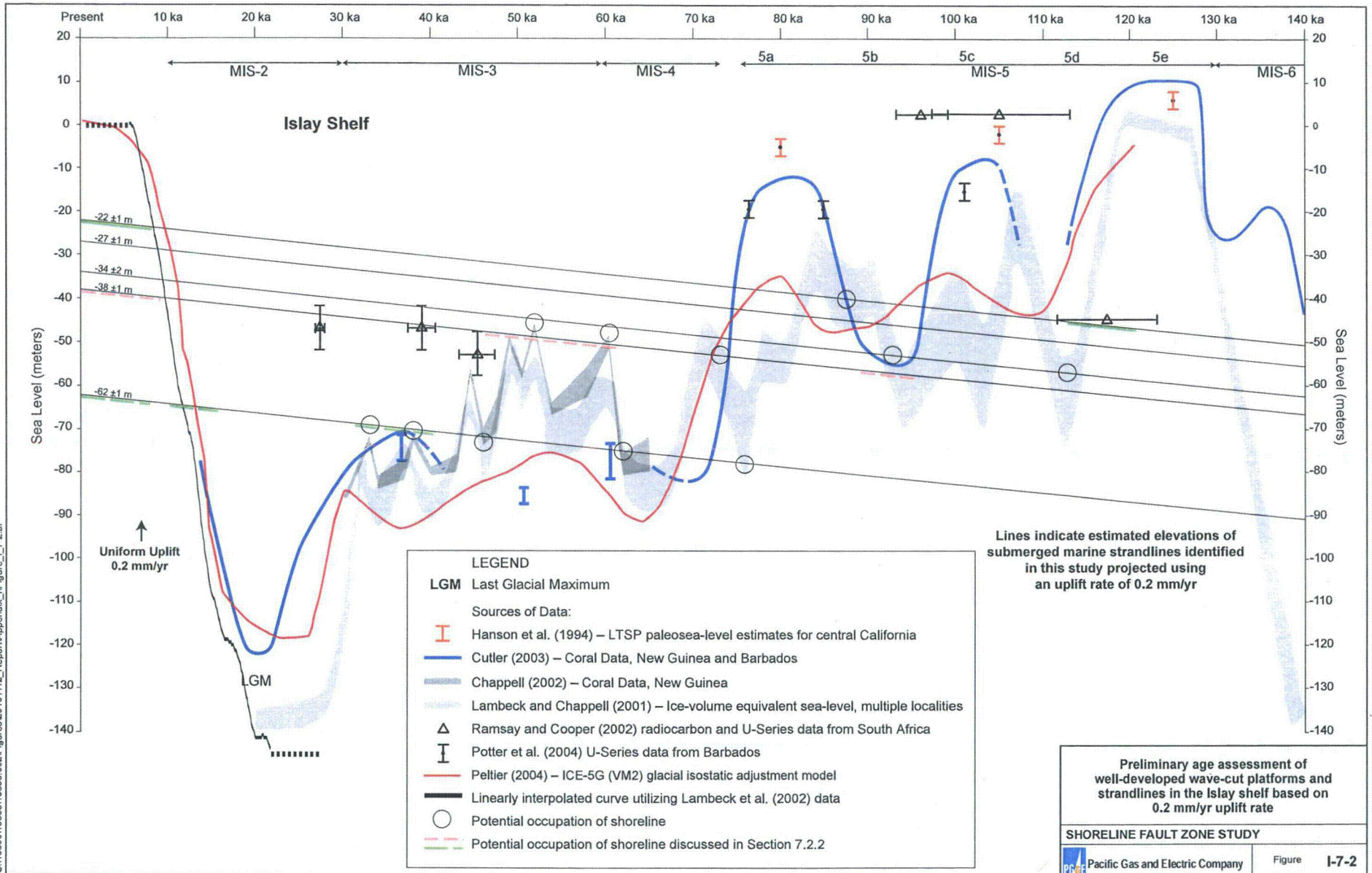
Notes:
1) Buried shoreline angle at elevation 7±1m constrained by boreholes.
2) Possible MIS 5a wave-cut platform uplifted in hanging wall of Rattlesnake fault.

Profiles on MIS 5a wave-cut platforms west of San Luis Hill and Olson Hill

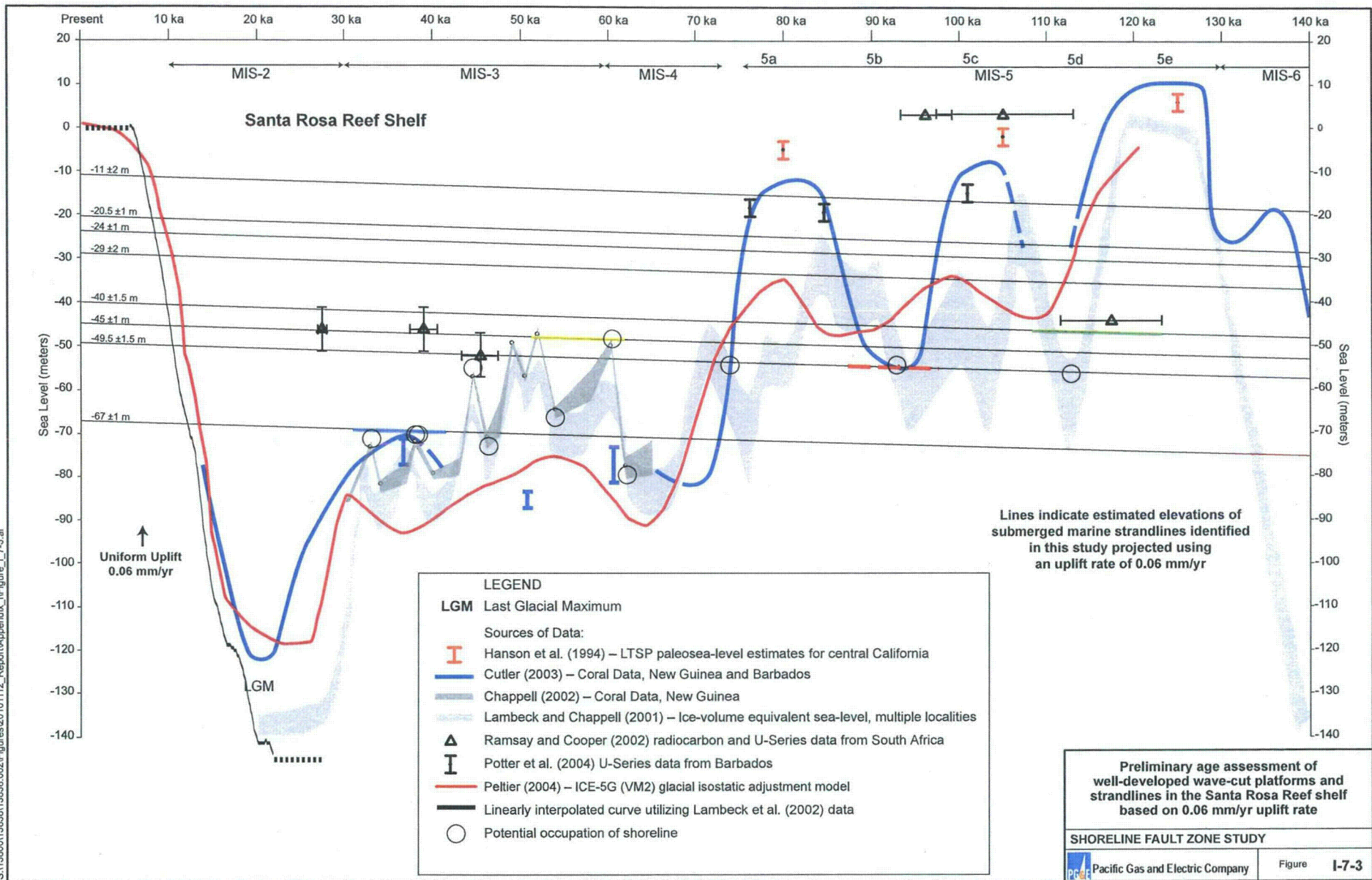
SHORELINE FAULT ZONE STUDY

Pacific Gas and Electric Company Figure I-7-1b

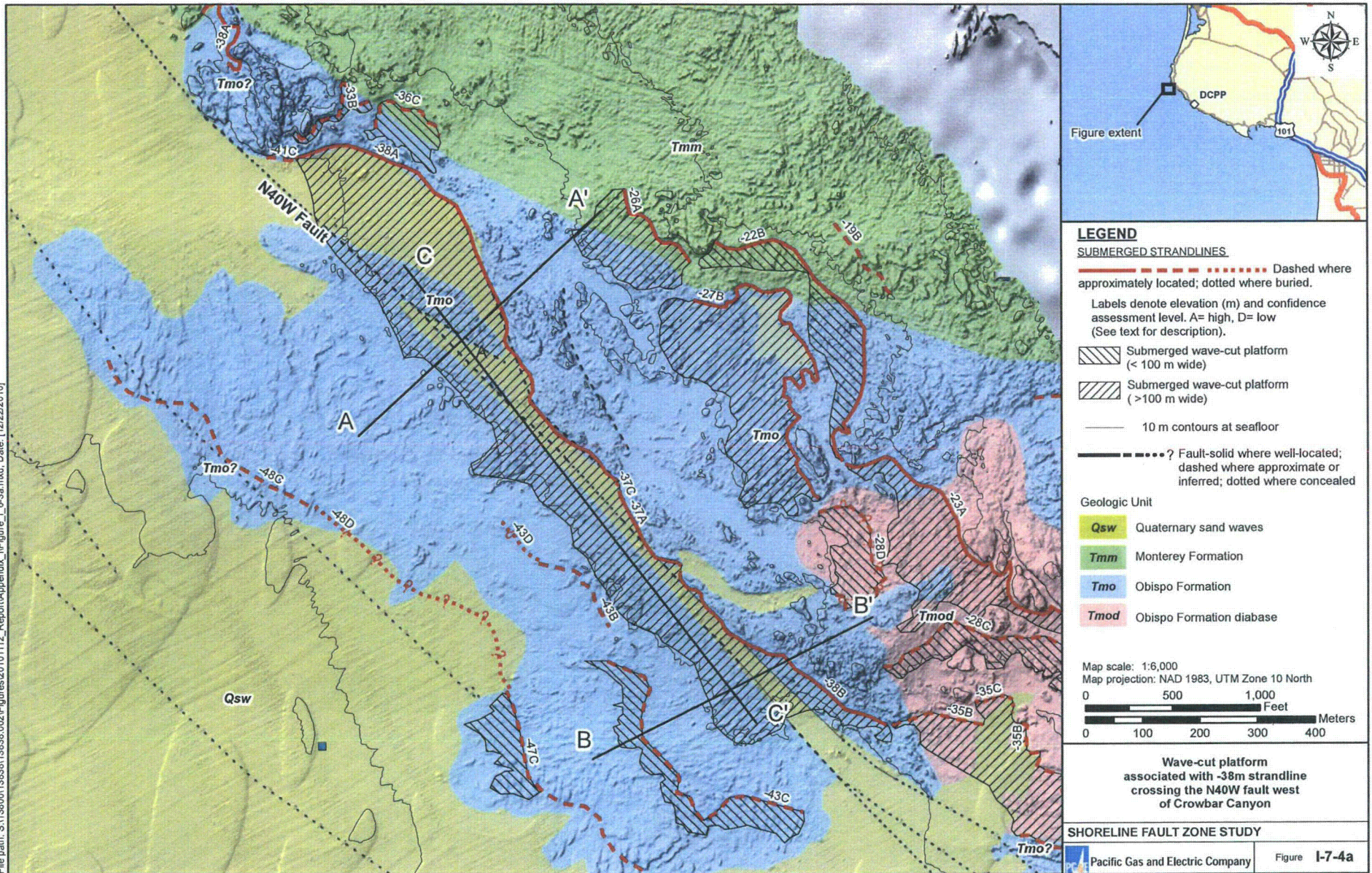
S:\138001\38381\3838_002\Figures\20101112_Report\Appendix_I\Figure_I_7-2.ai

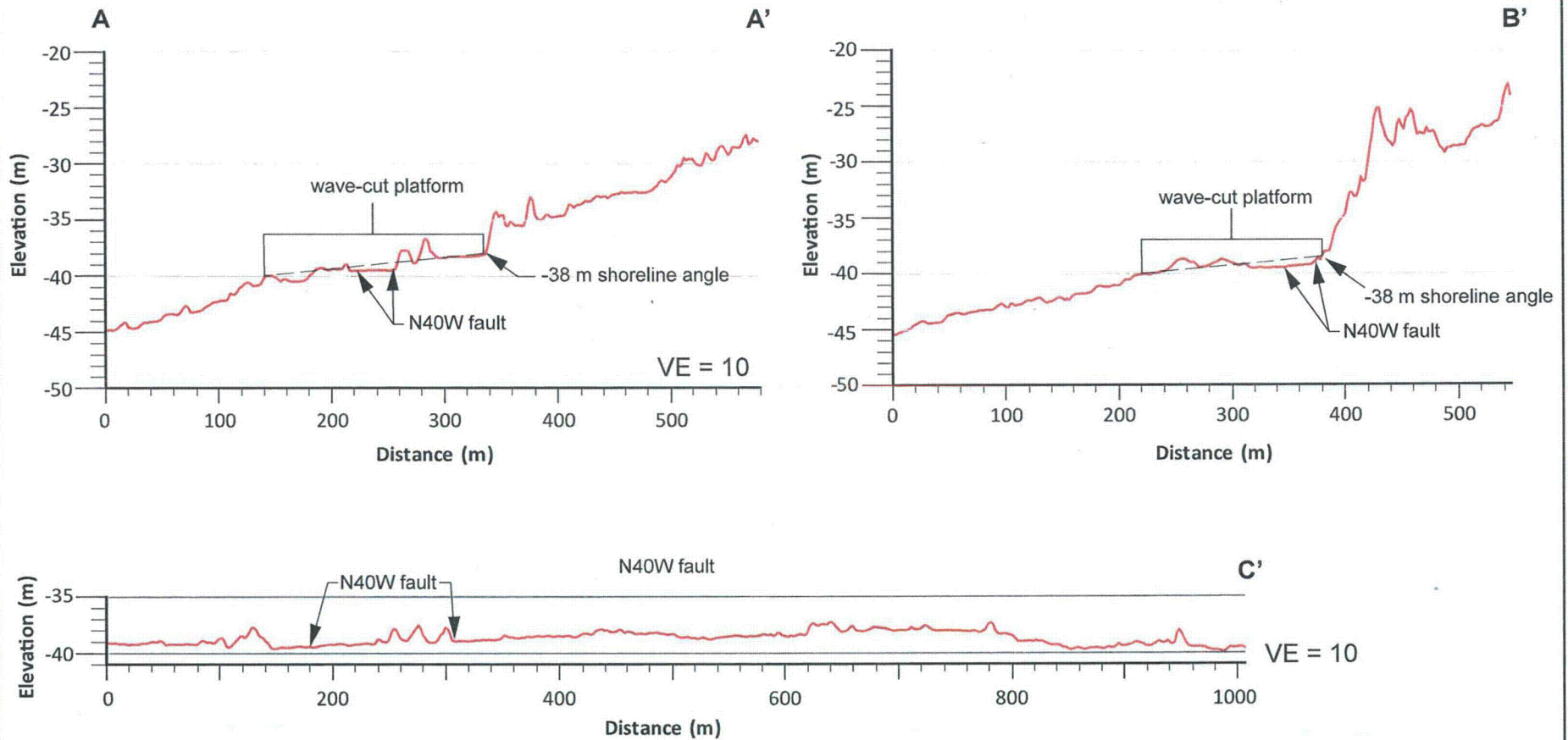


S:\1380013888\13886.02\Figures\20101112_Report\Appendix_I\Figure_I-7-3.ai



File path: S:\13900\13938\13938_02\Figures\20101112_Report\Appendix_I\Figure_I_6-3a.mxd; Date: [12/22/2010]





Note:

- 1) Although the N40W fault is locally associated with scarps within the wave-cut platform (such as the one shown in profile A), profiles show no persistent vertical separation of the wave-cut platform across the N40W fault.

Profiles showing wave-cut platform associated with -38 m strandline crossing the N40W fault west of Crowbar Canyon

SHORELINE FAULT ZONE STUDY

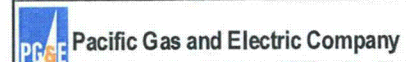
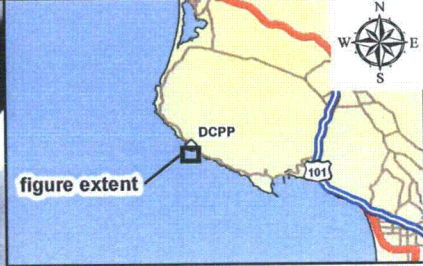
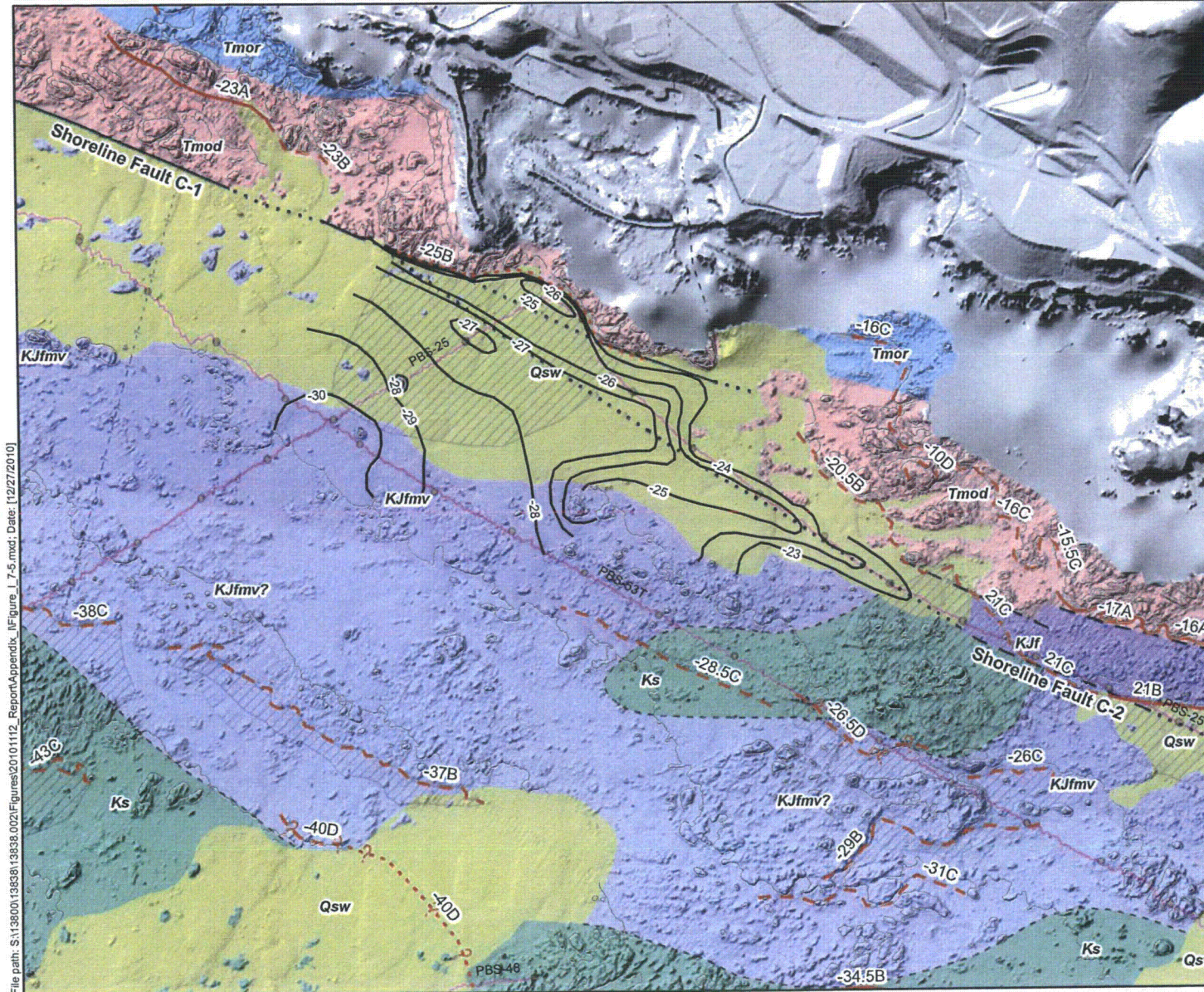


Figure I-7-4b



LEGEND

SUBMERGED STRANDLINES

- Dashed where approximately located; dotted where buried.
- Labels denote elevation (m) and confidence assessment level. A= high, D= low (See text for description).

Geologic Unit

	Qsw	Quaternary sand waves
	Tmor	Resistant Obispo Formation
	Tmod	Obispo Formation diabase
	Ks	Cretaceous sandstone
	KJfmv?	Franciscan Complex

Map scale: 1:6,000
 Map projection: NAD 1983, UTM Zone 10 North

0 500 1,000 Feet
 0 100 200 300 400 Meters

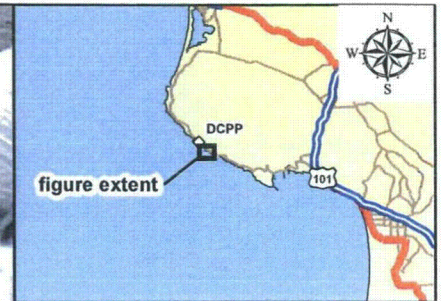
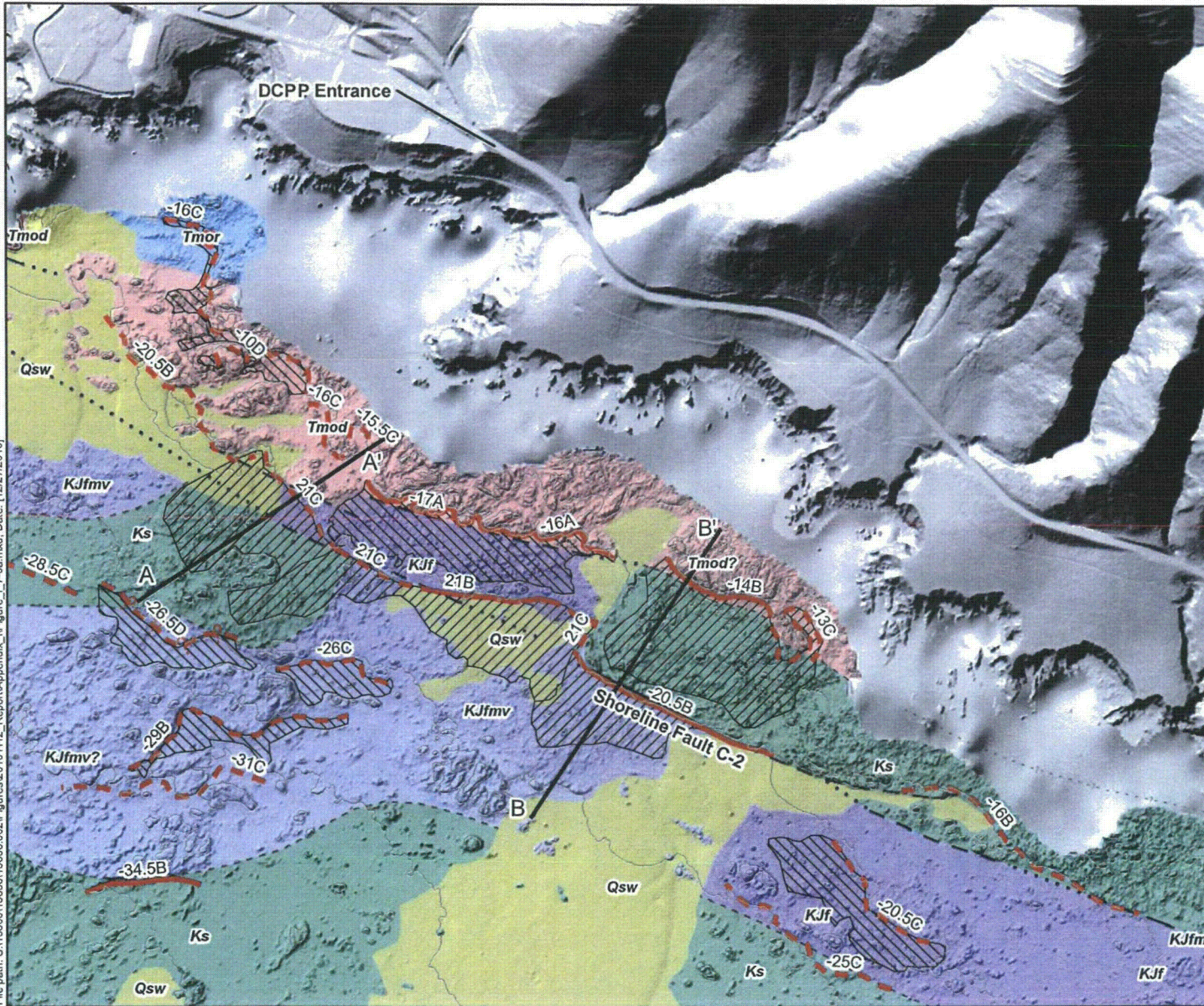
The -25m wave-cut platform across the North Central segment of the Shoreline fault zone at DCPD

SHORELINE FAULT ZONE STUDY

Pacific Gas and Electric Company Figure I-7-5

File path: S:\13800\13838\002\Figures\20101112_Report\Appendix_I\Figure_I_7-5.mxd; Date: 12/27/2010

File path: S:\138001\38381\3838_002\Figures\20101112_Report\Appendix_I\Figure_I-7-6a.mxd; Date: [12/27/2010]



LEGEND

SUBMERGED STRANDLINES.
 - - - - - Dashed where approximately located; dotted where buried.
 Labels denote elevation (m) and confidence assessment level. A= high, D= low (See text for description).

Submerged wave-cut platform (< 100 m wide)
 Submerged wave-cut platform (>100 m wide)
 ——— 5 m bathymetric contours

— - - - - Fault-solid where well-located; dashed where approximate or inferred; dotted where concealed

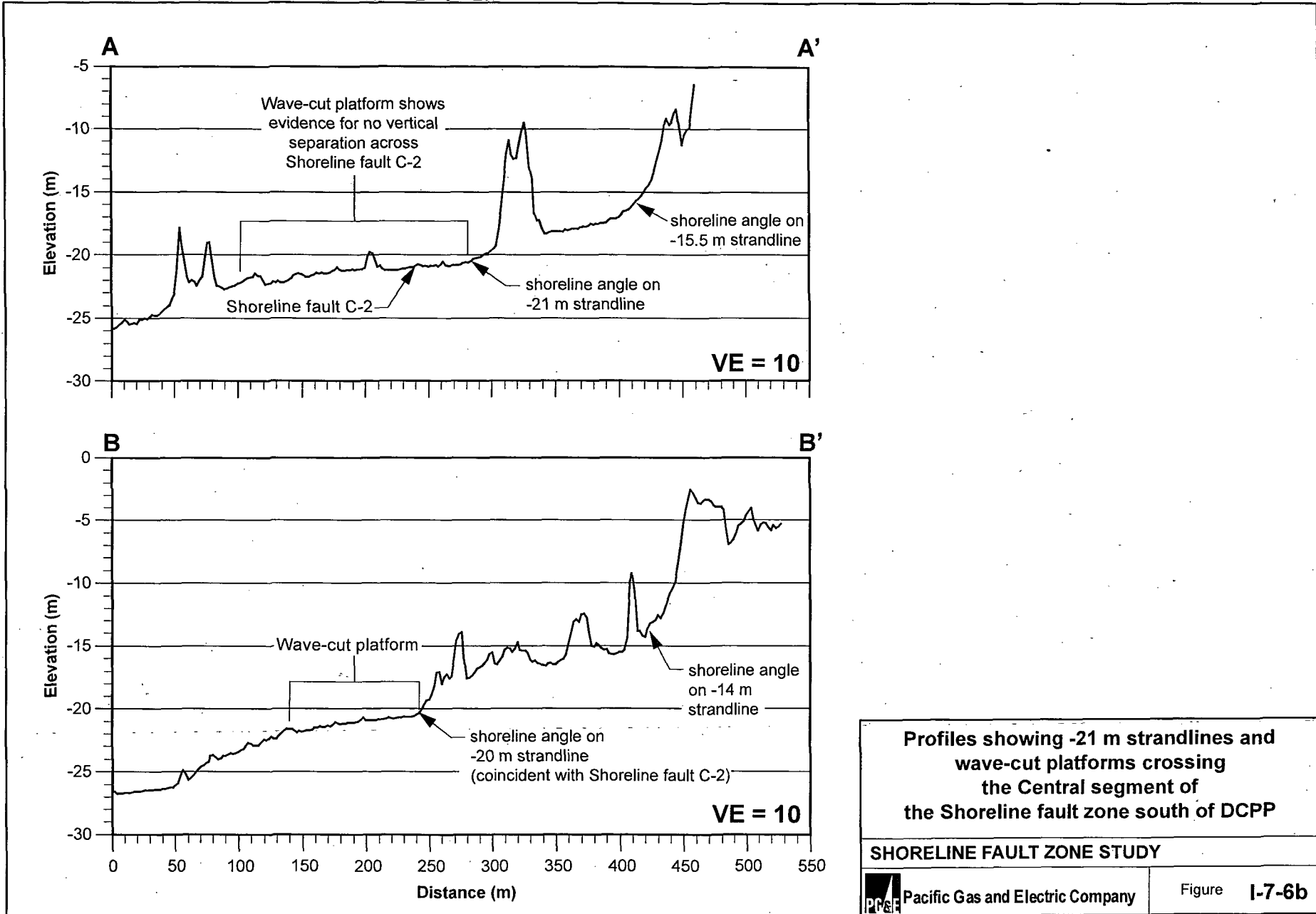
Geologic Unit

Qsw	Quaternary sand waves
Tmor	Resistant Obispo Formation
Tmod	Obispo Formation diabase
Ks	Cretaceous sandstone
KJfmv?	Franciscan Complex

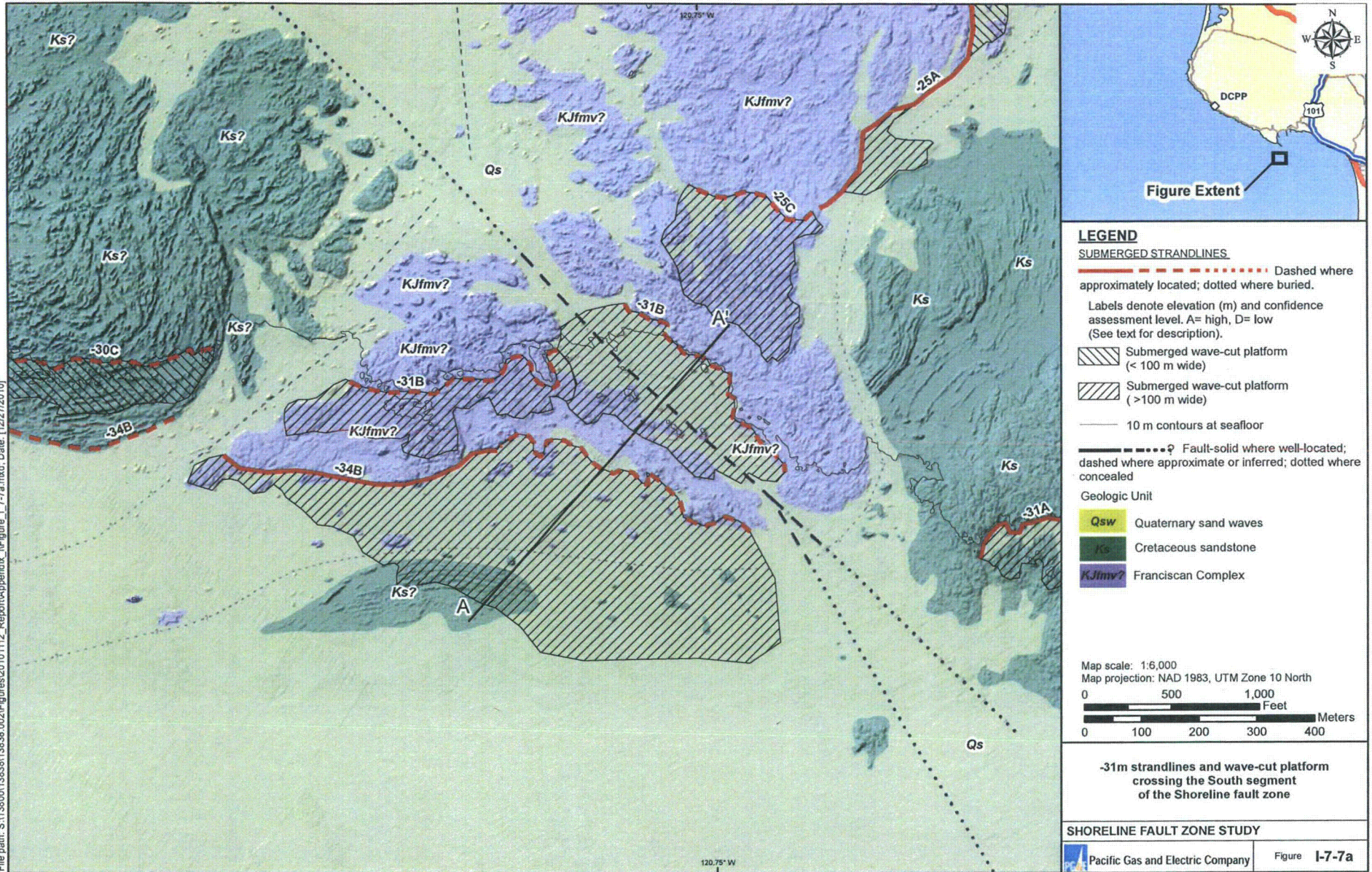
Map scale: 1:6,000
 Map projection: NAD 1983, UTM Zone 10 North

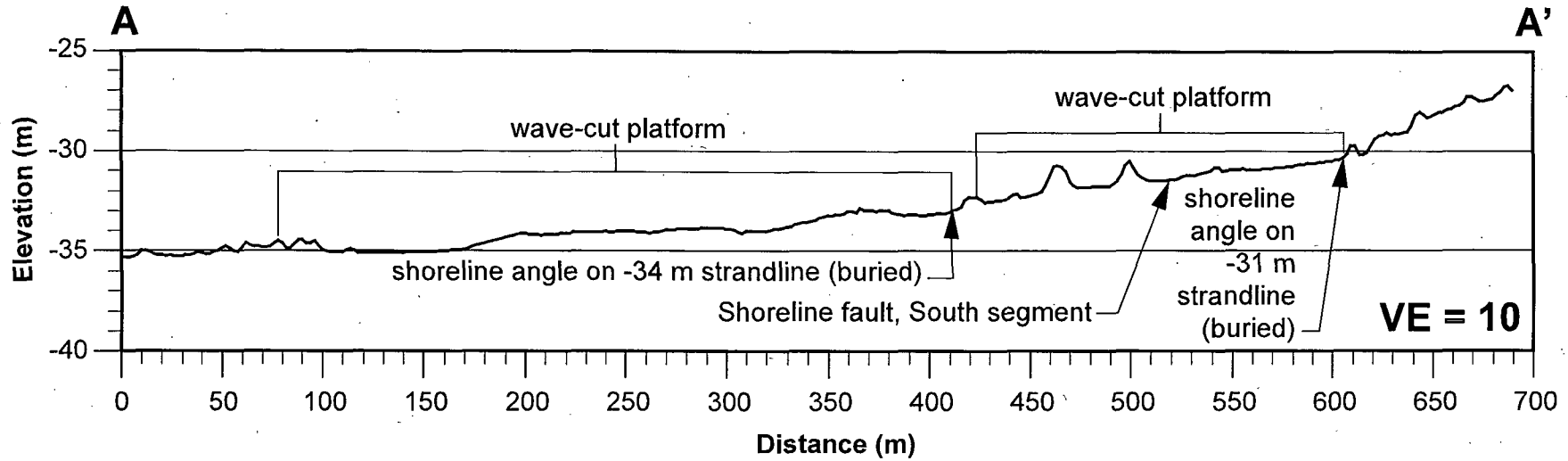
0 500 1,000 Feet
 0 100 200 300 400 Meters

-21m strandlines and wave-cut platforms crossing the Central segment of the Shoreline fault zone south of DCP



File path: S:\138001\38338\13838_002\Figures\2010101112_Report\Appendix_I\Figure_I-7-7a.mxd; Date: [12/27/2010]





Note:
 1) Wave-cut platform associated with -31 m strandline shows evidence for no vertical separation across South segment of Shoreline fault zone.

**Profile showing -31 m wave-cut platform
 across the South segment
 of the Shoreline fault zone**

SHORELINE FAULT ZONE STUDY

 Pacific Gas and Electric Company

Figure **I-7-7b**